32788

CI/SfB
(99.4) q4 (L31)
Date November 1994

BRANZ

STUDY REPORT

NO. 48 (1994)

A LITERATURE SURVEY OF ELECTRICAL TECHNIQUES FOR MEASURING CONCRETE MOISTURE PROFILES

J.W. Lovell-Smith

The work reported here was jointly funded by the Building Research Levy and the Foundation for Research, Science and Technology from the Public Good Science Fund

ISSN: 0113-3675

PREFACE

The Building Research Association of New Zealand (BRANZ) commissioned this report as part of its ongoing research into the drying of concrete floors, to develop a top surface-mounted technique for measuring moisture profiles in drying concrete.

ACKNOWLEDGEMENTS

The author wishes to acknowledge the assistance of Dr Malcolm Cunningham of BRANZ; Professor Roger Keey, Department of Chemical and Process Engineering, Dr Vasil Kerdemelidas, Department of Electrical and Electronic Engineering, Dr Colin Hooker and Dr Bob Bennett, Department of Physics, all of the University of Canterbury.

This report is intended for scientific researchers.

A LITERATURE SURVEY OF ELECTRICAL TECHNIQUES FOR MEASURING CONCRETE MOISTURE PROFILES

BRANZ Study Report SR 48

J.W. Lovell-Smith

REFERENCE

Lovell-Smith, J.W. 1994. A literature survey of electrical techniques for measuring concrete moisture profiles. Building Research Association of New Zealand Study Report SR 48. Judgeford, New Zealand.

KEYWORDS

Cement, concrete, curing, digital filters, drying, electric conductivity, electrodes, hydration, inverse methods, measuring instruments, moisture content, measurements, mortar, permeability, permittivity, polarisation, porosity, relative humidity, resistivity, surveys

ABSTRACT

Failure of polyvinyl chloride sheet flooring and other impervious materials on concrete base slabs, due to entrapped moisture, is a recurring problem. However, no clear guidelines exist to aid designers in deciding how long a concrete slab will take to dry out. A literature survey was carried out to determine which of two electrical techniques for measuring moisture profiles in concrete slabs was the most feasible and worthwhile developing for research purposes. The first part of the survey deals with the nature of concrete and hydrating cement paste insofar as it concerns the way water is held and located and is able to move within the matrix. Following a survey of the way in which the moisture condition may be characterised by the dielectric properties, techniques of profile recovery using dielectric (microwave) and resistivity techniques are discussed. It is recommended that the resistivity technique be pursued, as much of the technology exists and need only be modified. Dielectric techniques are less extensively reported in the literature. The ability of a microwave technique to resolve sufficiently deep profiles remains uncertain. Nevertheless effort in developing microwave techniques should proceed so as to capitalise on the complementarity of the two approaches.

CONTENTS

Page

FIGURES **Page**

Page

1.0 INTRODUCTION

Failure of polyvinyl chloride sheet flooring and other impervious materials on concrete base slabs, due to entrapped moisture, is a recurring problem. No clear guidelines exist to aid designers in deciding how long a concrete slab will take to dry out.

"Under most exposure conditions the moisture in concrete is not uniformly distributed and the distribution varies with exposure time...Furthermore the pore structure in which the moisture is held varies with time due to chemical and physical changes in the products of cement hydration" (Parrott 1990, p.1).

Characterisation of the moisture condition of concrete requires determination of a moisture profile. This generally involves drilling to extract core-samples or placing relative humidity probes at selected depths.

The present project is intended to develop a top surface mounted technique for measuring such moisture profiles in concrete. This literature survey was carried out in order to assess the viability of various techniques for research purposes. If a technique is successfully developed, longer term possibilities of commercialising an instrument may be considered.

The ideal technique "should be able to quantify the amounts of free, adsorbed and bound water...and be able to monitor variations of moisture and relative humidity non destructively as a function of time and spatial location" (Parrott 1990, pp.1-2). Parrott identified techniques based on electric properties (specifically microwave and resistive methods) as offering the most promise, although these methods are subject to several confounding influences. Concrete resistivity is sensitive to a number of other factors besides moisture content, including the degree of cement hydration, the initial mix proportions, and temperature. Microwave methods may be restricted because they may not be used to investigate at depths required, with sufficient resolution.

The first part of this report questions how and where moisture is held in cement paste as it cures and dries. Next, consideration is given to moisture mobility and to general transport properties of the paste. In Section 3.0, the origin and nature of dielectric properties are investigated. Experimental studies of these properties are presented, and possibilities for profile recovery from dielectric measurements are outlined. The purely resistive properties of concrete are considered in Section 4.0, preceding an outline of the theory of Geoelectric sounding, discussion of software and factors likely to be important when transferring this technology to concrete floor slabs. This section concludes with a short discussion of some resistivity meters which are commercially available.

2.0 MOISTURE IN CONCRETE

2.1 The Chemistry and Structure of Hydrating Cement Paste

The chemistry of concrete has been described by many authors. In the following sections, major sources include Neville (1981), Czernin (1980), Mindess and Young (1981), and Double (1983).

"Concrete is made by adding water to a mixture of cement, sand (fine aggregate) and coarse aggregate. Hydration takes place between the water and cement, producing a matrix of compounds, which is known as cement paste. This matrix locks together the coarse and fine aggregate particles to form a material with considerable compressive strength. The coarse and fine aggregates are cheap, high-strength fillers and are not normally regarded as active constituents, these being limited to cement and water." (Whittington and Wilson 1986, p. 265).

A concrete mix is normally defined by the mass ratios of constituents:
(a) water cement ratio [w/c]
(b) cement/sand/aggregate ratio
(c) cement/total-aggregate ratio [c/a or a/c]

In the surveyed literature, reference is made both to pure cement pastes and concrete. Brodersen and Nilsson (1992) note that studies have shown that "the cement paste in ordinary concrete occurs in narrow layers (typically about 0.1 mm) between the embedded sand and gravel particles. Results obtained from studying the microstructure of bulk samples of pure paste may therefore be misleading" (p. 407, referring to Diamond, 1987).

The main constituents of unhydrated cement are tricalcium silicate and dicalcium silicate, tricalcium aluminate and tricalcium aluminoferrite . "It is customary in cement chemistry to indicate the individual ...[cement] minerals by the following abbreviated notation:

$CaO = C$
$SiO_2 = S$
$Al_2O_3 = A$
$Fe_2O_3 = F$

Thus the compound $3CaO.SiO_2$ [tricalcium silicate] is referred to as C_3S and $2CaO.SiO_3$ [dicalcium silicate] as C_2S etc." (Czernin 1980, p26). Similarly tricalcium aluminate and tricalcium aluminoferrite are abbreviated to C_3A and C_4F respectively.

The chemical composition of a typical ordinary Portland cement (OPC) is given in Table 1; approximate composition limits of OPC are presented in Table 2.

When water is added to cement a complex series of chemical reactions take place. When tricalcium silicate passes into solution, the aqueous solution is unstable and soon decomposes into hydrated calcium silicate and calcium hydroxide. The calcium silicate hydrate, being insoluble, is precipitated from the solution. Dicalcium silicate reacts in a similar fashion, but more slowly. The calcium silicate hydrates, which are precipitated in gel form on the surface of cement grains, are considered to conform to the following overall formula:

$3CaO.2SiO_2.3H_2O$

which is abbreviated to C-S-H by cement chemists (Czernin 1980).

A summarised scheme of the hydration process taken from Double (1983) is shown in Figure 1. Calcium silicate hydrate is a "colloidal precipitate, which is mainly amorphous and has a rather variable composition. This occupies 60% (by volume) of the hydration products and is therefore the main binding agent in hardened cement. Calcium hydroxide is a by-product of the hydration of the calcium silicates and contributes a further 20% (by volume) approximately. The rest comprises various calcium sulphoaluminate and aluminoferrite hydrates, which are products of the hydration of the aluminate phases and gypsum. Gypsum (ca. 2%) is deliberately added to Portland cement to control the rapid hydration of C_3A, which otherwise tends to produce premature 'flash setting' of the cement. Apart from calcium hydroxide, crystalline products of hydration detectable by X-ray diffraction include ettringite [$3CaO.Al_2O_3.3CaSO_4.32H_2O$]...and calcium monosulphoaluminate [$3CaO.Al_2O_3.$-$CaSO_4$]" (Double, 1983 p. 53).

When water is added, calcium silicate hydrate [C-S-H] is rapidly precipitated on the surface of individual cement grains, forming a spiny protective coating which inhibits the access of water and retards hydration for a time known as the induction period. Osmotic pressure effects, due to the selectively permeable character of the colloidal gel, may be responsible for the rupture of the coating. This leads to accelerated hydration and secondary growth of gel (see Figure 2). "The acceleration period is followed by a gradually decreasing rate of reaction and this is attributed to later infilling and accretion by hydration products. Effectively, as the layers of hydration products thicken by growth around the cement grains and as free water in the microstructure is consumed, longer range diffusional processes dominate and progressively slow down hydration." (ibid p. 59).

Schematic representations of the sequence of hydration of cement are shown in Figure 3, while Figures 4 and 5 show some optical and electron micrographs of hydrating cement pastes.

Most secondary gel forms below the spines. As this secondary hydration layer grows, each cement grain effectively increases in size and the spines of calcium silicate hydrate begin to intermesh, beginning the formation of a solid bond between two cement grains and hence the formation of the solid matrix.

Thus the "structure of cement gel consists of irregular fibres of silicate growing from the surface of the cement grains and bridging the spaces between them....In fully aged cement there is considerable in-filling of the structure by fine-grained silicate-hydrate gel and by growth of crystalline hydration products. [Fine-grained and compact textured structures] are also formed on the inside of the grain coating " (Whittington and Wilson 1986, p. 266).

"Because of its variable composition, C-S-H is not a well-crystallised material; in fact it is very nearly amorphous...As a consequence of [the] very finely divided state of C-S-H, hydrated cement pastes have very high surface areas...most C-S-H preparations...[having] surface areas in the range 250 to 450 m^2/g" (Mindess and Young 1981, pp. 87-88). By contrast unhydrated cement has a specific surface of 0.2 to 0.5 m^2/g (Neville 1981).

Calcium silicate hydrate gel is considered to have a degenerate clay structure in which the layers are crumpled and randomly arranged, so that the spaces between the layers are irregular and vary considerably in size (see Figures 6 and 7).

There are several classification schemes for pores. Spaces having diameters less than 5 nm are called 'gel' pores and are considered to be part of the calcium silicate hydrate structure. In OPC, gel pores account for roughly 28% of the total volume of gel. Those pores in which capillary effects can occur (i.e., a meniscus can form), are called 'capillary' pores. Generally speaking these are the remnants of water-filled space that exists between the partially hydrated cement grains. They have diameters in the range 5 nm to 200 nm (McGlone 1990). Table 3 shows a slightly different classification scheme from Mindess and Young (1981).

As hydration continues, capillary pore volume is replaced by gel and the pore-size distribution shifts toward smaller diameters (Figure 8). Consequently, the "randomly oriented, interconnected pore network ...[developed after the cement paste first sets]... is in a constant state of change as filamentary pores which were continuous through the paste sample, become restricted or even blocked by gel growth. As access to pores becomes blocked, the continuous paths through the hardened cement paste...become more circuitous, hence as hydration continues, the pore tortuosity increases" (McCarter and Garvin 1989, p. 1773).

2.2 Moisture content

2.2.1 Where water is held

There are three main ways in which water is held in cement paste. Firstly, chemically combined water forms part of the hydrated compounds, and interlayer water is held between the clay-like layers of the gel by surface forces. Secondly, as cement paste consists of particles connected over only a small fraction of their total surface, part of the water is within the field of force of the solid phase although external to it, i.e., it is adsorbed. Thirdly there is the pore water contained within gel and capillary pores (see Figure 7).

2.2.2 Porosity

Capillary porosity, (the ratio of capillary pore volume to the total volume of paste or concrete) is largely a function of the initial w/c ratio, since it depends on the spacing of the individual unhydrated grains of cement (see Figures 9 and 10), and may range from 0% to about 40%. Because equilibrium vapour pressure inside pores depends on their size, the larger capillary pores are empty at relative humidities barely less than 100% (Mc Glone, 1990, see Figure 11 showing vapour pressure vs pore diameter). If the relative humidity (RH) falls below about 45%, the capillary pores will empty, at a rate depending also on how segmented they have become (Whittington and Wilson 1986). Gel pores remain full at much lower RH, reflecting their smaller diameters.

2.2.3 Definitions and measurements of water content

Moisture levels are commonly given as a fraction of the total mass or weight (e.g., Woelfl and Lauer 1979, Hashida et al, 1990). The measurement of moisture content by weight is a measure of the evaporable water content. This measure divides water according to whether or not it can be driven off at a certain relative humidity (for example by oven drying at 105 °C for 24 hours as in Berg et al. (1992), or until the weight has become constant as in Woelfl and Lauer 1979). The division between evaporable and non-evaporable water is somewhat arbitrary, since there is a continuum of binding energies between water and a porous material with a continuous range of pore-sizes (see Table 4).

Non-evaporable water, however, can be thought of as containing all chemically combined water and some not held by chemical bonds. "In well hydrated cement, non-evaporable water is about 18% of the mass of the original unhydrated cement...[rising] to about 23% in fully hydrated cement" (Whittington and Wilson 1986).

The most common in-situ moisture measurement is by using relative humidity (RH) probes (see for example Keey 1992 and Wiederhold 1987). Parrott (1980) and Hashida et al. (1990) describe their use with concrete samples.

The relationship between moisture content by weight and RH takes the form of a hysteresis loop (see Figure 12).

> "A very wet solid, on exposure to an atmosphere of fixed relative humidity, will lose moisture until the equilibrium amount in the solid is attained. Further moisture can be removed only by reducing the relative humidity, and a completely dry material can exist solely in a moisture free environment.
>
> "The amount of moisture ultimately retained depends upon whether the equilibrium has been approached by wetting (adsorption) or by drying (desorption). There is a closed loop hysteresis and the desorption isotherm always shows the larger equilibrium moisture content at a reduced vapour pressure" (Keey 1972, p. 23).

Hedenblad and Nilsson (1985) show that the degree of capillary saturation may be a more useful measure of mobile moisture than relative humidity, since capillary saturation takes into account the relative capillary pore space in different samples of concrete. In a slab having a homogeneous RH of 100%, whereas percent moisture content by weight actually decreased from top to bottom, capillary saturation increased, i.e., the pores were more saturated near the bottom. Without knowledge of the pore size distribution, RH may not be a very useful measure.

2.2.4 Moisture content data in the literature

Moisture profiles are reported in Hashida et al. (1990), Parrott (1990,1991) and Hedenblad and Nilsson (1985)(see Figure 13). From his data, Parrott (1990,1991) has derived empirical formulae relating RH at different depths (d in mm) from the surface of a slab in a constant ambient relative humidity (RHa). His 1991 formula is

$$RH = RH_a + (100 - RH_a)e^{(-kT)} \qquad (1)$$

$$\text{where } k = 0.8 - 0.14T + 0.01T^2$$

$$T = \frac{t}{t_{1/2}}$$

$$t = \text{time in days}$$

$$t_{1/2} = 10d, \text{ for } d < 41.4$$

$$= 3d, \text{ for } d \geq 41.4$$

Although this formula may not be very useful in predicting moisture profiles in the field, where ambient RH and temperatures vary widely, it may be used as an indication of expected profiles in controlled conditions. Profiles based on Parrott's formula are given in Figure 14. In the laboratory, RH may be controlled using various saturated salts (see Table 5). It is a feature of Parrott's formula that RH does not depend on w/c content or porosity. Nilsson (1977) and Berg et al. (1992), on the other hand, show that greater porosity is associated with faster drying. In the latter paper for example, evaporation proceeds more than twice as fast from samples with w/c=0.78 than from samples with w/c=0.5. This study used 80 mm cube samples of cement mortar whereas Parrot's samples were larger 100 mm cubes and of concrete.

2.3 Migration of Moisture

2.3.1 Drying

Keey (1972) distinguishes four phases of moisture movement as porous solids dry out (Figure 15). "In the first phase, the moisture flows as liquid under a hydraulic gradient. Initially the pores are full, but gradually air pockets appear to replace the moisture lost. In the second phase, the moisture has withdrawn to the waists of pores, and moisture can migrate either by creeping along the capillary walls or by successive evaporation and condensation between

liquid bridges...[a process] described as liquid-assisted vapour transfer. On further drying, these liquid bridges evaporate entirely leaving only adsorbed moisture behind; moisture moves by unhindered diffusion of vapour. The final stage is one of desorption-adsorption: any moisture that vaporizes is condensed, and the body is in hygrothermal equilibrium with its environment" (Keey 1972, p. 127, see also Figure 16).

It may be convenient, however, to think of the drying of concrete as a two-stage process. During the first stage the concrete is more or less saturated, and the drying rate is determined by the rate of surface evaporation, which itself is strongly influenced by air velocity and the condition of the surface. Once the surface dries out, "there is an abrupt interface between a shallow dry surface layer and a wet internal region. The drying rate is faster near the interface as pores in this region give up their moisture, effectively into the dry surface layer, far easier than the pores deeper down where there are fewer sites for excess moisture to go" (McGlone 1990, p. 4). As drying progresses, the interface moves deeper into the concrete and becomes less sharply defined. Figure 17 illustrates this process. The moisture condition at the interface may be represented by Figure 18, which shows how this two-stage relates to the four-stage process in Figure 16.

2.3.2 Relative humidity gradient

McGlone (1990) shows that the RH gradient (or equivalently, the gradient in the water vapour pressure) is the dominant driving force in the isothermal diffusion of moisture through concrete. He derives a mass transport equation from physical principles thus:

$$\frac{\partial h}{\partial t} = -\frac{1}{S_h}\frac{\partial}{\partial x}(D_h \frac{\partial h}{\partial x}) - (\frac{\partial h}{\partial t})h_{dr} \qquad (2)$$

where S_h is defined as the slope of the sorption isotherm, h is the relative humidity and D_h is a diffusion coefficient which is dependent on material properties, especially the internal (pore) RH, the w/c ratio and the temperature. This coefficient must be determined experimentally. The last term in the equation refers to the removal of water due to the hydration reaction (often termed self-desiccation) and is strongly dependent on the RH in the capillary pores. Hydration can take place only when vapour pressure in the capillaries is sufficiently high, i.e., RH greater than 80%. Hydration at maximum rate can proceed only under conditions of saturation (Neville 1981, pp. 308-309). This is illustrated by Figure 18, in which the water taken up by the cement over 6 months is closely related to the value of $(\partial h/\partial t)h_{dr}$ at different vapour pressures.

However, Hashida et al, (1990) suggest that although RH averages out in a drying concrete slab once it has been sealed, moisture does not redistribute, remaining at higher levels deeper within the slab (see Figures 19 and 20). This is not surprising since relatively little mass transfer is necessary to reach vapour pressure equilibrium but it does call into question the relationship between RH and moisture content. In a sealed slab other influences such as temperature gradients may become more important in shifting moisture than RH gradients. As Roper (1992) points out "the pore structures of most in situ concretes are such as to allow moisture diffusion under conditions of thermal gradients and differential pressures. Water vapour may accumulate and condense at the interface between the concrete and impervious coatings when differential temperature gradients, such that the surroundings are lower than the core, are present through the section" (p. 260).

2.3.3 Permeability

Moisture content and transport do not depend only on porosity. Permeability, the ease with which liquids or gases can travel through a porous material, is also important. The coefficient of permeability, k, is given by Darcy's equation

$$\frac{dq}{dt} = \frac{Ak\Delta h}{L} \qquad (3)$$

where dq/dt is the volume flow rate
A is the cross-sectional area of the sample
Δh is the drop in hydraulic head through the sample
L is the thickness.

Permeability is dependent on the w/c ratio, the a/c ratio, and the degree of hydration insofar as all three factors affect the porosity and the pore size distribution. In general, concretes made with lower w/c ratios, or cured under conditions of higher RH, or cured for longer, have lower permeability's because they have lower porosity's (Figures 21-23, 25). However, the same volume of pore space will result in a lower permeability if the pores are segmented and disconnected, or are on average smaller (Figure 24). "Although the porosity of... cement gel is 28%, its permeability is low ... because of the extremely fine texture of the gel and the very small size of the gel pores. The permeability of a hydrated paste as a whole is greater because of the presence of larger capillary pores, and in fact, permeability is largely a function of capillary porosity" (from Neville and Brooks 1987, p. 263).

Studies of the structure and transport properties in porous materials have resulted in percolation theory, first named in 1957, and now a well established field within general research on fractal structures (Brodersen and Nilsson 1992). Permeability is related to the connectivity or percolation of phases within the microstructure. "A percolating phase forms a three dimensional spanning cluster, while a phase that has not percolated consists of isolated clusters...The set time of a paste, mortar or concrete is determined by the point at which the total solids within the microstructure become connected, forming a rigid backbone that has a non-zero elastic stiffness. As hydration continues, the solid phases (hydration products, unhydrated cement, and mineral admixtures) become highly connected. This connectivity is responsible for the load-bearing capacity of cement-based materials....The transport properties of such materials are determined to a large degree by the amount and connectivity of the capillary porosity within the microstructure " (Bentz and Garboczi 1991 pp.325-326). These authors describe a three-dimensional microstructure simulation model which captures such relevant aspects as the discontinuity of the pore space, diffusivities, and characterisation of the cement-aggregate interfacial zone (see also Ping et al. 1991).

Even if connectivity of capillary pores is very low, moisture may move between capillary pores via inter-connecting gel pores. Permeability may not seem to be a very useful concept, since a relatively impermeable concrete may only impede moisture transport without actually preventing it. Nevertheless, as is shown below, the permeability does influence electrical properties. Thus, it is important that the relationships between permeability, porosity and other properties are clearly delineated.

2.3.4 Carbonation, corrosion and shrinkage

Carbonation occurs when carbon dioxide is absorbed by the hydrated hardened cement paste and reacts with calcium hydroxide

$$Ca(OH)_2 + CO_2 \rightarrow CaCO_3 + H_2O \qquad (4)$$

or with the silicates

$$3CaO.2SiO_2.3H_2O + 3CO_2 \rightarrow 3CaCO_3 + 2SiO_2 + 3H_2O \quad (5)$$

The overall effect is to lower the pH level of concrete.

The normally alkaline cement paste protects reinforcing steel from corrosion through the formation of a very thin oxide layer on the steel surface. Neutralisation of the paste pH 'depassivates' the steel. Corrosion of the steel will take place providing water, oxygen and carbon dioxide all have access.

"Concrete that is saturated with water offers high resistance to penetration of carbon dioxide, because this gas must first dissolve in the pore water before it can make its way by diffusion, at a slow rate, into the concrete" (Czernin 1980 pp. 132-133). At low relative humidities, "the rate of carbonation is restricted as the amount of evaporable water available to dissolve the carbon dioxide diminishes. The rate of carbonation appears to reach a maximum at intermediate relative humidities...[and can lead to corrosion] if the relative humidity at the steel surface is sufficiently high...[The] rate of corrosion rises sharply as the local relative humidity rises above 75%" (Parrott 1991, pp. 51).

The process of carbonation is attended by shrinkage, possibly as a result of the dissolution of 'bulky' crystals of hydrated lime, reincorporated as carbonate with a higher packing density (Czernin 1980, pp. 102). Excessive shrinkage can lead to the formation of micro-cracks. It has been noted that the permeability of concrete is greater than can be accounted for from the actual permeability of the cement paste. The presence of large voids formed by 'bleeding' (uneven sedimentation of the concrete mix before setting takes place) and cracks formed due to shrinkage as the concrete sets and later if carbonation takes place, may radically increase the permeability and porosity of the concrete. "The actual water-tightness of a structure is...largely determined by the flow that can occur through cracks in the concrete, rather than through the concrete itself" (Campbell-Allen 1992, pp. 204-205).

3.0 DIELECTRIC PROPERTIES

3.1 Introduction

When an electric field is applied to a material such as cement paste, some ions and electrons may be free to drift through the material, producing a conduction effect. Other charges, although not free to drift, will be displaced from an equilibrium position. This creates electric dipoles, the formation of which is referred to as polarisation. Macroscopically, the combined effect of the individual dipole moments is represented by the electric polarisation vector $\underline{P}$, defined as the dipole moment per unit volume.

The polarisability of a material is reflected in its dielectric constant ε (also known as the relative permittivity). The permittivity is complex with the real part ε_r' associated with a change in phase of an alternating field. The imaginary part ε_r'', sometimes called the loss factor, is related to the attenuation of the field (see below).

3.2 Polarisation and Permittivity

Theoretical treatment of the permittivity of homogeneous materials may be found in various texts such as Balanis (1989).

In a homogeneous dielectric, there are three possible mechanisms for producing polarisation in response to an external electric field:

1. Dipole or orientational polarisation; the rotation of existing dipoles or polar molecules such as water.
2. Ionic or molecular polarisation; the relative displacement of positive and negative ions.
3. Electronic polarisation; the displacement of electron clouds relative to the atomic nucleus in an applied field.

If a free charge is placed in a material subject to a static electric field, the charge density at that point will decay exponentially as charge migrates to the surface. The time τ_r that it takes for the free charge density to decay to e^{-1} of its initial value, is known as its relaxation time constant which may be shown to be given by $\tau_r = \varepsilon/\sigma$ where ε is the permittivity and σ the conductivity of the material (Balanis 1989, pp. 60-61).

Under the action of an alternating electric field, the polarisation will oscillate and energy may be transferred or 'lost' to the medium. "The occurrence of dielectric loss can generally be understood as follows: at very low frequencies, the polarisation easily follows the alternating field, thus its contribution to the dielectric constant is maximal, and no loss occurs. At very high frequencies the field alternates too fast for polarisation to arise and there is no contribution to the dielectric constant and no energy is lost in the medium. Somewhere between these two extremes, the polarisation begins to lag behind the field and energy is dissipated. The loss factor has a maximum at a frequency f_m related to a characteristic time $\tau = 1/(2\pi f_m)$" (van Beek 1967, p. 72)

Modelling a dielectric as a collection of uncoupled dipoles of charge Q and mass m and concentration N dipoles per unit volume which are free to oscillate in an alternating field of frequency ω, yields for the real part of the relative permittivity

$$\varepsilon_r' = 1 + \frac{\frac{NQ^2}{m}(\omega_0^2 - \omega^2)^2}{(\omega_0^2 - \omega^2)^2 + \left(\frac{\omega d}{m}\right)^2} \qquad (6)$$

and the imaginary part

$$\varepsilon_r'' = \frac{NQ^2}{m} \frac{\frac{\omega d^2}{m}}{(\omega_0^2 - \omega^2)^2 + \left(\frac{\omega d}{m}\right)^2} \tag{7}$$

where $\varepsilon_r = \varepsilon_r' - j\varepsilon_r''$ (8)

and d is a damping factor, s the restoring force constant in this simple model ,

and $\omega_0 = \sqrt{\frac{s}{m}}$ (9)

is the natural undamped resonant frequency.

The real and imaginary parts of equation (8) are plotted as a function of frequency in Figure 25. The imaginary part (loss factor) peaks at the natural damped frequency of the medium. Variations of the permittivity for a typical dielectric are shown in Figure 26, where susceptibility

$$\chi = 1 - \varepsilon \tag{10}$$

For a time harmonic electric field

$$E(t) = E_0 e^{jwt} \tag{11}$$

the displacement current density is given by

$$\underline{J}_D = \frac{\partial D}{\partial t} \tag{12}$$

where the electric flux density

$$\underline{J}_D = j\omega\varepsilon\underline{E} = (\omega\varepsilon'' + j\omega\varepsilon')\underline{E} \tag{13}$$

The total current density of a material in an alternating electric field is given by

$$\begin{aligned}
\underline{J}_D &= \underline{J}_c + \frac{\partial D}{\partial t} \\
&= (\sigma_s + \omega\varepsilon'')\underline{E} + j\omega\varepsilon'\underline{E} \\
&= (\sigma_s + \sigma_a + j\omega\varepsilon')\underline{E} \\
&= (\sigma_e + j\omega\varepsilon')\underline{E} \\
&= j\omega\varepsilon'[1 - j\tan\delta_{e]}]\underline{E} \\
&= j\omega\varepsilon'[1 - (\tan\delta_{s]} + \tan\delta_{a]}]\underline{E}
\end{aligned}$$

where $\underline{J}_c$ = the static field current density

σ_s = the static conductivity

σ_a = the alternating conductivity

σ_e = the effective conductivity $= (\sigma_s + \sigma_a)$

$\tan\delta_{s]}$ = the static electric loss tangent $= \frac{\sigma_s}{\omega\varepsilon'}$

$\tan\delta_a$ = the alternating electric loss tangent $= \frac{\varepsilon''}{\varepsilon'}$

(14)

The Debye (Balanis 1989, von Hippel 1954) equation enables the calculation of the complex relative permittivity for many materials as a function of frequency, provided the real part of the relative permittivity is known at zero frequency (denoted ε'_{rs}) and at very high frequency (denoted $\varepsilon'_{r\infty}$). Thus

$$\varepsilon'_{r\infty} = \varepsilon'_{r\infty} + \frac{\varepsilon'_{rs-}\varepsilon'_{r\infty}}{1+(\omega\tau_e)^2}$$

$$\text{and } \varepsilon^{\cdot}_{r}(\omega) = \frac{\varepsilon'_{rs-}\varepsilon'_{r\infty}}{1+(\omega\tau_e)^2} \qquad (15)$$

where τ_e is a relaxation time constant related to the static field time constant by

$$\tau_e = \frac{\varepsilon'_{rs}-2}{\varepsilon'_{r\infty}+2}\tau_s \qquad (16)$$

3.3 The dielectric behaviour of concrete

3.3.1 Theoretical Considerations

Van Beek (1967) has considered the dielectric behaviour of heterogeneous materials in some detail. In such materials, the build up of charges at the interfaces between two components results in interfacial or Maxwell-Wagner polarisation providing contributions to the permittivity, in addition to those associated with purely homogenous dielectrics (Figure 27).

Beginning with a two-layer system, formulae modelling the permittivity of variously shaped pores or particles dispersed in a medium of different permittivity may be derived. It is possible, given van Beek's formulae, to model the dielectric constant of concrete as a function of moisture content. Treating the cement gel as a system of needles (saturated gel pores) of permittivity ε_w, dispersed in a medium (calcium-silicate-hydrate) of permittivity ε_{CSH} , the gel permittivity ε_g may be obtained. As noted above, the ratio of gel pore volume to total gel volume (gel porosity) is constant at 0.28. Removal of water from gel pores could be modelled by (a) replacing the dielectric constant ε_w by ε_a , the permittivity of moist air, or (b) reducing the volume fraction of saturated gel pores from the minimum value of 0.28.

The range of larger, capillary pores could be treated as a separate problem. For the present purpose, rarely will the gel dry out enough to empty the gel pores. The moisture content of the capillary pores is of direct interest. Early in the curing history capillary pores are well connected. Later, as they become segmented, they may be viewed as a system of dispersed cylinders (of permittivity ε_{cw} when saturated or ε_a when dry) in the gel medium (of permittivity ε_g), thus giving the permittivity of cement paste as a function of capillary porosity (in which case the volume fraction reduces with time) and of water content (in which the permittivity of the dispersed cylinders changes from ε_{cw} to ε_a).

Finally, concrete may be regarded as a system of dispersed spheroids (aggregate) of permittivity ε_{agg} in a medium of permittivity ε_p (cement paste).

3.3.2 Experimental Studies

Several papers describe the electrical characteristics of cement paste and mortar in the first 24 hours after gauging (adding water to unhydrated cement).

Wilson and Whittington (1990) developed a model of the electrical characteristics of concrete over the frequency range of 1-100 MHz. As well as Maxwell-Wagner effects they included viscous conduction effects, which limit the ability of an ion to respond to an alternating electric field above a cutoff frequency, in other words, severely damping ionic polarisation. Measurements of permittivity and conductivity were made on a concrete sample sandwiched between parallel plates. This open-circuited transmission line was connected via coaxial cable to a Hewlett Packard HP444191A RF impedance analyser. The model was moderately successful in describing the frequency response of fresh concrete; however, it is clear that the actual response is far more complex (see Figure 28).

McCarter and Curran (1984,1985) measured the continuous variation in resistivity and permittivity of cement paste, which was setting in a coaxial test-cell, at a frequency of 1 kHz. They note a sudden decrease in resistivity and increase in permittivity, coincident with an increase in ionic concentration with onset of the secondary hydration stage. Much later in the curing history however the paste will be changing less chemically and variations in electrical properties will more likely reflect physical rather than chemical changes (Figure 29).

Moukawa et al. (1991) measured conductivity and permittivity at a microwave frequency (10 GHz), using a long sample in a waveguide with results similar to those of McCarter and Curran' (Figure 30).

In studies of cement pastes and mortar moist cured for 28 and 100 days, McCarter and Garvin (1989) obtained characteristic impedance plots over the 20 Hz-110 MHz frequency range. Lower moisture contents were associated with greater reactance and resistance and the form of the characteristic curve was shifted to higher frequencies (Figure 31).

The studies described above use measurement methods not suitable for non-destructive determination of moisture profiles.

Battilana (1989) in a paper describing electromagnetic screening, discusses three contributions to the attenuation of a signal passing through a reinforced concrete wall. Attenuation due to:

(i) surface reflection

$$M = 20\ln\left[\frac{(\lambda_o + \lambda_1)^2}{4\lambda_o\lambda_1}\right] \qquad (17)$$

(ii) dissipation within the concrete

$$D = \frac{20\pi}{\ln 10}\frac{\lambda_1 t}{\lambda_o^{\,2}}\varepsilon'' \qquad (18)$$

(iii) reinforcing bars

$$B = 10\ln\left(1+\left[\frac{\lambda_1}{2s}\ln\left(\frac{s}{\pi d}\right)\right]^2\right) \qquad (19)$$

where λ_0 and λ_0 are the wavelengths in air and concrete respectively, t is the thickness of the wall, d is the diameter of the reinforcing bars and *s* the spacing between them.

The attenuation can be expressed in terms of the real and imaginary parts of the complex permittivity, however it is not obvious how the permittivity could be recovered from such measurements (Figure 32).

The determination of permittivity and conductivity using open ended waveguides is discussed in Gardiol (1984) and Marsland and Evans (1987) Otto and Chew (1991) describe the use of a large open-ended coaxial probe for measurement of the average complex permittivity of samples with large-grain inhomogeneities, such as rocks and concretes (Figure 33). Depth of penetration of the electromagnetic field depends on frequency and probe diameter.

As Parrott (1990) points out, permittivity measurements at microwave frequencies have the advantage that free water has a high loss factor at microwave frequencies, whilst bound and adsorbed water are effectively seen as solid since they contribute little to permittivity above 8 GHz. Dissolved salts which contribute greatly to conductivity, and hence may be mistaken for a higher water content of lower concentration, have little effect on permittivity above a few GHz. At high frequencies, the trade-off between high resolution but low depth penetration, somewhat weakens these advantages for determination of moisture profiles. An early study by Bhargarva and Lundberg (1972), using rectangular resonant cavities shows that the effective depth of penetration for 0.3 GHz microwaves is 150 mm. This reduced to 60 mm as the frequency increased to 0.8 GHz (Figure 34). Larger open ended coaxial probes may allow greater depth penetration at higher frequencies.

3.4 Profile Recovery from Dielectric Measurements

To recover or "invert" conductivity and/or permittivity profiles, a range of dielectric measurements must be taken as a function of changing angle of incidence or reflection at a set (monochromatic) frequency; or as a function of frequency at a certain angle of incidence; or in the case of pure resistivity measurements, as a function of the distance between probes driving current into the medium.

Papers describing dielectric profile inversion using permittivity measurements are still largely theoretical (see, for example, Ladouceur and Jordan 1985, Habashy et al. 1990, Tijhuis and van der Worm 1984, Tamil and Jordan 1991, and Ge and Chen 1991). Tijhuis (1984) presented a numerical method to compute either the permittivity (or susceptibility) or conductivity profile from the reflected field of an electromagnetic pulse of finite duration. Although his examples of profile recovery are impressive, the ability of the method to handle data noise is not discussed. Whether the short time scales involved in measurements over a thin dielectric slab are resolvable is questionable too.

Sanadiki and Mostafavi (1991) discuss the inversion of inhomogeneous continuously varying dielectric profiles using rectangular open-ended waveguides. The measured data, simulated in their paper, consists of the self-admittance of the waveguide in contact with the dielectric. The resolution of the model depends on the number of layers L, taken to approximate the continuous profile. Self-admittance data must then be taken for at least as many frequencies as layers. It was found that convergence to the correct profile was best achieved by initially assuming a five-layer profile, finding the best fit, and using optimised parameters based on this model as initial guesses (based on simple interpolations) for a six-layer model. Continuing this refinement process, all the fairly simple profiles studied were successfully inverted using no more than thirteen layers (Figure 35). The method appeared to be fairly robust when simple additive Gaussian noise (30 and 40 dB) was introduced, although the number of iterations at each step of the refinement process was considerably increased.

Analytical formulation of the self admittance of an open-ended waveguide radiating into an inhomogeneous dielectric with a continuously varying dielectric permittivity or conductivity does not yet exist in the literature (Sanadiki and Mostafavi 1991). However, that for a rectangular waveguide excited by its dominant mode (TE_{10}) radiating into a stratified dielectric, has been formulated by Galejs (1969).

4.0 RESISTIVITY

4.1 The Resistivity of Cement Paste, Mortar and Concrete

Many studies have focussed on purely resistive properties of cement based materials rather than the broader dielectric properties. In general, the resistivity of porous material decreases with increasing moisture content However, as noted above, resistivity increases with increasing cement hydration and decreasing w/c ratio (see Figures 29 and 36), which may be caused by their effects on capillary porosity and the volume of pore fluid.

When concrete is continuously moist-cured, resistivity rises from around 4 ohm-m at initial set to about 40 ohm-m for w/c=0.6 or up to 80 ohm-m for w/c=0.4 (Hughes et al. 1985). Air-cured concrete samples attain much higher resistivities as the concrete dries out. The effect on porosity of curing in the relatively low RH of the open air is revealed by Woelfl and Lauer (1979), who show that the resistance of an air-cured sample re-immersed in water falls below that of a sample continuously moist-cured (Figures 37 and 38).

4.1.1 Frequency Effects

As noted above, the dielectric constant and hence conductivity is highly frequency dependent. At low frequencies ionic conduction predominates. As the cement paste cures, the rate of change of resistivity can be "regarded as the rate at which water and charges are removed from the aqueous phase (i.e., capillary water) and reflects a combination of grain segmentation and growth of the gel as it extends, constricts and blocks the continuous capillaries within the paste and the fractional volume of free evaporable water within these capillaries" McCarter (1987, p59). At higher frequencies, conductivity will be enhanced by the frequency dependent component of the dielectric constant, which mostly caused by surface conduction effects on the adsorbed gel water. "The difference between high and low frequency dependent measurements will give a qualitative indication of the proportion of current flowing through the gel water and hence give a measure of the gel-space ratio within the paste" (McCarter 1987, p59). The gel-space ratio is defined as the ratio of the volume of hydrated cement to the total volume of hydrated cement plus the capillary pores. This information may useful in distinguishing moisture able to migrate easily through concrete in response to temperature and RH gradients, from that which is fairly strongly held in position within the gel.

Having considered this use of frequency effects in purely resistive measurements, the remainder of this section will be concerned with resistivity at fairly low frequencies (<3 kHz).

4.1.2 Conduction Paths

Whittington et al. (1981) consider three possible conduction paths through concrete: through the aggregate and paste in series, through the aggregate particles in contact with one another, through the paste itself. As typical aggregate resistivities (at around 500-5000 ohm-m) are higher than cement paste by several orders of magnitude, the authors show that more than 90% of the current is conducted through the paste alone, the rest being conducted through the aggregate and paste in series. They conclude that the paste is a controlling factor in the overall resistivity of the concrete and that anything which affects the electrical conductivity of the paste will affect the overall conductivity of the concrete.

Archie's law (Archie, 1942), i.e.,

$$R_o = R_w \varphi^{-m} \qquad (20)$$

was proposed to describe the resistivity, R_o, of consolidated and unconsolidated sandstone filled with water, in terms of the resistivity R_w, of the water in the sandstone, the fractional volume φ of water contained within the rock and a shape or consolidation factor (m).

As concrete consists of particles of many sizes (aggregate) in a cement paste matrix, Whittington et al. (1981) modified Archie's law to describe the resistivity ρ_c of concrete consisting of nonconducting particles of various shapes (shape factor m) and sizes embedded within a matrix (cement paste) of resistivity ρ_m . If the fractional volume of cement paste is φ then

$$\rho_c = \rho_m A \varphi^{-m} \qquad (21)$$

where A=1.04 and m=1.20 for their particular mix.

This formula could be of use when predicting resistivities of concrete of known a/c ratios when the paste resistivity is known. Bear in mind, however, that considering the aggregate to be nonconducting may not always be an appropriate approximation.

As the resistivity of bone-dry cement paste can be up to 10^9 ohm-m (Neville 1981), significant conduction of electricity takes place only via the water content of cement paste. While electronic conduction may take place through cement compounds - i.e., through the gel, gel-water and unreacted cement particles it is accepted that at low frequencies, conduction through moist cement is primarily by means of ions in the evaporable water in the cement paste, the principal ions being Ca^{++}, Na^+, K^+, OH^-, and SO_4^- (Whittington et al. 1981).

It follows that resistivity will be greater in pores small enough to significantly impede ionic travel, hence resistivity will be related to both permeability and the pore size distribution.

These authors state the virtual inseparability of the ionic and electronic conduction effects since the hydrating cement compounds control the concentration and type of ions in the evaporable water; and the water itself in cement paste is fluctuating between evaporable water, adsorbed water, interlayer water and chemically combined water. Nevertheless, investigation of the resistivities of the various conduction paths seems warranted.

The resistivity of the concrete will thus depend on:

(i) the resistivity, porosity and permeability of the aggregate,
(ii) the relative proportions of aggregate, cement and water,
(iii) the size and shape distributions of the aggregate,
(iv) the capillary and gel pore size distributions.
(v) the connectivity of the pores or, more generally, the connectivity or percolation of the phases within the microstructure of the cement paste and
(vi) the relative humidity /moisture content and condition of the pores.

Whereas (i)-(iii) may be predetermined,(iv)-(vi) will be influenced by the initial mix proportions and the curing history. This includes the initial water/cement ratio as well as the subsequent ambient humidity and temperature conditions.

4.1.3 Resistivity versus Moisture Content

Few studies directly relate moisture content and resistivity. Woelfl and Lauer (1979) measured the electrical resistance of moist-cured concrete samples subsequently dried, weighed, and placed in RH-controlled environments. These samples would be expected to have lower moisture content than those left to dry out (from moist curing) in the same RH. A transformation from resistance to resistivity suggests that at 100% RH resistivities are around 200 ohm-m rising to 1400 ohm-m when the samples hold 55% of their maximum water content (Figure 39). On the other hand where data for w/c and a/c ratios from other sources is compared (e.g. Hughes et al. 1985), maximum resistivity at 55% moisture content is about 500 ohm-m. If the same scaling factor is used on Woelfl and Lauer's air-dried specimen resistivities of 5000 ohm-m are reached.

Tashiro et al. (1987) measured the resistivity of hardened cement pastes as a function of curing time, evaporable moisture content w (measured by successive drying and weighing cycles) and cement type. They found that the resistivity could be expressed as

$$\rho = \rho_o e^{c/w} \qquad (22)$$

where c is an intrinsic quantity reflecting the microstructure of capillary pores in the paste (c being the slope of the log(r) vs 1/w plot; see Figure 40). As hydration progresses and the pore size distribution changes, the same high resistivities are obtained with higher evaporable moisture content, suggesting that conduction pathways are becoming restricted.

Berg et al. (1992) report a detailed study of the dielectric properties of cement mortar as a function of water content. They describe the bulk dielectric response of the mortar by an equivalent circuit consisting of a resistance in parallel with a constant phase element (CPE). The resistive element represents the dc (direct current) conductance of the sample. Defining the relative water content p as the volume fraction of evaporable water in the sample divided by its initial volume fraction, the conductance can be described as a power law of p, above a threshold value pc (see Figure 41). This conductance threshold is analogous to the percolation threshold which occurs in random networks, that is, the sharp decrease in conductivity occurs when continuous paths of water through the sample begin to break up. "An estimate based on the measured internal surface area of cement paste shows that the conductance threshold occurs at roughly the value of p expected for monolayer coverage of the pore walls with evaporable water" (Berg et al 1992, p. 5900).

For w/c ratios between 0.5 and 0.78, the conductivity G is proportional to $(p-pc)^t$ with $pc=0.05 \pm 0.003$ and $t=2.7 \pm 0.15$ The power law roughly agrees with the exponential relationship of Tashiro et al. (1987).

We have seen that current is mainly carried by the evaporable water. Low resistivity basically indicates the presence of water. Conductivity is enhanced by dissolved salts and the presence of continuous pore pathways through the concrete. A lower w/c content with optimal moist curing conditions will minimise the pore volume and increase the tortuosity. The presence of full pores will be hidden in measurement by the lack of complete low resistance paths.

A porous concrete with nearly empty pores may be indistinguishable from a relatively saturated but impermeable concrete, giving identical resistivity readings. The volume of water able to cause problems with concrete floor coverings may or may not be equal in the two cases. In practice, this means that resistivity measurements may be sensitive to the permeability and degree of saturation of concrete but insensitive to the porosity of the concrete itself.

4.2 Profile Recovery from Resistivity Measurements

4.2.1 Introduction

Recovery of resistivity profiles from measurements of apparent resistivity at the surface, has been extensively studied and practised in geophysics (see for example Parasnis 1982). Of the variety of two- and four-probe arrays in use (see Figure 42), the Schlumberger and Wenner arrays seem most appropriate when transferring the technology to concrete resistivity sounding. Various dipole-dipole arrays have advantages in geoelectric sounding where the terrain is uneven or inaccessible. These are irrelevant, however, for the present purpose which is concerned with planar surfaces.

Roy and Apparao (1971) show that the Schlumberger array has greater depth penetration than the Wenner array for a given current probe spacing, so that an instrument based on this array may be shorter. On the other hand, the Wenner array apparently gives greater vertical resolution. It would not be difficult, in the long term, to electronically sample a multi-probe array to enable both Wenner and Schlumberger readings.

For the full development of the theory of vertical electric sounding (VES), the reader is referred to Koefoed (1979). A less extensive treatment may be found in Parasnis (1982) which is a general text on geophysical prospecting. A brief outline of the theory follows. Flow charts giving more detail may be found in the appendices.

4.2.2 Apparent Resistivity

If current I, is injected into a homogeneous, semiinfinite slab of resistivity ρ , the potential V at a distance r, is given by

$$V(r) = \frac{I\rho}{2\pi r} \tag{23}$$

In practice, two current electrodes are used - a positive electrode 'A', and a negative electrode 'B' - giving a potential of

$$V(r) = \frac{I\rho}{2\pi}\left(\frac{1}{r} - \frac{1}{r'}\right) \tag{24}$$

should $V \rightarrow 0$ as $r \rightarrow \infty$ (see Appendix 1).

The resistivity determined by an ideal Schlumberger array (see Appendix 1) is given by

$$\rho_s = \frac{\pi s^2}{I}\left|\frac{dV}{dx}\right| \tag{25}$$

In practice the potential gradient dV/dx is found by measuring the potential difference between two electrodes, M and N, a distance 2b apart. That is

$$\frac{dV}{dx} \approx \frac{\Delta V}{2b} \tag{26}$$

where the distance 2b is much less than the current electrode separation 2s. The measured resistivity then becomes

$$\rho = \frac{\pi s^2}{2b}\left|\frac{\Delta V}{I}\right| \tag{27}$$

In general, the potential difference between two probes 'M' and 'N' at the surface, is given by

$$\Delta V = \frac{I\rho G}{2\pi} \tag{28}$$

That is, the resistivity of the homogeneous slab is determined to be

$$\rho = \frac{2\pi\Delta V}{IG} \tag{29}$$

where $$G = \frac{1}{AM} - \frac{1}{BM} - \frac{1}{AN} + \frac{1}{BN} \tag{30}$$

For the Wenner array, G=1/a, so that

$$\rho = 2\pi a \frac{\Delta V}{I} \tag{31}$$

If the slab is not homogeneous, but horizontally stratified (see Appendix 2), the potential, V, at a point, r, from a current, I, injected at a point may be shown to be

$$V(r) = \frac{I}{2\pi} \int_0^\infty T(\lambda) J_o(\lambda r) \partial\lambda \tag{32}$$

where $T(\lambda)$ is known as the Resistivity Transform, which is a function of all the layer resistivities and thicknesses, λ is a variable of integration, and $J_o(\lambda r)$ is the zeroth order Bessel function of the first kind.

The transform $T(\lambda)$ may be calculated from the layer parameters using simple recurrence relations (see Appendix 2). The reverse process of using recurrence relations to recover the profile from the transform is less straight forward. A brief description of this process, using a modified transform function, is given in Section 4.3.1 on Direct Methods.

Substituting equation (32) into equation (25) gives the 'apparent resistivity' ρ_a for the Schlumberger array on a horizontally stratified slab. That is

$$\rho_a(s) = s^2 \int_0^\infty T(\lambda) J_1(\lambda r) \lambda \partial\lambda \tag{33}$$

Hankel's inversion (Arfken, 1985) may be applied to this equation to give an expression for the resistivity transform in terms of the apparent resistivity (see Appendix 3)

$$T(\lambda) = \int_0^\infty \rho_a(s) J_1(\lambda s) / s \partial s \tag{34}$$

Vertical electric sounding (VES) involves determination of the apparent resistivity at a range of spacings. In the analysis in following sections the terms VES curve and apparent resistivity curve are used synonomously.

4.2.3 Digital Linear Filters - Ghosh's Filters

In order to recover the layer parameters (i.e., of the resistivity profile within the slab), it is necessary to calculate ρ_a from $T(\lambda)$ and/or calculate $T(\lambda)$ from ρ_a . However, ρ_a and $T(\lambda)$ are not readily evaluated using equations (33) and (34) respectively. Instead, a linear digital filter is normally used. O'Neill and Merrick (1984) give a good overview of filter design. The following summary is based on this paper, which closely follows the original paper by Ghosh (1971) who first introduced the practical method to Geophysics.

Appendix 3 shows how the filter is determined. Defining λ and s in terms of new variables x and y

$$s = e^{x} \quad \text{and} \quad \lambda = e^{-y} \tag{35}$$

the convolution integral

$$T(y) = \int_0^\infty \rho_a(x) J_1[e^{(x-y)}]dx \tag{36}$$

is obtained, which in the frequency domain becomes

$$F(f) = G(f) \cdot H(f) \tag{37}$$

where $T(y) \leftrightarrow F(f)$ and $\rho(a) \leftrightarrow G(f)$ are Fourier transform pairs, and $H(f)$ is the resistivity filter characteristic.

To determine $H(f)$, a partial apparent resistivity curve $\Delta\rho_a(x)$ is chosen whose exact resistivity transform $\Delta T(y)$ is known. Thus, from the transform pairs

$$\Delta\rho_a(x) \leftrightarrow \Delta G(f) \quad \text{and} \quad \Delta T(y) \leftrightarrow \Delta F(f) \tag{38}$$

the filter characteristic

$$H(f) = \frac{\Delta F(f)}{\Delta G(f)} \tag{39}$$

is obtained.

The filter characteristic is digitised by subjecting it to a sinc function input, the frequency spectrum of which is a block function of height Δx and width / Δx. Δx is the largest constant sampling interval, above which, accurate reconstruction of a function from its sample values cannot be achieved. Thus

$$\begin{array}{c}\text{the spectrum of} \\ \text{sinc response}\end{array} = \begin{array}{c}\text{the sinc} \\ \text{response}\end{array} \text{X} \begin{array}{c}\text{the filter} \\ \text{characteristic}\end{array}$$

$$= \begin{cases} \Delta x \cdot H & f \le \dfrac{1}{2\ \Delta x} \\ 0 & f < \dfrac{1}{2\ \Delta x} \end{cases} \tag{40}$$

$\frac{1}{2\ \Delta x}$ is known as the Nyquist Frequency.

The inverse Fourier transformation of the resulting sinc response spectrum gives the sinc response of the filter, sampled values of which constitute the required digital filter.

Hence, in the space domain, the discrete equivalent of equation (36) may be written

$$T_m = \sum_i a_i R_{m-i} \tag{41}$$

where a_i is called the i th forward filter coefficient and R_{m-i} is the m-i th sampled resistivity from the apparent resistivity curve (see Appendix 4).

To calculate the apparent resistivity from the resistivity transform we note

$$G(f) = \frac{F(f)}{H(f)} \qquad (42)$$

The inverse filter sinc response is then obtained as in the forward case, replacing (Hf) by its inverse. The digital values of apparent resistivity are then given by

$$R_m = \sum_j b_j T_{m-j} \qquad (43)$$

$$m = 0, 1. 2...$$

where b_j is the inverse filter coefficient (44)

T_{m-j} is the sampled resistivity transform

4.2.4 Guptasarma's Filters

The accuracy of Ghosh's filter is unacceptable for resistivity curves that have steep descending branches such as are likely to be found in drying concrete slabs exposed to low ambient relative humidities. His method, however, has been used and improved by many, including Koefoed (1972), Das and Ghosh (1974), Anderson (1975) and O'Neill (1975). Guptasarma (1982) published seven-, eleven-, and nineteen-point filters which are substantially more accurate than existing equivalent filters.

The filters are used in a slightly different way from Ghosh-type filters, compromising computational time for accuracy. Apparent resistive curves calculated for steeply descending and then ascending profiles are shown in Figure 43. While both filters have difficulty responding to this extreme profile (the sudden drop in resistivity being due to a reinforcing bar perhaps) the seven-point Guptasarma filter responds more faithfully than the Ghosh type. Clearly, the filter must be appropriate to the of profile.

The use of the two types of filters is shown in Appendix 5. With Ghosh-type filters, values of λ used to calculate $T(\lambda)$ from the layer parameters must be chosen to be logarithmically spaced at a rate of three data points per decade, although later Ghosh type filters generally use more. Once the resistivity transform is found at each value of λ, it is convolved with the digital filter to obtain the apparent resistivity ρ_a.

Guptasarma's seven-point filter, for example, requires, at each chosen spacing, a reduced range of λ given by

$$\lambda_r = \frac{10^{a_r}}{s} \qquad (45)$$

where a_r is the rth abscissa corresponding to the filter coefficient φ_r, r = 1,2,..7

$T(\lambda_r)$ is then calculated for each value of λ_r. The apparent resistivity at the particular spacing is found by convolving the coefficients against the reduced $T(\lambda_r)$, thus:

$$\rho_a(s) = \sum_{r=1}^{7} \varphi_r T(\lambda_r, s) \qquad (46)$$

The seven-point Guptasarma filter requires roughly seven times as much computational time as a Ghosh type filter, since the relatively lengthy recursive generation of $T(\lambda)$ from layer parameters must be carried out seven times for each spacing value, compared with only once per spacing using a Ghosh filter.

4.3 Profile Recovery Methods

Many ways of automatic recovery of resistivity profiles from VES curves have been developed. Two broad groups, indirect and direct methods are outlined in Appendix 6.

4.3.1 Direct Methods

Direct methods are suggested and/or used by Ghosh (1971), Depperman (1973), Marsden (1973), Patella (1975), Koefoed (1972), Szaraniec (1980) and Basokur (1990). Slichter (1933) first pointed to the possibility of direct interpretation of VES data, by fitting the transform curve to families of two- and three-layer resistivity transform templates. Pekeris (1940) introduced a modified kernel function G(s), the logarithm of which has the important propert of being a linear function of λ. The slope of the function is controlled by the top layer thickness whereas its intercept with the ordinate axis G is controlled by the ratio of the resistivities of the top two layers.

Once the modified resistivity transform is calculated in some way (which was not easy before the introduction of the linear filter method) an alternation of two steps followed. In the first step, the first part of the transform curve (i.e., for small s) is approximated by a straight line from which the resistivities of the first two layers and the thickness of the first layer can be derived. The second step is what is known as "the reduction of the transform function to a lower boundary plane" (e.g., Koefoed 1976) in which the contribution to the transform curve made by the top layer is stripped away using a simple reduction formula. The effective boundary plane (i.e., the earth-air interface) is now the top of the second layer. The two steps are iterated until a reduced transform curve is obtained that completely represents the linear function for the bottom two layers (Koefoed 1976, Parasnis 1982).

Basokur (1990) published a program for the direct interpretation of VES curves written in Basic, which has been transcribed into Microsoft QuickBasic by the author. This has been rather disappointing in its requirement for the user to determine the branch points from the resistivity transform curve (i.e., those points indicating existence of separate layers). Modifications may increase the automaticity and the user-friendliness of the interpretation; however, it may not be worthwhile proceeding in this direction. Direct interpretation methods suffer from error growth and propagation at each iteration. Error in determining layer parameters at the first iteration is carried into the next iteration which may, in addition, generate its own error. There is, in fact, guaranteed initial uncertainty in generation of the transform function, since forward filters require extrapolation of the VES curve. Finally, there is no obvious way to optimise the solution using direct methods; rather, as in Marsden (1973), a direct method may be used to generate the initial model for use in an indirect methods.

4.3.2 Indirect Methods

Indirect methods require the initial input of a trial model. From this, the resistivity transform is calculated using recurrence relations (Appendix 2). Then, an inverse linear filter is digitally convolved with the transform to obtain a trial apparent resistivity curve. This is compared with the actual VES curve. On the basis of this fit, layer parameters of the trial model may be adjusted or accepted. This process of optimisation may be automatic or user input may be requested. The new or modified trial model is used to generate a new trial apparent resistivity curve and the process continues until some pre-defined cutoff is reached.

One step per cycle is saved if comparisons are made in the resistivity transform domain (see Appendix 6). In this case a forward filter is used. However, as noted above, use of the forward filter requires extrapolation of the apparent resistivity curve at each end of the spacing range, thus using data that are not actually measured. It is also necessary to smooth the data. Both operations introduce sources of error. When comparing in the apparent resistivity domain, the unprocessed data are used for comparison purposes only and the influence of the user's personal judgement is kept to a minimum (Johansen, 1975, Merrick, 1977). Working in the apparent resistivity domain thus allows the fullest interpretation of incomplete sounding curves since no information is lost or distorted through extrapolation.

4.4 Two Indirect Methods of Profile Recovery

Once appropriately fast and accurate inverse filters are chosen, the key problem in indirect profile recovery is optimising the fit between the calculated and the actual apparent resistivity curves. Two papers proposing entirely different indirect methods look particularly promising.

4.4.1 Merrick (1977, see algorithm, Appendix 7)

Given a set of m of apparent resistivity data $\underline{\rho}^*_{a_i}$

which are due to an *n*-layer earth characterised by thicknesses

$$\underline{h}^* = (h_j^*); \quad j = 1,2,\ldots n - \tag{47}$$

and resistivities

$$\underline{\rho}^* = (\rho_k^*); \quad k = 1,2,\ldots n \tag{48}$$

which are combined into a single vector

$$\underline{P}^* = (P_j^*) = (h_1^*, h_2^* \ldots h_{n-1}^*; \rho_n^*, \rho_{n+1}^* \cdots \rho_{2n-1}^*) \tag{49}$$

A trial model $\underline{P}$ will give the trial apparent resistivity ρ_{a_i}.

Comparing data through their logarithms in order to reduce the bias toward high apparent resistivities, the sum of squares

$$\Phi = \sum_{i=1}^{m} \{\log(\rho_{a_i}^*) - \log(\rho_{a_i})\}^2 = \sum_{i=1}^{m} \{R^* - R\}^2 \tag{50}$$

is a suitable measure of the goodness of fit.

Writing $\Delta\underline{P} = \underline{P}^* - \underline{P}$ and $\Delta\underline{R} = \underline{R}^* - \underline{R}$ the problem of minimising Φ may be linearised by defining a matrix $\underline{\underline{A}}$ which maps the parameter correction vector $\Delta\underline{P}$ into the vector of data deviations $\Delta\underline{R}$. That is

$$\underline{\underline{A}}\,\Delta\underline{P} = \Delta\underline{R} \tag{51}$$

This process is equivalent to linearising the apparent resistivity function by a Taylor series expansion about a trial model

$$R_i(\underline{P} + \Delta\underline{P}) = R_i(\underline{P}) + \sum_{j=1}^{2n-1} \left(\frac{\partial R_i}{\partial P_j}\right)\Delta\underline{P}_j \qquad (52)$$

provided that the elements a_{ij} of the matrix $\underline{\underline{A}}$, are defined to be normalised apparent resistivity derivatives with respect to each model parameter

$$a_{ij} = \frac{\partial R_i}{\partial P_j} = \frac{1}{\rho_{a_i}} \frac{\partial \rho_{a_i}}{\partial P_j} \qquad (53)$$

The derivatives are found by convolving a digital filter {b(k)} with transform derivatives

$$\frac{\partial \rho_{a_i}}{\partial P_j} = \sum_k b(k) \frac{\partial T_{i-k}}{\partial P_j} \qquad (54)$$

defined recursively (Johansen 1975).

Because apparent resistivity is a non-linear function of the model parameters, there is no exact inverse $\underline{\underline{A}}^{-1}$ giving $\Delta\underline{P}$ when $\Delta\underline{R}$ is known. However, a generalised inverse $\underline{\underline{A}}^{+}$ may be found such that

$$\Delta\underline{P} = \underline{\underline{A}}^{+}\Delta\underline{R} \qquad (55)$$

in a least squares sense. $\underline{\underline{A}}^{+}$ may be found by singular value decomposition or approximated by the Marquardt method (Marquardt 1963) or using the pseudoinverse (pinv.m) function in Matlab.

A program based on Merrick's method has been developed by the former DSIR Geology and Geophysics Groundwater Division, reported in Broadbent and Callander (1991). This method seems to promise speed and accuracy.

4.4.2 Zohdy (1989)

Zohdy (1989) notes the following properties of Wenner and Schlumberger sounding curves:

(a) Computed apparent resistivities are always positive
(b) The form of a sounding curve follows the form of the true resistivity-depth curve.
(c) A sounding curve is always "out of phase" with the resistivity-depth curve and is always shifted to the right of the resistivity-depth curve.
(d) The amplitude of a sounding curve is always less than or equal to that of the true resistivity-depth curve, and,
(e) Changing the true resistivity of a thick layer changes the apparent resistivity along a corresponding segment of the sounding curve.

Assuming then, that the VES curve is related fairly directly in form to the resistivity profile, Zohdy notes that the problem becomes one of how to shift the VES curve more "in phase" with the actual layering, and how to scale the apparent resistivities to the actual resistivities (see Figure 44).

An outline of the method is given in Appendix 8, showing the two main iterative loops. The depth-shifting loop is entered by taking the actual VES curve as the initial trial model, by setting model depths equal to the spacings and setting trial layer resistivities equal to the apparent resistivities. The resistivity transform is calculated and then the trial apparent resistivity curve which is compared with the actual VES curve and the RMS difference recorded. By multiplication by a shift factor (e.g., 0.9) the trial depths are shifted to the left, and the cycle repeated. The RMS should normally be smaller (final shift-factors appear to lie in the

range 0.4 - 0.6 for Schlumberger readings). The cycle is repeated until the RMS reaches a minimum or other cutoff. The apparent resistivity curve from the best-fit trial model from this cycle is used as input to the resistivity-scaling loop.

On the basis of point (e) above, each trial layer resistivity is scaled up or down by multiplying it by the actual apparent resistivity divided by the trial apparent resistivity. The cycle is repeated until again an RMS minimum or some other cutoff point is reached.

Although sharing the advantages of indirect methods generally, this method provides some ability to cope with noisy or anomalous data. As the best fitting trial apparent-resistivity-curve represents a smoothing of the actual VES curve, it may be used as the initial input to another round of interpretation, although, as Zohdy shows, this does not always work well.

As the VES curve is used as the initial model, when a Ghosh-type filter is used, the spacings must be logarithmically separated as noted above. If the data points were not measured at appropriate spacings, the VES curve must be interpolated at logarithmic intervals. This can represent a loss of information since the logarithmic end points may be some distance within the spacing range. Guptasarma's filter can thus be an advantage here as it does not require logarithmic spacing.

The method described above produces a nearly continuous profile with step-sizes controlled by the scaled spacing. In earlier papers, Zohdy (1974, 1975) demonstrated how to obtain information on discrete layers using, what he terms, a "modified Dar Zarrouk" curve. This, however, is likely to be unnecessary here. Apart from the presence of reinforcing steel, where the resistivity will effectively plunge to zero, (masking any deeper layering), one would expect moisture and resistivity profiles in concrete to be continuous. The method described above would seem to be ideally suited for the measurement of resistivity profiles, and hence moisture profiles in concrete slabs.

4.5 Commercial Software

Although custom-written software is necessary to suit the particular requirements of resistive modelling of concrete slabs as opposed those of natural terrain, it may be useful to investigate commercially available software.

There is at least one commercial program based on Zohdy's method. This is EMDRIP see Appendix 9. Another program "GEOL" (Appendix 10) reported by Tselentis and Delis (1991), appears to follow Zohdy's methods, but may incorporate other interpretation schemes. A demonstration copy of ResiX-Plus by Emix (Appendix 11), appears to use methods more related to Merrick's than to Zohdy's, and includes various features such as equivalence analysis and interactive, graphically based, modelling. The main drawback of this program is its limitation to 6 layers.

4.6 Application to Concrete Resistivity Sounding

A number of factors must be considered when applying VES technology to resistivity profile recovery from concrete slabs.

4.6.1 Electrode Spacing and Aggregate Size

Figure 45 shows the effect of probe spacing on the scatter of resistivity measurements due to resistive inhomogeneity of concrete brought about by the highly resistive aggregate. When the spacings between electrodes are the order of, or smaller than, the maximum aggregate size, apparent resistivity readings exhibit considerable scatter. is is because the probes are close

enough for the larger pieces of aggregate to begin to be resolved. This unwanted noise in the data may be reduced considerably by averaging over a large number of measurements at slightly different locations. In Millard's 1991 study, even after averaging over 20 readings, the scatter when the distance between the current probes equalled the maximum aggregate size, had a standard deviation of about 10%. This reduced to about 5% when the spacing was doubled. In the present study, the concrete specifications indicate a maximum particle size of 19 mm. If minimum spacings are about 40 mm for 5% standard deviation, Zohdy's shift factor of 0.5 above, suggests that the accuracy of profile recovery for depths less than 20 mm, will be poor.

4.6.2 Electrode Contact Area

It is clear from Figure 46, that "the four-point method is very insensitive to the electrode contact area: diameters from as small as 1 mm up to 40 mm for an electrode spacing of 50 mm caused less than a 6% variation in the measurements" (Millard 1991, p. 77). Although a large contact area will reduce probe-concrete interface resistance, the area must be small enough to maintain the approximation to the ideal array of four points.

4.6.3 Finite Distance Between Potential Probes

The derivation of equation (27) above, required the approximation

$$\frac{dV}{dx} = \frac{\Delta V}{2b} \qquad (56)$$

to be made. It is sometimes stated (without proof) that the requirement that $b<<s$, is satisfied by $b<s/5$ (Bibby and Fisk, 1988). It is often necessary, however, to use larger potential probe spacings to increase sensitivity, and Bibby and Fisk derive a correction factor

$$F = \frac{1}{6}\left[\frac{\partial^2 \ln \rho_s}{\partial \ln s^2} + \left(\frac{\partial \ln \rho_s}{\partial \ln s}\right)^2 - 5\frac{\partial \ln \rho_s}{\partial \ln s}\right] \qquad (57)$$

such that the ideal Schlumberger apparent resistivity (where $b \rightarrow 0$) is given in terms of the measured apparent resistivity

$$\rho_s(s) = \frac{\rho_a(s,b)}{[1+(\frac{b}{s})^2 F + O(\frac{b}{s})^4]} \qquad (58)$$

They show that for VES curves with steeply descending branches (where the apparent resistivity drops away sharply with depth) the correction factor may be as high as 17% for b/L = 0.2 (Figure 47). Drying concrete may be expected to have resistivity profiles of this type. Although the correction factor uses derivatives of the ideal Schumberger sounding curve, in practice, derivatives of the smoothed field sounding curve may be used since it can be shown that

$$\frac{\partial \ln \rho_a(s,b)}{\partial \ln s} = \frac{\partial \ln \rho_s}{\partial \ln s}[1+O(\frac{b}{s})^2] \qquad (59)$$

and

$$\frac{\partial^2 \ln \rho_a(s,b)}{\partial \ln s^2} = \frac{\partial^2 \ln \rho_s}{\partial \ln s^2}[1+O(\frac{b}{s})^2] \qquad (60)$$

The correction factor would be used as follows. A profile recovery program would be run using the raw VES curve and the correction factor would then be calculated using the best-fit trial apparent resistivity curve. The program would be run again using the best trial model from the first run as the initial trial model: and the corrected curve used in place of the VES curve.

4.6.4 Effect of Reinforcing

The presence of highly conductive layers such as reinforcing rods or mesh, will tend to prevent recovery of the deeper profile. To minimise the effect of reinforcing bars, their location must be identified (e.g., by using a magnetic 'covermeter', Webb 1990) and soundings taken in a line midway between and parallel to the bars. This may enable some deeper profile recovery. A reinforcing mesh, however, cannot be so treated. Bars crossing at right angles to the array are "lateral inhomogeneities" which, at mesh sizes standard in concrete floors, are too closely spaced, to correct for by any methods used in Geophysics. The mesh must be treated as a highly conductive layer by averaging over a range of measurements, covering several grid spacings. Some possible profiles, theoretical VES curves and recovered profiles are shown in Figure 48. In general, wider spacings are required for the recovery of profiles below more highly conductive layers.

4.6.5 Edge Effects

In general, concrete floors are large enough to be considered infinite in lateral extent if the array is located appropriately. For deep soundings, or where the surface has been wet and relatively conductive, larger array spacings may be necessary, so, proximity to edges may affect measurements.

Millard (1991) found that locating a Wenner array perpendicular to an edge caused little variation in apparent resistivity. The error caused by one electrode making contact at the end of a section was found to be less than 10%. An array parallel to an edge had an error of less than 10% only when the array was more than twice the electrode spacing from the edge (Figure 49).

Correction factors for such boundary effects have been derived by Valdez (1954), in a paper introducing the Wenner array as a means of resistivity measurements of semiconductors. His work suggests that the true apparent resistivity for perpendicular contact is about 0.7 of that measured. Apparent resistivity measured by an array twice the spacing from a parallel boundary must be multiplied by 0.96 (Figure 51).

4.7 Commercial Instruments for the Measurement of Apparent Resistivity

Several resistivity meters are on the market:

CMT (Instruments) SCRIBE Digital Resistivity Array Meter has two probes requiring pre-drilled holes (to 8 mm depth) and conducting gel (Swarfega). However Millard (1991) notes that more accuracy is obtained using four probes .

The Colebrand Resistivity Logger uses a four-probe Wenner array of hollow spring-loaded probes filled with a conducting gel to maintain good electrical contact with the concrete surface (Appendix 13).

The C.N.S. Electronics Ltd Resistivity meter (Appendix 12), also uses a Wenner array, but with adjustable spacing and dry probes. The resistance of the probe-concrete interface may vary greatly from probe to probe. Variation of the current-probe interfaces will affect the current greatly, requiring a low current warning circuit. Variation of the voltage-probe

interfaces will result in variation of the common-mode voltage. A common-mode rejection ratio of at least 110 dB is necessary. The C.N.S. meter probably uses circuitry based on U.K. Patent Application 2156084A (Ewins 1985). The principles are described by Ewins (1990).

Note: The analysis in previous sections, has presumed direct current (dc). In practice, to avoid polarisation effects, use is made of fairly low-frequency square waves (26 Hz -2 kHz) which are sampled in both negative and positive dc sections.

Resistivity measurements are used in industry mainly for corrosion assessment. Low resistivity readings indicate high permeability and hence potential for, or existence of, corrosion of reinforcement. It is worth noting that the existence of an instrument able to take resistivity profiles can only enhance the determination of corrosion potential.

5.0 DISCUSSION

A useful measure of concrete moisture content is the evaporable water content, which is held within the capillary pores and more tightly in gel pores. As hydration progresses, the total pore volume reduces and the pore size distribution shifts in favour of smaller diameters. This results in a lower, and generally more tightly held, volume of water. Relative humidity probes provide another useful view of the moisture state within concrete. Formulae have been empirically derived to determine relative humidity profiles as a function of time, ambient relative humidity and concrete type. The relationship between relative humidity and the evaporable water content may be represented by an adsorption/desorption hysteresis curve.

Although four phases of moisture movement through a porous solid are recognised, the drying of concrete may be seen as a two-stage process in which moisture near the drying surface moves to the surface through vapour diffusion. Deeper below the surface, pores are mostly full and water flows as liquid, the wet-dry interface moving more deeply as drying progresses. Diffusion is driven by the RH gradient and may be described by a mass transport equation using empirically determined sorption curves.

However, sorption curves are normally generated using samples progressively dried and weighed or placed in environments of fixed RH. It is not clear how valid such curves are for use with concrete slabs. In the only study specifically measuring both RH and evaporable water in samples with moisture gradients, Hashida et al. (1990) found that the relationship broke down once the drying face had been sealed.

As hydration proceeds, the reduction in pore-size and the accompanying increasing segmentation of capillary pores have major effects on the dielectric properties of concrete. Many papers describe how these properties, which are also a function of the frequency of the exciting field, vary with time and concrete type. A relationship between moisture condition and complex permittivity can be derived, on the basis of van Beek's (1967) work, once certain assumptions about pore size and shape and about the permittivity of the pore fluid are made. Berg et al (1992), have attempted to derive the relationship using fractal geometry and percolation theory, a work incomplete to date. Whether such relationships can be determined and validated is not crucial to the problem of recovering moisture profiles using dielectric properties. This is because simple calibration curves could be empirically determined for various concrete types and conditions.

Given the relationship between moisture condition and electrical properties, a decision must be made as to which measuring technique can best recover an electrical profile. The work of Sandaniki and Motafavi (1991) and Otto and Chew (1991) suggest the possibility of dielectric profile recovery, using a frequency sweep in the microwave range and a large open-ended waveguide. Questions still remain regarding the trade-off between the depth of view and resolution.

Much work has gone into investigating the purely resistive properties of concrete. Using a modified Archie's law, the resistivity of cement paste could be determined from the concrete resistivity. The dc resistivity reflects the conduction of ions through the pore fluid, higher resistivity being associated with hindered passage through the smaller gel pores when capillaries are empty. Berg et al (1992) and Tashiro et al. (1987) present empirically derived formulae specifically relating evaporable moisture content to resistivity.

The theory of Vertical Electric Sounding from Geophysics, and the associated software, seem readily adaptable for use with resistivity profiles in concrete. Work on this is proceeding, as is the adaptation of existing designs of meters developed to measure apparent resistivity. Although there are difficulties such as the masking effect of reinforcement and measurement scatter caused by larger pieces of aggregate, resistivity profiling using a Schlumberger array seems quite feasible and should be able to be quickly implemented. An instrument based on

this technique will have value in research into the changing moisture condition of concrete floor slabs. A commercialised instrument would still have application in three dimensional mapping of steel reinforcement corrosion potential, even if use in moisture profiling was not realisable.

6.0 CONCLUSION

This report concludes that the moisture condition of a concrete slab may be characterised by a vertical profile of the evaporable water content. Various studies suggest that the evaporable water content of concrete may be expressed as a function of its electrical properties. Recovery of dielectric profiles using a surface mounted microwave instrument seems quite feasible, although it is not possible yet to determine its ability to resolve profiles deep within a concrete slab. It is the opinion of the author that investigations should continue into the use of this technique. However the main effort in this project should be directed toward the development of resistivity sounding techniques, given the advanced state of the science of Vertical Electric Sounding in Geophysics and the existence of resistivity meters designed to measure apparent resistivity using four-probe arrays.

REFERENCES

Anderson, W.L. 1975. Improved digital filters for evaluating Fourier and Hankel transform integrals. Report No. USGS-GD-75-012, US Geological Survey, Denver, Colorado.

Archie, G.E. 1942. The electrical resistivity log as an aid in determining some reservoir characteristics. Transactions of the American Institute of Mining and Metallurgical Engineers, Vol. 146: 54-62.

Arfken, G. 1985 Mathematical Methods For Physicists. Third Edition, Academic Press, London.

Balanis, C.A. 1989. Advanced Engineering Electromagnetics. Wiley, New York.

Basokur, A.T. 1990. Microcomputer program for the direct interpretation of resistivity sounding data. Computers and Geosciences, Vol. 14(4): 587-601.

Battilana, J.A. 1989. Electromagnetic Screening by reinforced concrete. Magazine of Concrete Research, Vol. 41(148):163-169, September 1989.

Bentz, D.P. and Garboczi, E.J. 1991. Percolation of phases in a three-dimensional microstructual cement paste model. Cement and Concrete Research, Vol. 21: 325-344.

Bentz, D.P. and Garboczi, E.J. 1991. Reply: "Percolation of phases in a three-dimensional microstructual cement past model", Cement and Concrete Research, Vol. 21: 1187-1188.

Berg, A., Niklasson, G.A., Hedberg, H. and Nilsson, L.O. 1992. Dielectric properties as a function of water content. Journal of Applied Physics, Vol. 71(12): 5897-5903.

Bhargava, J. and Lundberg, K. 1972. Determination of the moisture content of concrete by microwave-resonance method. Materiaux et Constructions, Vol. 5(27): 165-168.

Bibby, H.M. and Fisk, G.F. 1988. Correction for finite distance between potential electrodes in Schlumberger resistivity soundings: Proceedings 10th New Zealand Geothermal Workshop, Auckland. University of Auckland Press, New Zealand, 133-138.

Broadbent, M. and Callander, P.F. 1991. A resistivity survey near Waimakariri river. NZ Journal of Geology and Geophysics, Vol 34: 441-453.

Brodersen, K. and Nilsson, K. 1992. Pores and cracks in cemented waste and concrete. Cement and Concrete Research, Vol. 22: 405-417.

Campbell-Allen, D. 1992. Properties of hardened concrete. in: Australian Concrete Technology, pp. 172-212. Ryan, W.G. and Samarin, A. (Eds.) Longman Cheshire, Melbourne.

Czernin, W. 1980, Cement Chemistry and Physics For Engineers. Crosby Lockwood and Son Ltd, London.

Das, U.C. and Ghosh, D.P. 1974. The determination of filter coefficients for the computation of standard curves for dipole resistivity sounding. Geophysical Prospecting, Vol. 22: 765-780.

Depperman, K. 1973. An interpretation system for geo-electrical sounding graphs, Geophysical Prospecting, Vol. 21: 424-463.

Diamond, S. 1987. in Microstructural Development During Hydration of Cement. Materials Research Society Symposium, Vol. 85, p. 21.

Double, D.D. 1983. New developments in understanding the chemistry of cement hydration. Philosophical Transactions of the Royal Society, London, A, Vol. 310: 53-66.

Ewins, A.J. 1985. A Resistivity Meter. UK Patent Application 2156084A.

Ewins, A.J. 1990. Resistivity measurements in concrete. British Journal of Nondestructive Testing, Vol. 32(3): 120-126.

Galejs, J. 1969. Antennas in Inhomogeneous Media. Pergamon, New York.

Gardiol, F.E. 1984. Introduction to Microwaves. Artech House, Dedham, Mass., U.S.A.

Ge, D.B. and Chen, L.-J. 1991. A direct profile inversion for weakly conducting layered medium. IEEE Transactions on Antennas and Propagation, Vol. 39(7): 907-909.

Ghosh, D.P. 1971. The Application of linear filter theory to the direct interpretation of geoelectrical resistivity sounding measurements. Geophysical Prospecting, Vol. 19: 192-217.

Guptasarma, D. 1982. Optimization of short digital linear filters for increased accuracy. Geophysical Prospecting, Vol. 30: 501-514.

Habashy, T.M., Chow, E.Y. and Dudley, D.G. 1990. Profile inversion using the renormalised source-type integral equation approach. IEEE Transactions on Antennas and Propagation, Vol. 38(5): 668-682.

Hashida, H., Tanaka, K. and Koike, M. 1990. Moisture distribution in concrete before and after application of the finish. Building Research and Practice, No.5: 303-308.

Hedenblad, G. and Nilsson L.-O. 1985. Degree of capillary saturation: a tool for better evaluation of the moisture content in concrete. Report TVBM-7005, Division of Building Materials, Lund Institute of Technology, Sweden.

Heiman,J.L. 1992. in Australian Concrete Technology. Ryan, W.G. and Samarin, A. (Eds.) Longman Cheshire, Melbourne.

Hughes, B.P., Soleit, A.K.O. and Brierly, R.W. 1985. New technique for determining the electrical resistivity of concrete. Magazine of Concrete Research, Vol. 37:133.

Johansen, H.K. 1975. An interactive computer/graphic-display-terminal system for interpretation of resistivity soundings. Geophysical Prospecting, Vol. 23: 449-458.

Keey, R.B. 1972. Drying Principles and Practice. Pergamon Press, Oxford.

Keey, R.B. 1992. Drying of Loose and Particulate Materials. Hemispere Publishing Corp., New York, U.S.A.

Koefoed, O. 1972. A note on the linear filter method of interpreting resistivity sounding data. Geophysical Prospecting, Vol. 20: 476-489.

Koefoed, O. 1976. Progress in the direct interpretation of resistivity soundings: an algorithm. Geophysical Prospecting, Vol. 24: 233-240.

Koefoed, O. 1979. Geosounding Principles. Elsevier, Amsterdam.

Ladouceur, H.D. and Jordan, A.K. 1985. Renormalisation of an inverse scattering theory for inhomogeneous dielectrics. Journal of the Optical Society of America, A, Vol. 2 (11): 1916-1921.

Marquardt, D.W. 1963. An algorithm for least-squares estimation of non-linear parameters. Journal of the Society for Industrial Applications of Mathematics, Vol. 11: 431-441.

Marsden, D. 1973. The automatic fitting of a resistivity sounding by a geometrical progression of depths. Geophysical Prospecting, Vol. 21: 266-280.

Marsland, T.P. and Evans, S. 1987. Dielectric measurements with an open-ended coaxial probe. IEE Proceedings, Vol. 134.(H40): 341-349.

McCarter, W.J. 1987. Gel formation during early hydration. Cement and Concrete Research, Vol. 17: 55-64.

McCarter, W.J. and Curran, P.N. 1984. The electrical response characteristics of setting cement paste. Magazine of Concrete Research, Vol. 36(126):42-49.

McCarter, W.J. and Curran, P.N. 1985. Discussion of the paper "The electrical response characteristics of setting cement paste", (McCarter and Curran, 1984). Magazine of Concrete Research, Vol. 37(130): 53-56.

McCarter, W.J. and Garvin, S. 1989. Dependence of electrical impedance of cement-based materials on their moisture condition. Journal of Physics D:Applied Physics, Vol. 22: 1773-1776.

McGlone, V.A. 1990. Drying rates of concrete floors. Unpublished BRANZ internal report, August 1990.

Merrick, N.P. 1977. A computer program for the inversion of Schlumberger sounding curves in the apparent resistivity domain. Hydrological report 1977/5,Water Resources Commission, N.S.W.

Millard, S.G. 1991. Reinforced concrete resistivity measurement techniques. Proceedings: Institute of Civil Engineers, Part 2, Vol. 91: 71-88.

Mindess, S. and Young, J.F. 1981. Concrete. Prentice-Hall, Englewood Cliffs, N.J.

Moukwa, M. Brodwin, M., Christo, S., Chang, J. and Shah, S.P. 1991. The influence of the hydration process upon the microwave properties of cements. Cement and Concrete Research, Vol. 21: 863-872.

Neville, A.M. 1981. Properties of Concrete. 3rd edition, Pitman, London.

Neville, A.M. and Brooks, J.J. 1987. Concrete Technology. Longman, Singapore.

Nilsson, L.-O. 1977. Moisture problems at concrete floors. Report TVBM-3002, Division of Building Materials, Lund Institute of Technology, Sweden.

O'Neill, D.J. 1975. Improved linear filter coefficients for application in apparent resistivity computations. Bulletin of the Australian Society of Exploration Geophysics, Vol. 6(4) December, 104-109.

O'Neill, D.J. and Merrick, N.P. 1984. A digital linear filter for resistivity sounding with a generalized electrode array. Geophysical Prospecting, Vol. 32: 105-123.

Ollivier, J.P. and Massat, M. 1992. Permeability and microstructure in concrete: a review of modelling. Cement and Concrete Research, Vol. 22: 503-514.

Otto, G.P. and Chew, W.C. 1991. Improved calibration of a large open-ended coaxial probe for dielectric measurements. IEEE Transactions on Instrumentation and Measurement, Vol. 40(4), 742-746.

Parasnis, D.S. 1982. Principles of Applied Geophysics. Chapman and Hall, London.

Parrott, L.J. 1991. Factors influencing the internal humidity in concrete. Magazine of Concrete Research, Vol. 43(154): 45-52.

Parrott, L.J. 1990. A review of methods to determine the moisture conditions in concrete. British Cement Association - C Series December.

Patella, D. 1975. A numerical computation procedure for the direct interpretation of geoelectrical soundings. Geophysical Prospecting, Vol. 23: 335-362.

Pekeris, C.L. 1940. Direct method in interpretation in resistivity prospecting. Geophysics, Vol. 5(1): 31-46.

Ping, X., Beaudoin, J.J. and Brousseau, R. 1991. Flat aggregate-portland cement paste interfaces, 2. Transition zone formation. Cement and Concrete Research, Vol. 21: 718-726.

Powers, T.C. 1958. Structure and physical properties of hardened portland cement paste. Journal of the American Ceramic Society, Vol. 41: 1-6.

Powers, T.C., Copeland, L.E., Hayes, J.C. and Mann, H.M. 1954. Permeability of Portland Cement paste. Journal of the American Concrete Institute, Vol. 51:285-298.

Roper, H. 1992. Surface Coatings and Treatments. In: Australian Concrete Technology. (pp. 258-268), Ryan, W.G. and Samarin, A. (Eds.) Longman Cheshire, Melbourne.

Roy, A, and Apparao, A.: 1971. Depth of investigation in direct current methods geophysics, Vol. 36(5) October, 943-959.

Ryan, W.G. and Samarin, A. (Eds.) 1992. Australian Concrete Technology. Longman Cheshire, Melbourne.

Sanadiki, B.A. and Mostafavi, M. 1991. Inversion of inhomogeneous continuously varying dielectric profiles using open-ended waveguides. IEEE Transactions on Antennas and Propagation, Vol. 39(2): 158-168.

Slichter, L.B. 1933. The interpretation of the resistivity prospecting method for horizantal structures. Physics, Vol 4: 307-322.

Szaraniec, E. 1980. Direct resistivity interpretation by accumulation of layers. Geophysical Prospecting, Vol. 28(2): 257-268.

Tamil, L. and Jordan, A.K. 1991. Spectral inverse scattering theory for inhomogeneous dielectric waveguides and devices. Proceedings of the IEEE, Vol. 79(10): 1519-1528.

Tashiro, C., Ishida, H. and Shimamura, S. 1987. Dependence of the electrical resistivity on evaporable water content in hardened cement paste. Journal of Materials Science Letters, Vol. 6: 1579-1381.

Thompson, F. 1989. Moisture measurement using microwaves. Measurement and Control, Vol. 22: 210-215.

Tijhuis, A.G. 1991. Iterative determination of permittivity and conductivity profiles of a dielectric slab in the time domain. IEEE Transactions on Antennas and Propagation, Vol. 29(2): 239-245.

Tijhuis, A.G. and van der Worm, C. 1984. Iterative approach to the frequency-domain solution of the inverse- scattering problem for an inhomogeneous lossless dielectric slab. IEEE Transactions on Antennas and Propagation, Vol. 32(7): 711-716.

Tselentis, G. and Delis, G. 1991. Geoel: an IBM PC algorithm for the automatic processing and graphic presentation of geoelectric data. In: European Association of Exploration Geophysicists, 3rd Meeting and Technical Exhibition Florence, May, Technical Programme and Abstracts of Papers.

Valdez, L.B. 1954. Resistivity Measurements on Germanium for Transistors. Proceedings of the IRE: Institute of Radio Engineers, Vol. 42: 420-427.

van Beek, L.K.H. 1967. Dielectric behaviour of Heterogeneous Systems. In: Progress in Dielectrics, pp. 69-114, Birks, J.B. (Ed.), Heywood Books, London.

von Hippel, A.R. 1954. Dielectrics and Waves. MIT Press, Cambridge, Massachusetts.

Webb, C. 1990. Testing equipment and methods. Concrete, December: pp. 1-36.

Whittington, H.W. and Wilson ,J.G. 1986. Low-frequency electrical characteristics of fresh concrete. Proceedings IEE, Vol. 133(A5): 265-271

Whittington, H.W., McCarter, J. and Forde, M.C. 1981. The conduction of electricity through concrete. Magazine of Concrete Research, Vol. 33(114):48-60.

Wiederhold, P. 1987. Humidity Measurements. in Handbook of Industrial Drying, pp. 881-914, Mujumdar, A. (Ed.), Dekker, New York.

Wilkins, N.J.M. 1982. Resistivity of concrete. (Internal Paper), United Kingdom Atomic Energy Association, Harwell, Materials Development Division, January.

Wilson, J.G. and Whittington, H.W. 1985. Discussion:The electrical response characteristics ofsetting cement paste. Magazine of Concrete Research, Vol. 37(130): 52-56.

Wilson, J.G. and Whittington, H.W. 1990. Variations in the electrical properties of concrete with change in frequency. IEEE Proceedings, Vol. 137(A5): 246-254.

Wilson, J.G. Whittington, H.W. and Forde, M.C. 1983. Microprocessor based system for automatic measurement of concrete resistivity. Journal of Physics E: Scientific Instruments. Vol. 16: 700-705.

Woelfl, G.A. and Lauer, K. 1979. The electrical resistivity of concrete with emphasis on the use of electrical resistance for measuring moisture content. Cement, Concrete and Aggregates, Vol. 1(2): 64-67.

Zohdy, A.A.R. 1974, Use of Dar Zarrouk curves in the interpretation of vertical electrical sounding data U.S. Geological Survey Bulletin 1313-D.41.

Zohdy, A.A.R. 1975. Automatic Interpretation of Schlumberger Sounding Curves, Using Modified Dar Zarrouk Functions. U.S. Geological Survey Bulletin 1313- E16

Zohdy, A.A.R. 1989. A new method for the automatic interpretation of Schlumberger and Wenner sounding curves. Geophysics, Vol. 54(2): 245-253.

APPENDIX 1. Resistivity of a Homogeneous Earth

Point current on homogeneous earth of resistivity ρ

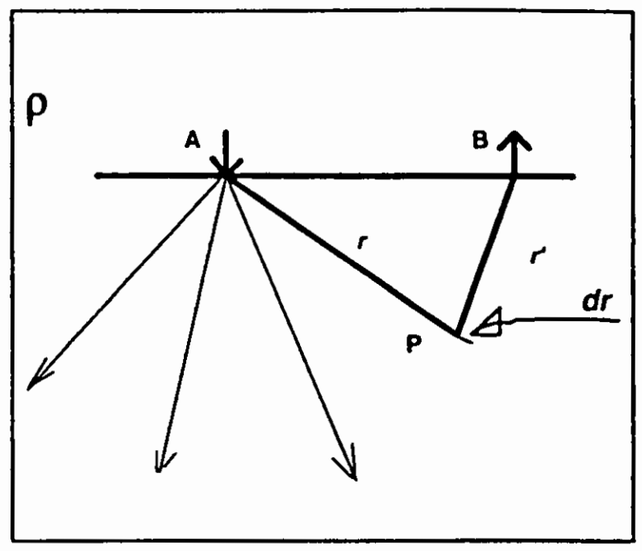

The resistance dR across a shell of thickness dr at a distance r from the point source is

$$dR = \frac{\rho dr}{2\pi r^2}$$

The potential at r is given by

$$V(r) = -\int_{r=0} I dR = -\int_{r=0} \frac{I\rho dr}{2\pi r^2}$$

that is:

$$V(r) = \frac{I\rho}{2\pi r}$$

In practice a positive electrode A, and a collecting electrode B are used. The potential at any point r from A and r' from B is then

$$V(r) = \frac{I\rho}{2\pi}\left(\frac{1}{r} - \frac{1}{r'}\right)$$

Resistivity determination by measurement of the potential difference between two 'voltage' probes M and N.

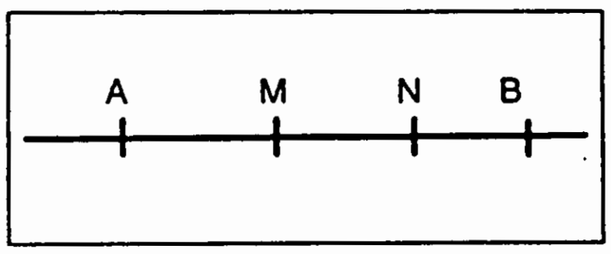

$$\text{At M } V_m = \frac{I\rho}{2\pi}\left(\frac{1}{AM} - \frac{1}{BM}\right)$$

$$\text{at N } V_n = \frac{I\rho}{2\pi}\left(\frac{1}{AN} - \frac{1}{BN}\right)$$

$$\text{so } \Delta V = V_m - V_n = \frac{I\rho G}{2\pi}$$

Thus the resistivity of a homogeneous earth is given by

$$\rho = \frac{2\pi}{G}\frac{\Delta V}{I} \text{ where } G = \frac{1}{AM} - \frac{1}{BM} - \frac{1}{AN} + \frac{1}{BN}$$

For the Wenner Array,

$$G = 1/a$$

$$\text{thus } \rho_w = 2\pi a \frac{\Delta V}{I}$$

Resistivity measurement using the Schlumberger array

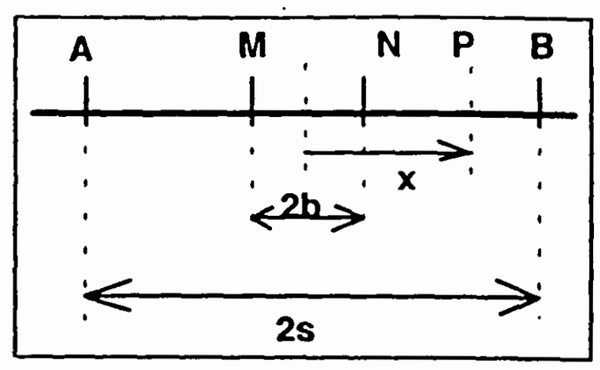

At point P

$$V = \frac{I\rho}{2\pi}\left(\frac{1}{(s+x)} - \frac{1}{(s-x)}\right)$$

thus $$\frac{dV}{dx} = -\frac{I\rho}{2\pi}\left(\frac{1}{(s+x)^2} - \frac{1}{(s-x)^2}\right)$$

$$= -\frac{I\rho}{2\pi s^2} \quad \text{at} \quad x = 0$$

when $MN \rightarrow 0$, ie, for the ideal Schlumberger array,

$$\rho_s = -\frac{\pi s^2}{I}\frac{dV}{dx}$$

To measure resistivity in practice, ΔV is measured between probes M and N and the approximation $\frac{dV}{dx} \approx -\frac{\Delta V}{2b}$, is made, giving the measured resistivity for the Schlumberger array:

$$\rho_{ms} = -\frac{\pi s^2}{2b}\left|\frac{\Delta V}{I}\right|$$

APPENDIX 2. Apparent Resistivity of a Horizontally Stratified Earth

Point current on a horizontally stratified earth

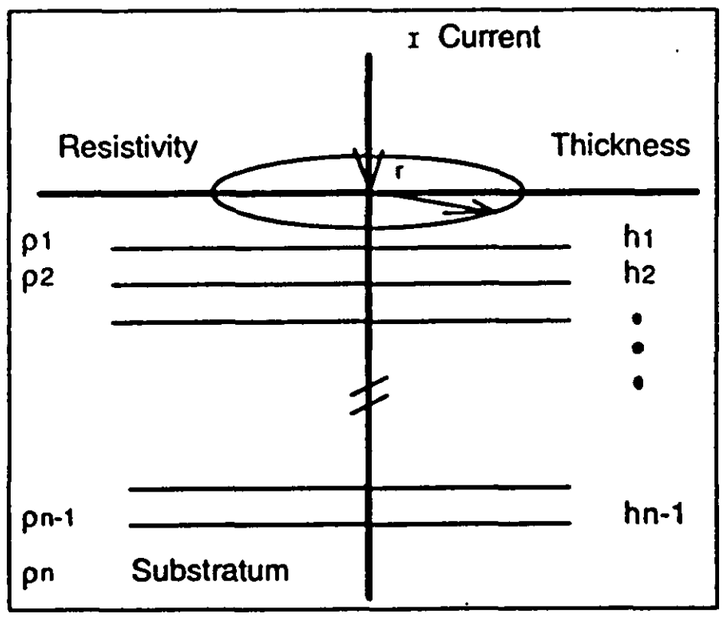

It can be shown (e.g., Koefoed 1979), that the potential at the surface, a distance r from a point source of current I, is given by

$$V(r) = \frac{I\rho_1}{2\pi}\left[\frac{1}{r} + 2\int_0^\infty k(\lambda)J_0(\lambda)d\lambda\right]$$

$$= \frac{I}{2\pi}\left[\rho_1\int_0^\infty (1+2k(\lambda))J_0(\lambda)d\lambda\right]$$

$$\text{ie } V(r) = \frac{I}{2\pi}\int_0^\infty T(\lambda)J_0(\lambda r)d\lambda \qquad (1)$$

where $T(\lambda)$ = the resistivity transform = $\rho_1(1+2k(\lambda))$

λ = an integration variable = $1/s$ usually.

ρ_1 = resistivity of the top layer.

$k(\lambda)$ = the characteristic function, a function of all layer thicknesses and resistivities

$J_0(\lambda r)$ = zeroth order Bessel equation of the first kind

The resistivity transform may be obtained from the layer parameters using **recurrence relations.**

(a) Let $u_{j-1}(\lambda) = e^{-2h_{j-1}\lambda}$

and $k_{j-1} = \dfrac{\rho_{j-1} - \rho_j}{\rho_{j-1} + \rho_j}$ (reflection coefficient)

and $w_j(\lambda) = \rho_j \dfrac{(1-u_j)}{(1+u_j)}$

(b) Obtain $T_{n-1}(\lambda)$ = the resistivity transform for the substratum and bottom layer

$$= \rho_{n-1}\left(\frac{1-k_{n-1}u_{n-1}}{1+k_{n-1}u_{n-1}}\right)$$

(c) Reiterate $T_j(\lambda) = \dfrac{w_j(\lambda) + T_{j+1}(\lambda)}{1 + w_j(\lambda)T_{j+1}(\lambda)/\rho_j^2}$ for subsequent layers, until $T_1(\lambda)$ is obtained.

For an Ideal Schlumberger Array the **apparent resistivity** of a stratified earth is given by,

$$\rho_{ms} = \frac{\pi s^2}{I}\left|\frac{dV}{dr}\right| \qquad (2)$$

Differentiating (1), and substituting into (2) gives

$$\rho_a(s) = s^2\int_0^\infty T(\lambda)J_1(\lambda r)\lambda d\lambda \qquad (3)$$

Where $J_1(\lambda r)$ is the first order Bessel equation of the first kind.

Use of the transform

Either $T(\lambda)$ is substituted into (3) and the result solved to find ρ_a or (3) may be inverted to obtain $T(\lambda)$ and hence the layer parameters. In both cases a numerical solution usually is sought with the aid of linear digital filters (see Appendix 3).

APPENDIX 3. Numerical Evaluation of the Relationship between Apparent Resistivity ρ_a and the Resistivity Transform

Design of digital filter (Ghosh 1971)

From equation (3) above, i.e.,

$$\rho_a(s) = s^2 \int_0^\infty T(\lambda) J_1(\lambda r) \lambda d\lambda \qquad (3)$$

Hankel's inversion is applied to obtain

$$T(\lambda) = \int_0^\infty \rho_a(s) J_1(\lambda s) / s \, ds \qquad (4)$$

The substitutions $s = e^x$ and $\lambda = e^{-y}$
are made, to obtain the equation

$$T(y) = \int_{-\infty}^{\infty} \rho_a(x) J_1[\exp(x-y)dx] \qquad (5)$$

which is a convolution integral in the space domain. This may be transformed to a simple product in the frequency domain, i.e.,

$$F(f) = G(f) \cdot H(f) \qquad (6)$$

where T(y) and the output function F(f) are Fourier transform pairs, as are $\rho_a(x)$ and the input function G(f), and exp(x-y)and H(f) which is known as the Filter Characteristic function.

A partial apparent resistivity curve $\Delta\rho_a(x)$ whose exact resistivity transform $\Delta T(\lambda)$ is known, is chosen so that from the transform pairs $\Delta\rho_a(x) \leftrightarrow \Delta G(f)$ and $\Delta T(\lambda) = \Delta F(f)$, the **Forward** filter characteristic may be determined as $H(f) = \frac{\Delta F(f)}{\Delta G(f)}$ Since equation (6) may be written $G(f) = F(f)/H(f)$, apparent resistivity may be obtained from the resistivity transform by determining the **Inverse** filter characteristic 1/H(F).

The responses of the forward and inverse filters to a sinc function (sinx/x) input are then sampled to obtain the coefficients which constitute the Forward and Inverse digital linear filters respectively.

APPENDIX 4. Use of Forward and Inverse Filters

Forward filter

Forward filters are used to generate the resistivity transform from an apparent resistivity curve.

The apparent resistivity curve is smoothed and sampled at logarithmically spaced intervals to give 'digitised' apparent resistivities : R_k = 1,2...m+r, where r is the number of filter coefficients and m the number of transform values required. Generally m is the number of measurements actually recorded at logarithmically spaced intervals, the balance being generated through extrapolation of the curve at each end.
The discrete equivalent of

$$T(\lambda) = \int_0^\infty \rho_a(s) J_1(\lambda s) / s ds$$

is

$$T_m = \sum_i^r a_i R_{m-i}$$

where a_i are the forward filter coefficients.
Forward filters are used in Direct methods of profile recovery and sometimes in Indirect methods (see Appendix 6).

Inverse filter

Applying recurrence relations to a model profile at logarithmic spacings s (and hence at values of λ , the 'digitised' resistivity transform T_k k=1,2...m+r is obtained.
The discrete equivalent of

$$\rho_a(s) = s^2 \int_0^\infty T(\lambda) J_1(\lambda r) \lambda d\lambda$$

is

$$R_m = \sum_j^r b_j T_{m-j}$$

where b_j are the inverse filter coefficients.

Inverse filters are used in Indirect methods of profile recovery.

APPENDIX 5. The Use of Two Types of Inverse Filter to Calculate Apparent Resistivity Curves from Model Profiles

Select current probe spacing range s=AB/2. For the concrete resistivity meter s will probably range from 0.02 to 0.5m.

Ghosh type filters

Logarithmically spaced values of *s* are required.

Select the number d, of spacings per decade, so that $s_{i+1} = 10^{1/d} \cdot s_i$ and $\lambda_i = 1/s_i$.

For each value of λ, the resistivity transform $T(\lambda)$ is calculated using recurrence relations on the model profile.

Inverse filter coefficients b_j are used to calculate the apparent resistivity. Thus at the ith spacing s_i, Ghosh's 9-point filter gives $\rho(s_i) = \sum_{j=-3}^{5} b_j T_{i-j}$.

Guptasarma type filters

There is no requirement for values of s to be logarithmically spaced.
For each value of *s*, (using the seven-point filter for example), values of λ_r are found using

$\lambda_r = 10^{a_r} / s$

where a_r are the abscissae for the filter coefficients.

The resistivity transform $T(\lambda_{i,r})$is calculated for each $\lambda_{i,r} = 10^{a_r} / s_i$ using recurrence relations.

Guptasarma's inverse filter coefficients φ_r are used to calculate apparent resistivity at spacing s_i thus

$$\rho(s_i) = \sum_{r=1}^{7} \varphi_r T(\lambda_{i,r}).$$

The main disadvantage of Gutasarma's filters is the heavier demand on processing time since 7,11 or 19 (for the 7,11 or 19 point filters) values of T must be calculated for each value of *s*, whereas when using Ghosh type filters, T is calculated over a fixed set of λ and used throughout. This disadvantage may be outweighed by the higher accuracy of Guptasarma's filters for steeply decreasing resistivities with increasing depth, and the ability to use non-logarithmically spaced current probe spacings.

APPENDIX 6. Methods of Profile Recovery

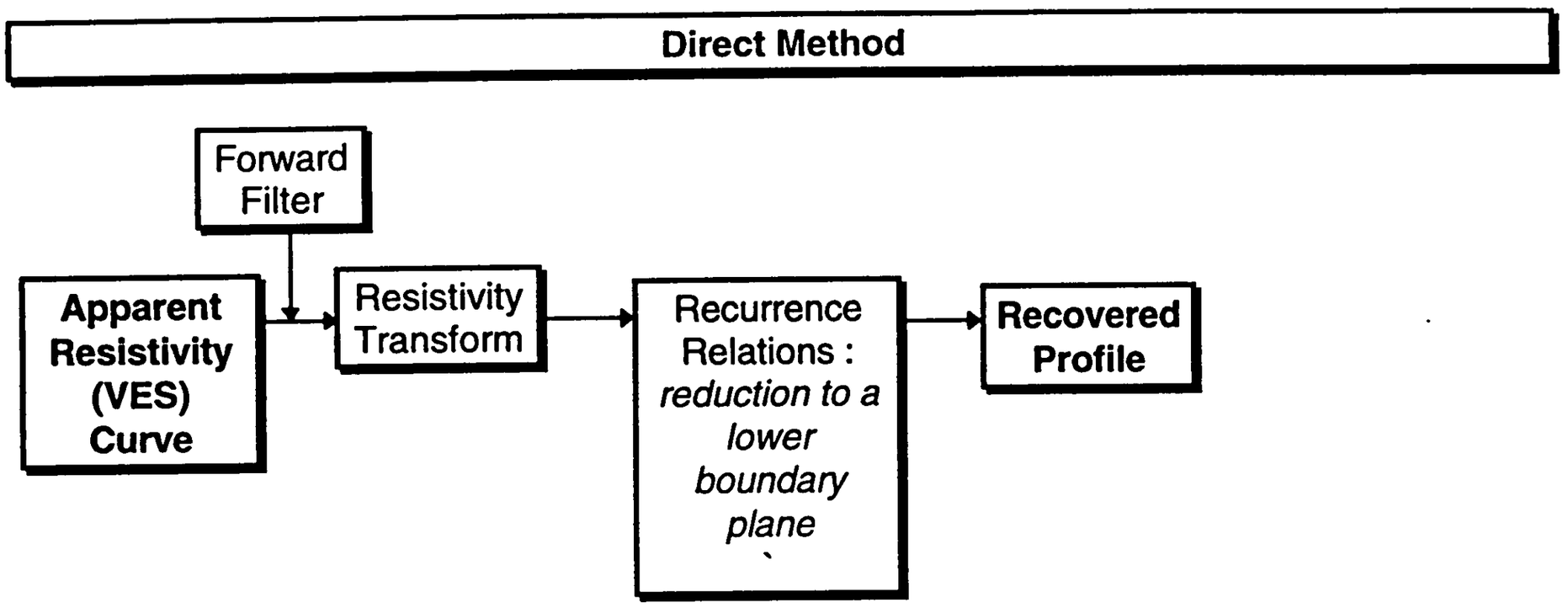

Indirect Methods

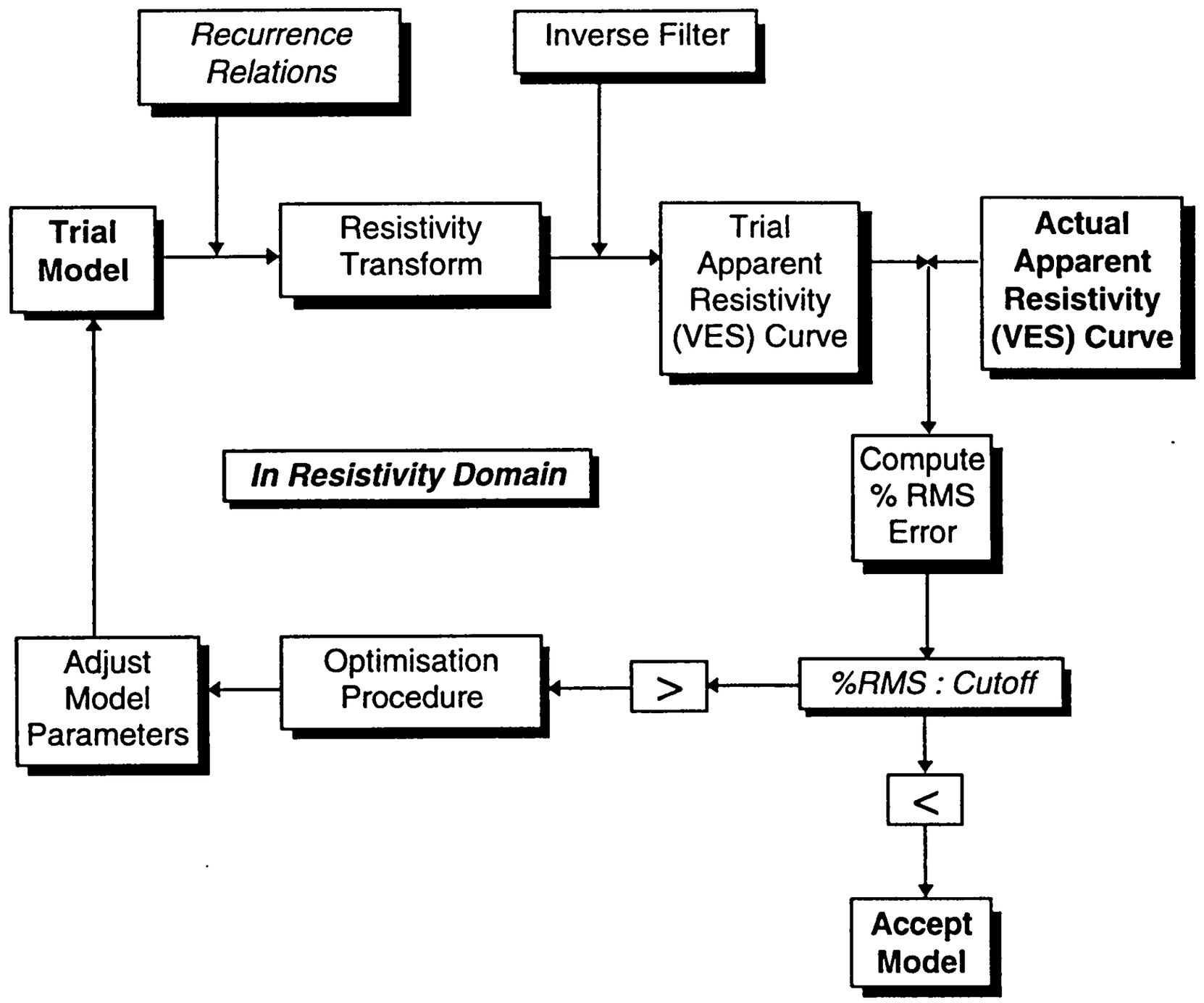

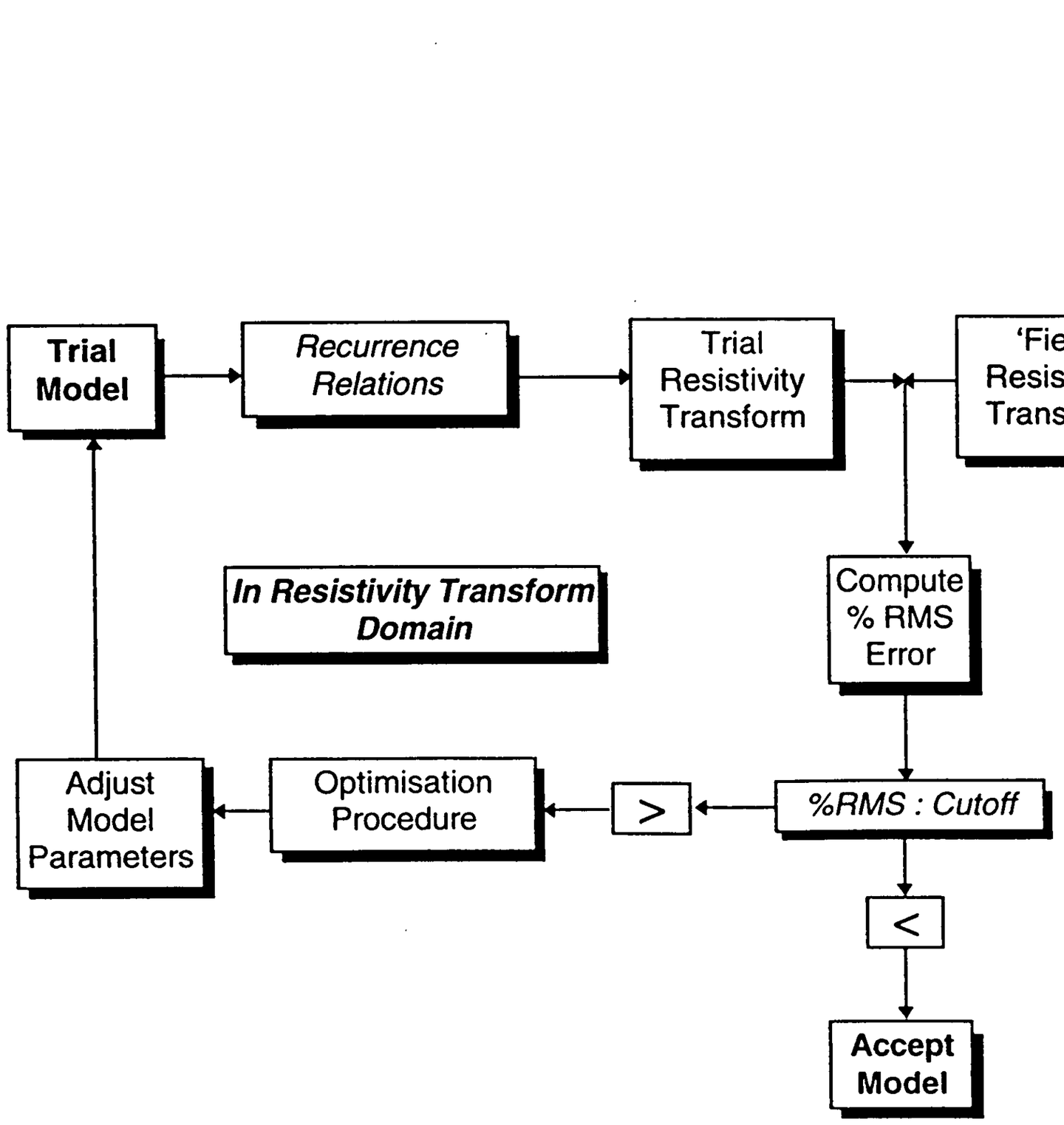

APPENDIX 7. Indirect Method based on Merrick (1977)

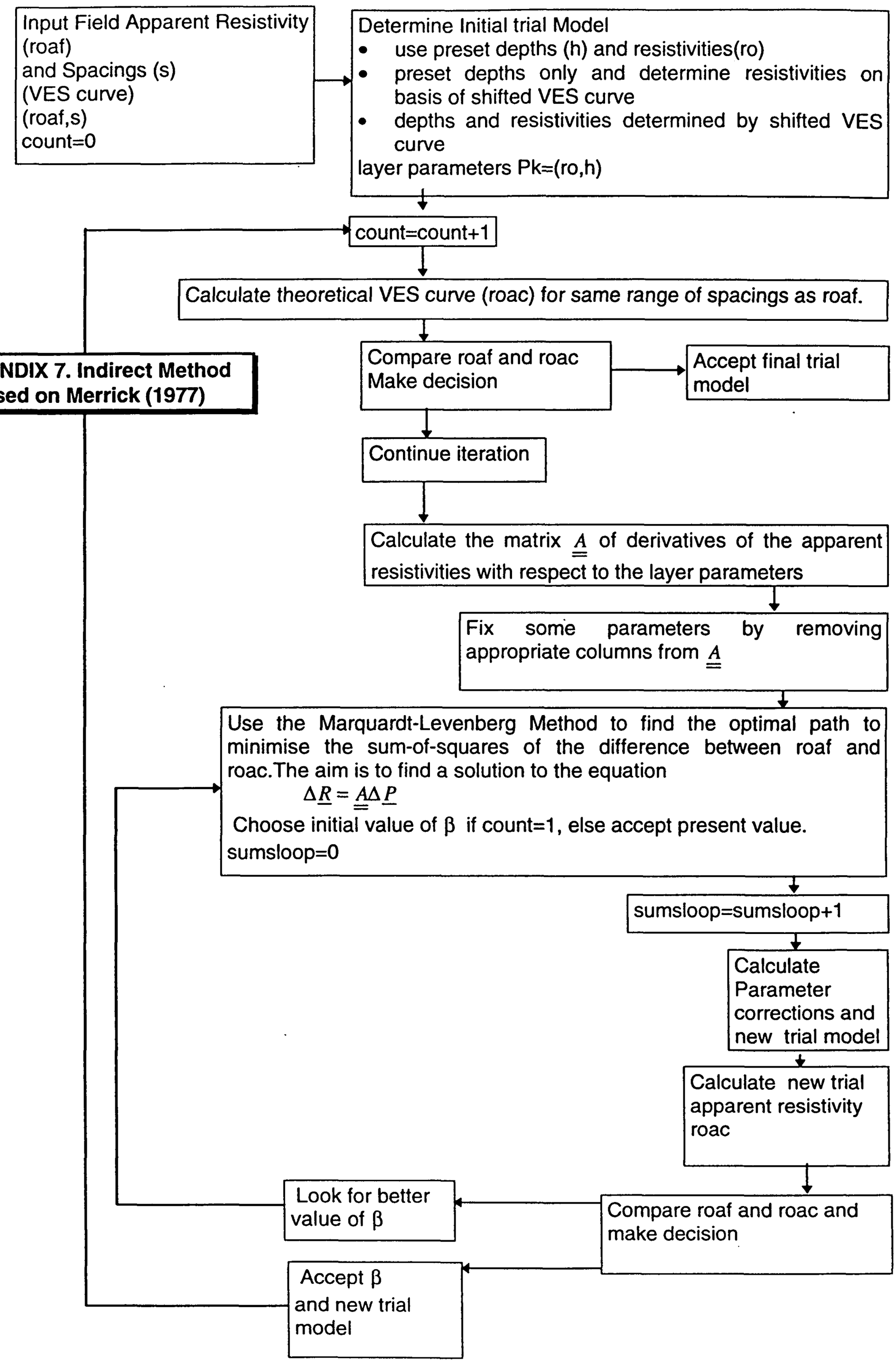

APPENDIX 8. Indirect Method based on Zohdy (1989)

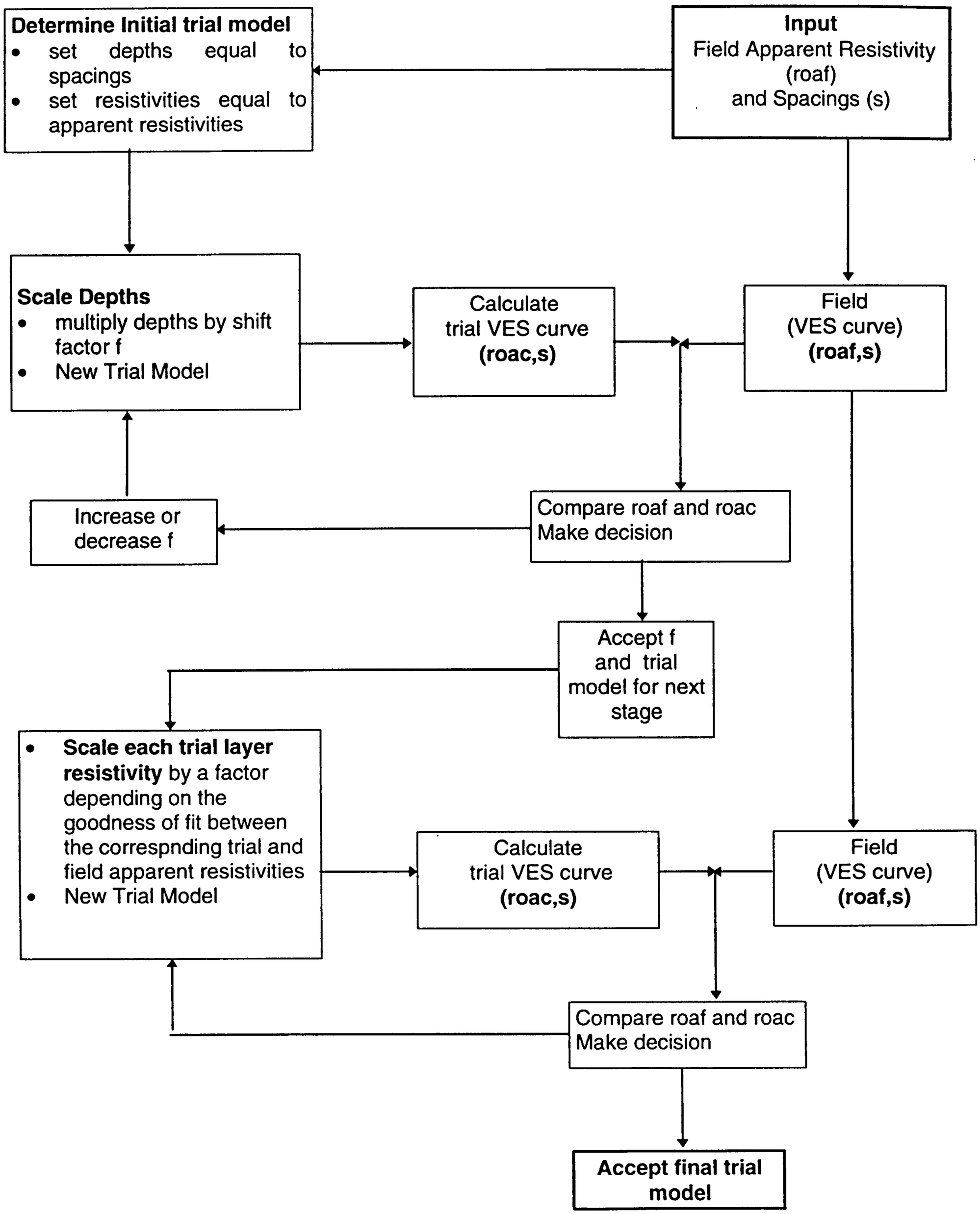

APPENDIX 9

EMDRIP

(Developed by Geo-Compu-Graph)

EMDRIP is a software package that implements Zohdy's routine for rapid, fully automatic inversion of dc resistivity vertical electronic sounding (VES) data. The routine marks a departure from the traditional view of inversion that requires the user to specify a fixed number of sub surface layers in advance of executing the program or to gamble on the program specifying the correct number of layers. **EMDRIP** is an acronym for Equivalent Multilayer Dc Resistivity Inversion Process.

EMDRIP is a fully automated inversion program that accommodates both Wenner and Schlumberger arrays. Six points per decade are used for Schlumberger arrays, and eight points per decade are used for Wenner arrays. The data points are evenly spaced on a logarithmic scale.

A utility module for keyboard input and editing of observed resistivity data is also included. The observed data are stored on disk. The observed data must be evenly spaced on a logarithmic scale. Electrode spacings and resistivities need not be in the same distance units.

Observed Data:

- 200 resistivity readings per sounding allowed.
- Data must be logarithmically evenly spaced.

Inversion

- AB/2 or a-spacings of 1 1000 distance units displayed on graph.
- Resistivities of 3 to 3000 ohm-distance units displayed.
- rms error calculated.

Schlumberger array resistivity inversion showing observed data (points), calculated anomaly (solid curve), and the generated equivalent multilayer resistivity model (stairstep curve).

System Requirements

IBM PC compatible 8086 or 80286 computer. 512K RAM, CGA, EGA, or VGA graphics capability. MS-DOS 2.1 or higher. Parallel port with DB-25 connector. Single disk drive, monochrome or colour monitor and printer (optional).

APPENDIX 10. Software Package GEOEL: An IBM PC algorithm for the automatic processing and graphic presentation of geoelectric data

G. - Akis Tselentis and George Delis
Hydroel Ltd, 4 Ioanninon Street, Ano Pefki, 151 21 Athens, Greece.

This paper addresses the problem of automatic processing and interpretation of geoelectric data with personal computers.

The main algorithm is divided into two processing stages. During the first processing stage, the field curve is approximated by a group of layers which are determined automatically by the program in such a way that the resulting theoretical curve describes as closely as possible the field curve. This operation is performed in the resistivity - space domain and the optimum number of layers needed to describe the resistivity distribution versus depth is determined from the algorithm.

The result is treated as the initial solution of the second processing stage which is based on adaptive linear filters for forward modelling and non linear least squares ridge regression for the assessment of the final geoelectric properties of the underground.

One strong point of the program is that it does not assume an initial model to start and that it can delineate all the bad data points without attempting to replace them by fictitious layers in the final solution.

The whole package is supported by a set of subprograms called up through a pull down menus session during which the geophysicist can perform all the commonly required interpretation tasks such as:

a) interactive data entering with simultaneous build up of the field curve
b) automatic or manual shifting of the various sections of the apparent resistivity curve
c) colour coded resistivity display of the solution
d) colour coded resistivity section of a traverse (something like resistivity tomography) taking into consideration the local sounding altitudes
e) specially designed data base for the organisation of geoelectric data and the solutions, etc. Furthermore, the programme supports all the well known printers including colour ones and it can be run from a laptop in the field for the on site processing of the data and the optimum design of a geoelectric survey.

APPENDIX 11. Software package RESIX

From Interprex Limited Product Catalogue, Third edition, 1991

Interprex offers five software tools that interpret resistivity and induced polarisation soundings in terms of 1 dimensional models. These tools belong to the RESIX family of productivity software. Use any one of these software packages to produce forward and inverse models of resistivity data, or induced polarisation data, or both. Please read the brief descriptions of each package in the RESIX family to discover which products best suit your needs.

The RESIX Family

The RESIX family of programs includes:

- RESIX
- RESIX IP
- RESIX PLUS, and
- BOSSIX and OFFIX

All packages in the RESIX family produce forward and inverse models in terms of layered earth models. Some packages are resistivity modelling packages only; others perform induced polarisation modelling as well.

Mathematical basis

For forward modelling, all RESIX family programs use an Anderson style adaptive linear digital filter for most common arrays to provide you with resistivity contrasts of up to 10,000 to 1. For stable results for inversion, all programs use the Inman style ridge regression approach of nonlinear least squares curve fitting.

The RESIX family of software can provide:

- Maximum of 10 earth layers for the forward model
- Maximum of 8 earth layers in the inversion
- Ability to fix model parameters
- Maximum of 60 data points
- Interactive or batch (unattended) mode
- Support for Schlumberger, Wenner, dipole-dipole, pole-dipole, polar-dipole, and equatorial arrays (some programs support additional arrays).
- Assigning sounding locations with XY coordinates and elevations
- Resolution matrix listings
- Access to ASCII and binary file formats

RESIX family Interprex Standard Features:

- Choice of menu or command language interface
- Spread sheet editors
- Forward modelling
- Inverse modelling
- Interactive graphics operation mode
- Paginated listings
- Hard copy colour output
- SET DIRECTORY command
- BATCH WRITE command
- DOS SHELL command

The additional features of individual programs are listed below:

RESIX is the base program in the RESIX FAMILY and provides all the capabilities listed above. Apparent resistivity versus spacing define the sounding curves in this program. RESIX can either automatically shift data with overlapping curve segments or allow you to shift the data yourself.

RESIX PLUS has all the features of RESIX and adds the ability to perform direct inversion. Direct Inversion calculations let you estimate a layered model directly from the data without having to construct the layers of the model manually. The direct inversion feature will save you substantial amounts of time. The extension of the input data curve for short and long electrode spacings as well as the resampling and transformation of the curve is automatic and transparent to the user, another valuable feature.

RESIX PLUS gives you a choice of two methods to define sounding curves. You may define sounding curves by apparent resistivity versus electrode spacing or with a spread sheet that sets the voltage, current and spacing for both the current and potential electrodes. The work sheet then calculates apparent resistivities as you enter the data in the cells, using formulae that account for the finite electrode spacings.

RESIX PLUS also provides equivalence analysis and automatic overlapping data shift features of RESIX. RESIX PLUS provides plate style output to graphics printers, laser printers and pen plotters.

BOSSIX and OFFIX interpret data taken with the Offset Wenner Sounding System and other DC resistivity methods. Both programs accommodate the data reduction techniques required for the offset sounding method. An interactive work sheet reduces the five resistance measurements taken with the offset Wenner sounding method. The output, in terms of apparent resistivity versus electrode spacing, interfaces directly with the rest of the programme and is completely transparent.

BOSSIX and OFFIX are programs based on RESIX PLUS and have all of the features of RESIX PLUS except automatic shifting of overlapping data segments.

BOSSIX is sold in North and South America for BOSS systems by Bison Instruments, Inc.; OFFIX is sold in Europe and Africa for the Offset Wenner Sounding system from Campus Geophysical Instruments, Ltd.

RESIX IP has all the capabilities of RESIX and adds the ability to interpret induced polarisation soundings. RESIX IP also has the added benefit of Equivalence analysis. RESIX IP gives you the choice of showing IP response as either PFE or mV-sec/V.

When performing inversion, RESIX IP can use up to 7 layers if both resistivity and polarisation parameters are included, or up to 10 layers if only resistivity parameters are sought. Forward curves in this program are defined by apparent resistivity (and IP response) versus spacing. RESIX IP can shift overlapping data segments either automatically or manually.

RESIX IP produces plate style output to graphics printers, laser printers and pen plotters, and produces paginated data listings on a printer.

APPENDIX 12. CNS resistivity meter

General specification

Display: 0-1999, Digital Panel Meter; decimal points and annuciators are automatically selected by the Range and Function switches, but the Resistivity Ranges are only shown as "kΩ', NOT 'kΩ.cm'.
An over-range indication is given by blanking off the last three digits.
A low-battery indication is given when the supply voltage falls below 3.6v.

Range switch: Six-position switch to select Ranges 1 to 6 (see Table for details).

Function switch: Three position toggle switch, centre biased to Resistivity Measurements - the Current or Resistance (R/10) functions may be temporarily selected by switching to the appropriate function as indicated.

Analogue output: 0 - 10v, full-scale, representing the FSR of the selected range and function. The o/p is available via a 'bnc' socket on the front panel or via pins 1 (sig.) & 2 (gnd) of the Remote Socket.

Remote function: The Resistivity Meter can be remotely switched ON & OFF by positive (3.5-30v) or negative (0 - 1.5v) logic signals on pins 4 or 5, respectively, with respect to pin 6 (gnd), of the Remote Socket. A 'closing' switch contact (between pins 3 & 4, or pins 5 & 6 of the Remote Socket) may alternatively be used.

Probe socket: 6-pin, front panel mounted for connection to the Wenner probe array. Connections:-

Pin	Connection
1	V1 (screen
2	Probe V_1
3	Probe V_2
4	V2 (screen)
5	Probe I1
6	Probe I2

Remote socket: 6-pin, back panel mounted for connection to an external power supply, remote ON/OFF signals and to provide an alternative analogue output. Connections:-

Pin	Connection
1	+ve Sig. o/p
2	-ve Sig. o/p (gnd)
3	+V power supply i/p
4	+ve logic i/p
5	-ve logic i/p
6	-V power supply i/p and logic gnd

Battery supplies: 4 x 1.5v 'C' type manganese-alkaline cells, or 4 x 1.25 'C; type Nickel-Cadmium rechargeable cells. An external voltage of 5/6 may be applied through pins 3 (+ve) & 6 (-ve) of the Remote socket.

Battery life: Approximately 34 hrs using Duracell type cells.

Approximately 10 hrs using Ni-Cd rechargeable cells.

Weight: Complete kit including leather carrying case 5.5 kilograms (12 lbs).

Designed by Taywood Engineering Ltd.

Description and specification of the resistivity meter

The resistivity meter has been designed specifically to measure the resistivity of concrete. Using a standard Wenner linear four probe array, a flat-topped ac waveform for the current source and sophisticated electronic circuitry, a true measure of the dc component (that is, resistance, not impedance) of resistivity is measured. The resulting measurement is not frequency dependent.

There are four basic ranges of full-scale measurement possible, 0 - 2 kΩ.cm, -=20kΩ.cm, 0 - 200kΩ.cm and 0 - 2MΩ.cm. The actual full-scale reading is 1999 and an over-range indication is given for readings greater than 1999. A ten-turn dial (the SPACING control) allows the probe spacing to be entered resulting in a true measurement of resistivity in Ω.cm. The range is 0 - 10 cm (that is, 1 cm/turn).

In addition to resistivity ranges, the RM has four ranges of ac resistance measurement (again, resistance not impedance) as measured between the two current probes, selected by a function switch. They are, 0- 20kΩ, 0 - 200kΩ, 0 - 2MΩ & 0 - 20MΩ. By setting the spacing control to 1.59 cm, and using a four probe technique, additional ac resistance measurements in the range of 0 - 200Ω and 0 - 2kΩ may be made using the two lower resistivity ranges.

One of the major problems with making concrete resistivity measurements is that of high contact resistances between the probes and the concrete. There are many ways in which these contact resistances may be reduced, but they are difficult to eliminate altogether. If high contact resistances exist there is no reason to suppose that they are identical on each probe. High, and substantially different, contact resistances on each of the probes can cause serious errors in the measurement of resistivity if instruments with sine-wave current sources are used. The RM uses a flat-topped current waveform and a patented technique to overcome this problem and will give accurate measurements in the presence of large and different probe contact resistances. It can also be used with 'buried' probes in concrete, if desired.

On each of the resistivity ranges the current drive to the current probes is limited to a maximum 'constant' value. The voltage drive to the current probes is also limited, to 25V pk-pk, so that in the event of high contact resistances between the current probes and the concrete, the current will reduce below its 'constant' value. The measured value of resistivity is proportional to the voltage measured on the voltage probes divided by the current flowing through the current probes; both voltage and current are measured and an analogue divider circuit is used to compute the resulting division. Thus, even when the current falls below its 'constant' value, an accurate measure of the resistivity is possible. However, the measurement becomes less accurate, and more variable, as the current reduces. Accurate results may still be obtained with current levels down to $^1/_{20}$th of the 'constant' value providing readings are stable.

The current flowing between the two current probes is only likely to reduce below its 'constant' value in the presence of high contact resistances on the current probes. Such contact resistances may easily be estimated using the ac resistance measurement function. If such an event occurs, greater accuracy and/or stability of reading, may be obtained by switching to a lower value of 'constant' current. The facility is provided for the two centre ranges of resistivity, 0 - 20kΩ.cm and 0 - 200 kΩ.cm.

The function switch is also used to provide an indication of the current flowing between the two current probes, so that an operator may know when the current of a particular range has fallen below its 'constant' value and switch to the alternative range (if available) using a lower current. The table below indicates the six ranges of the RM, the full-scale measurements of resistivity, resistance and current possible on each range, and the highest total contact resistance - between the two current probes - possible before the current falls below its 'constant' value.

Ranges of the resistivity meter

RANGE	FULL-SCALE READING			MAX. CONTACT RES
	P	R/10	I	
1	2kΩ.cm	20kΩ	2mA	12.5kΩ
2	20kΩ.cm	200kΩ	2mA	12.5kΩ
3	20kΩ.cm	200kΩ	200μA	125kΩ
4	200kΩ.cm	2MΩ	200μA	125kΩ
5	200kΩ.cm	2MΩ	20μA	1.25MΩ
6	2MΩ.cm	20MΩ	20μA	1.25MΩ

The maximum contact resistance quoted for each range is the nominal total contact resistance that can be tolerated between both current probes without reducing the value of the constant current drive. In practice, these may be increased by up to 20 times with some possible reduction in accuracy under certain conditions, see specification of resistivity measurements. The exception to this rule is on ranges 5 & 6 where contact resistances in excess of 1.25MΩ/ probe may produce erratic readings due to 'hum' pick-up and to stray capacitive effects associated with the probe/concrete interface.

Range selection resistors of ±1% tolerance are used in the RM, and the RM is therefore accurate to within ±2% of this tolerance when measuring resistance. The accuracy of resistivity measurements should be as good as those for resistance. However, when making concrete resistivity measurements, it must be remembered that what is measured is an 'apparent' resistivity. The results depend on the assumption that the concrete is of 'infinite' surface area and depth, and homogenous; concrete is rarely that. It is essential to have a good appreciation of the possible sources of error in making concrete resistivity measurements if sensible interpretation of the results is to be achieved.

The RM is battery powered and runs from type 'C' cells. These may be either standard or Manganese-Alkaline cells of 1.5V or No-Cd cells of 1.25V. NO charging facilities for Ni-Cds are provided. Standard 1.5V or Ni-Cd cells will provide approximately 10 hours operating time, whilst Duracell types will provide up to 34 hours operating time. A 'low-battery' indication is given by the Digital Panel Meter when the cells are exhausted. The full accuracy of the RM is maintained over the whole range of battery voltages.

An additional feature of the RM is its 0 - 10V analogue output, representing the measured function of the selected range. Also provided is a remote ON/OFF facility for the RM so that, together with its analogue output, it may be used with a logger for intermittent monitoring of concrete resistivities on a long-term basis. The remote ON/OFF function (situated on the back-panel) may be operated by means of positive or negative logic signals (in the range of 0 - 30V) or a closing relay contact. The remote control input socket has additional pins to allow the RM to be operated from an external power source, 5/6V @ 200mA being required.

Resistivity measurements

The resistivity ranges of the resistivity meter are calibrated for surface measurements using a standard Wenner linear 4-Probe array with equal spacing of 'x' cms between the probes. A current is driven between the outer ('current') probes and a voltage is developed and measured across the inner ('voltage') probes. Both current and voltage levels are measured and the resultant value of V/I is determined using an analogue divider circuit. Reversing either the 'current' or the 'voltage' probes will produce a -ve sign for the reading, which is of no significance, but see 'Accuracy' below.

Ranges: See table on previous page.

Current drive: Alternating, with a flat-topped, trapezoidal wave-form at a frequency of about 13Hz. The pk-pk level is nominally constant (see Table) but with a nominal voltage limit of 25v pk-pk.

Accuracy: **The basic accuracy is** ±2% of reading, ±3 digits, for current drives down to $^1/_{20}$th of the nominal 'constant' value assuming equal contact resistances on the 'current probes.

If high and unequal contact resistances exist on the current probes, additional errors can be generated which may effectively add, or subtract, an offset value of the reading. The RM has been designed to reduce these errors to a minimum, but is dependent upon the setting of the spacing control, "x" in cm and the ratio, 'r', being equal to I_C/I_A. For the various ranges, the 'worst case' additional errors are:

Ranges 1, 3 & 5: ± 1 digit/x/r

Ranges 2, 4 & 6: ± 0.1 digits/x/r

Typically, such errors will be much smaller than the 'worst case' value and can be ignored. However, when a reading is of the order of 20% of full-scale, or less, their existence and effect can be checked and substantially reduced by taking two resistivity readings - with and without the connections to the 'voltage' probe reversed - the mean of the two readings (ignoring signs) being a good estimate of the 'true' reading.

Probe spacing: Adjustable between 0 - 10 cm using a ten-turn dial (1 cm/turn). To prevent overloading of the circuitry the control must not be set below 1.59 cm.

Resistance measurements

A.C. resistance measurements can be made between the outer 'current' probes that are true resistance measurements, NOT impedance. The FSR values are as shown in the table on page 54 and are ten times the displayed values on the digital panel meter.

Ranges: See table on page 54

Accuracy: ± of reading, ±1 digit

Two additional ranges or resistance measurements can be made using a four-probe technique (i.e. outer 'current' probe connections connected to the nearest inner 'voltage' probe connections) and the resistivity ranges, and by setting the spacing control to 1.59 cm.

Ranges: $^1/_{10}$th of the selected resistivity range, in kΩ, NOT kΩ.cm. This gives ranges of 0 - 200Ω and 0 - 2kΩ using the two lower ranges of resistivity. (NB The other resistivity ranges can be used to measure resistance in this manner if so desired.)

Current measurements

The actual current flowing between the outer 'current' probes can be measured in order to determine if it has fallen below its nominal 'constant' value. The nominal 'constant" values, for each range are between +0% and -5% of the values shown in the table.

Accuracy: ±2% of reading, ±2 digits

Once the current, of a particular range, has fallen below its 'constant' value and the current drive is voltage limited, the resistance between the 'current' probes can be estimated from the formula:

$R = 25v/I$

where I is the current measured and 25v ±5%, is the nominal value of the current drive voltage limit.

Table 1: Approximate composition limits of ordinary Portland cement (Neville 1978, p. 11)

Oxide	Content (%)
CaO	60-67
SiO_2	17-25
Al_2O_3	3-8
Fe_2O_3	0.5-6.0
MgO	0.1-4.0
Alkalis	0.2-1.3
So_3	1-3

Table 2: Composition of a typical Portland cement (Neville 1978, p. 11)

Typical oxide composition	(%)	Hence, calculated compound composition	(%)
CaO	63	C_3A	10.8
SiO_2	20	C_3S	54.1
Al_2O_3	6	C_2S	16.6
Fe_2O_3	3	C_4AF	9.1
MgO	1½	Minor compounds	-
So3	2		
K_2O } Na_2O }	1		
Others	1		
Loss on ignition	2		
Insoluble residue	½		

Table 3: Classification of pore sizes in hydrated cement paste (Mindess and Young 1981, p. 99)

Designation	Diameter	Description	Role of Water	Paste Properties Affected
Capillary pores	10-0.05 μm (50 nm)	Large capillaries	Behaves as bulk water	Strength: permeability
	50~10 nm	Medium capillaires	Moderate surface tension forces generated	Strength: permeability; shrinkage at high humidities
Gel pores	10-2.5 nm	Small (gel) capillaries	Strong surface tension forces generated	Shrinkage to 50% RH
	2.5~-.5 nm	Micropores	Strongly absorbed water; no menisci form	Shrinkage; creep
	<~0.5 nm	Micropores "interlayer"	Structural water involved in bonding	Shinkage; creep

Table 4: Classification of Moisture Retention in Solids (Keey 1972, p 22)

Item	Chemically attached moisture (stoichiometric)		Physically attached moisture (non-stoichiometric)					Mechanically attached moisutre (non-stoichiometric)		
Order of bond energy, kJ/k mol	Ionic	Molecular	Adsorptive			Osmotic	Structural	Microcapillary	Macrocapillary	Unbound
		5000	3000					≥ 100	≥ 100	0
Conditions under which bond forms	hydration	crystallisation	hydrogen-bonding/ solvation	physiochemical absorportion		osmotic imbibition	dissolution in gels	capillary condensation		surface condensation
Reason for bond constitution	electrostatic field		molecular-force field			osmotic pressure	moisture inclusion on gelling	meniscus in capillary		surface adhesion
	between ions	between molecules	all molecules	outer/inner surface	inner surface					
Condition to disturb bond	chemical reaction	roasting	evaporation	desorption	deadsorption	more concentrated ambient solution	evaporation or mechanical dewatering	evaporation from capillaries into less humid air		surface evaporation into less humid air
Changes in character of solid skeleton and associated moisture	new compound is formed	new crystals are formed	moisture enters as solvate	moisture held in inter-miscellar pores	moisture held in molecular layers	large changes in physical appearance and properties, e.g. cohesive strength		little changes in moisture properties and nearly no changes in solid skeleton		
Examples	hydrate of lime	inorganic crystals	ionic/ molecular solutions	hydrophilic materials	hydrophobic materials	plant cells with aqueous solutions	gels with about 1% solid	capillary-porous bodies		non-porous hydrophilic materials
								$r \leq 10^{-7}$ m	$r \geq 10^{-7}$ m	

Table 5: Relative Humidity above saturated solutions of salts in water at 20°C (Keey 1972, p 29)

Material		Relative humidity, ψ
Lithium cloride	LiCl	0.0126
Potassium acetate	CH_3COOK	0.20
Calcium chloride	$CaCl_2$	0.323
Potassium carbonate	K_2CO_3	0.45
Sodium hydrogen sulphate	$NaHSO_4$	0.52
Sodium nitrate	$NaNO_2$	0.66
Sodium chlorate	$NaClO_3$	0.75
Ammonium chloride	NH_4Cl	0.792
Potassium bromide	KBr	0.84
Potassium chromate	K_2CrO_4	0.88
Potassium bromate	$NaBrO_3$	0.92
Sodium sulphate heptahydrate	$Na_2SO4\ 7\ H_2O$	0.95
Lead nitrate	$Pb(NO_3)_2$	0.98

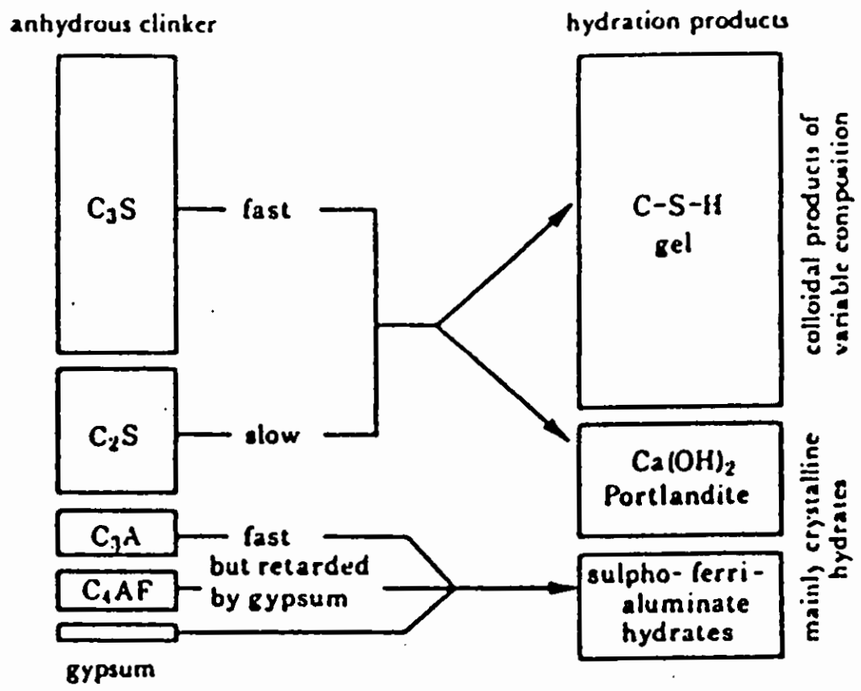

Figure 1: Summarised scheme of the hydration process. Schematic representation of the anhydrous constituents in Portland cement clinker and the products formed during hydration. The areas of the 'boxes' give the approximate volume proportions of the phases. (Double 1983, p.54)

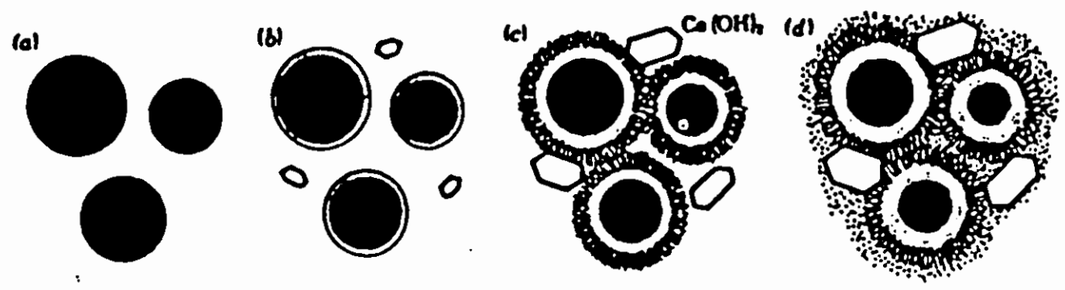

Figure 2: Schematic representation of the sequence of hydration of cement. (a) Cement grains in water. (b) Formation of protective colloidal coatings of C-S-H gel around cement grains. (c) Rupture of the protective coatings followed by secondary growth of C-S-H gel. (d) Later infilling of the microstructure by fine grained C-S-H gel and by growth of crystalline Calcium Hydroxide. (Double 1983, p.59)

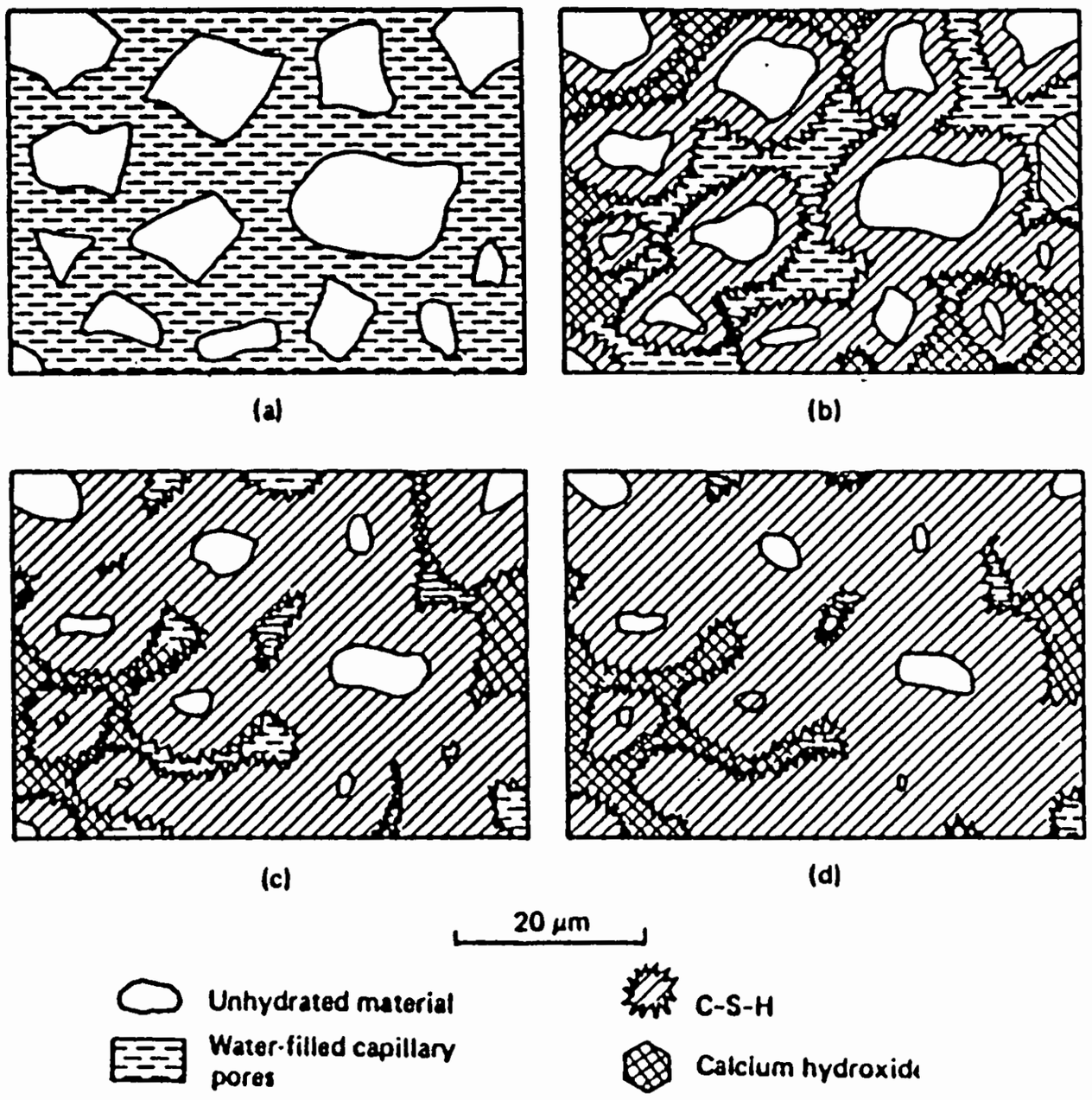

Figure 3: Schematic outline of microstructural development in Portland cement pastes. (Calcium Sulfoaluminates are included as part of C-S-H for convenience, although they will crystallise as separate phases.) (a) Initial mix. (b) 7 days. (c) 28 days. (d) 90 days. (Double 1983, p.59)

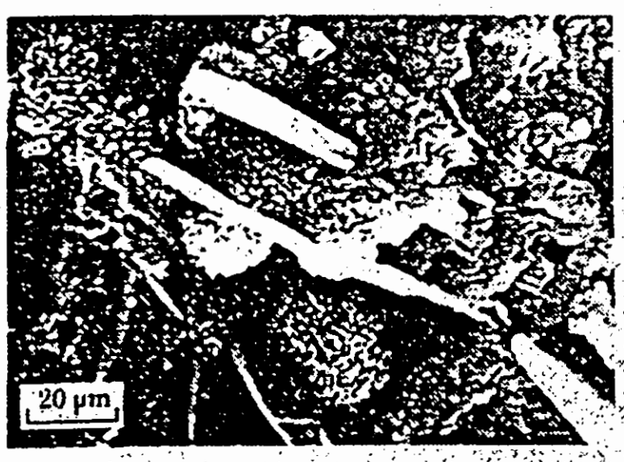

FIGURE 2. Fracture surface of a hardened cement paste showing fibrillar growth of C–S–H gel around the cement grains and plate-like crystals of calcium hydroxide (w/c ratio 0.7, age 40 days). Scanning electron micrograph.

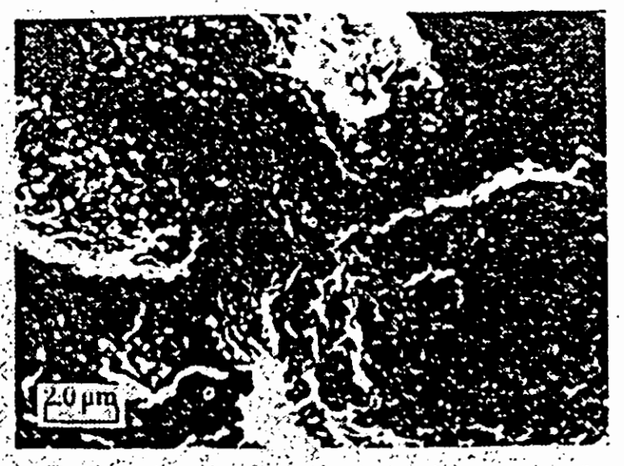

FIGURE 3. Fracture surface of a C_3S paste sample at early stages of hydration showing gel coatings around the particles and the beginning of the growth of fibrillar C–S–H gel product (w/c ratio 0.5, age 2 h). Scanning electron micrograph.

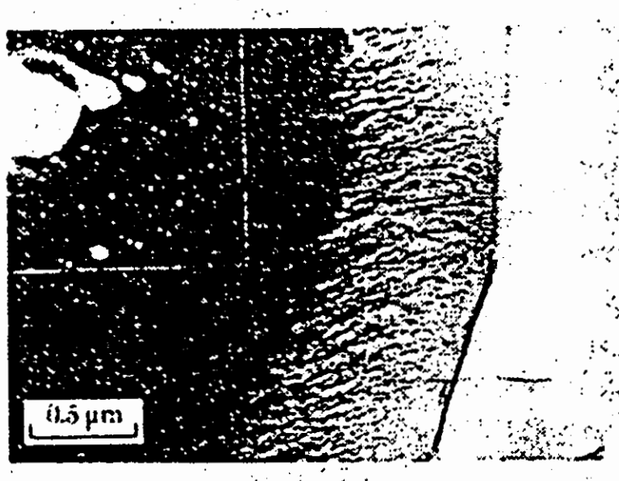

FIGURE 4. Colloidal gel coating formed on a grain of C_3S in a thinned slice of Portland cement clinker after dipping in water for 5 min. Transmission electron micrograph and selected area diffraction pattern (Groves 1981).

FIGURE 5. Secondary growth of C–S–H gel at the surfaces of cement grains after hydration for 21 h, the hydrate shows fibrillar and crumpled sheet type morphologies. Transmission electron micrograph.

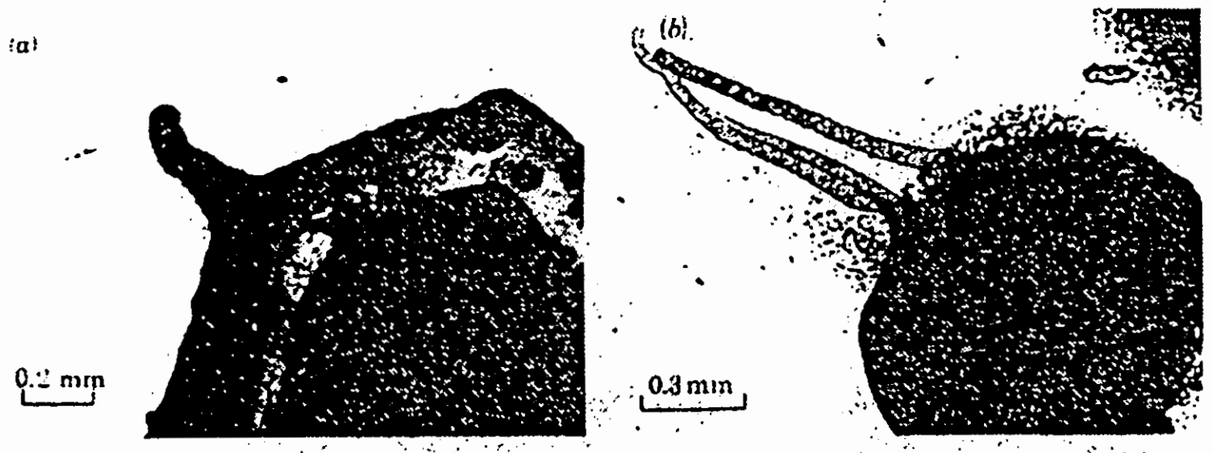

FIGURE 10. 'Silicate garden' obtained by immersing a grain of sodium silicate in dilute aqueous calcium nitrate solution. (*a*) Formation of colloidal C–S–H gel coating around the dissolving grain. (*b*) Tubular growths formed after osmotic rupture of the gel coating. Optical micrographs.

Figure 4: Micrographs of hydrating cement pastes
(Double 1983, p.54)

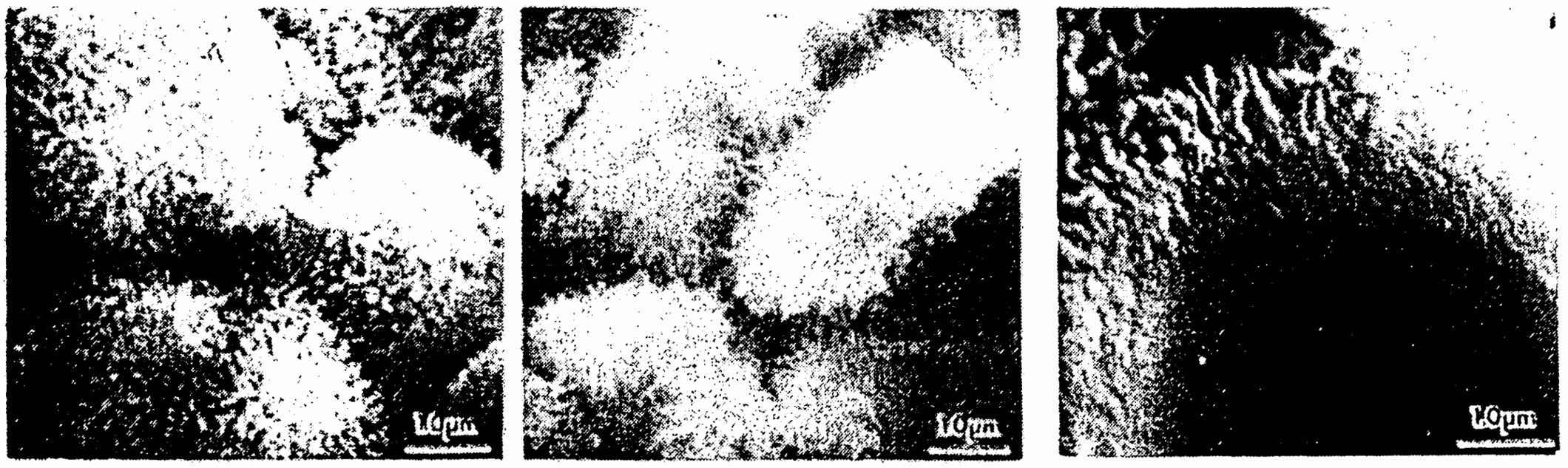

Figure 5: Micrographs of hydrating cement pastes
(Mindess and Young 1981, p.96)

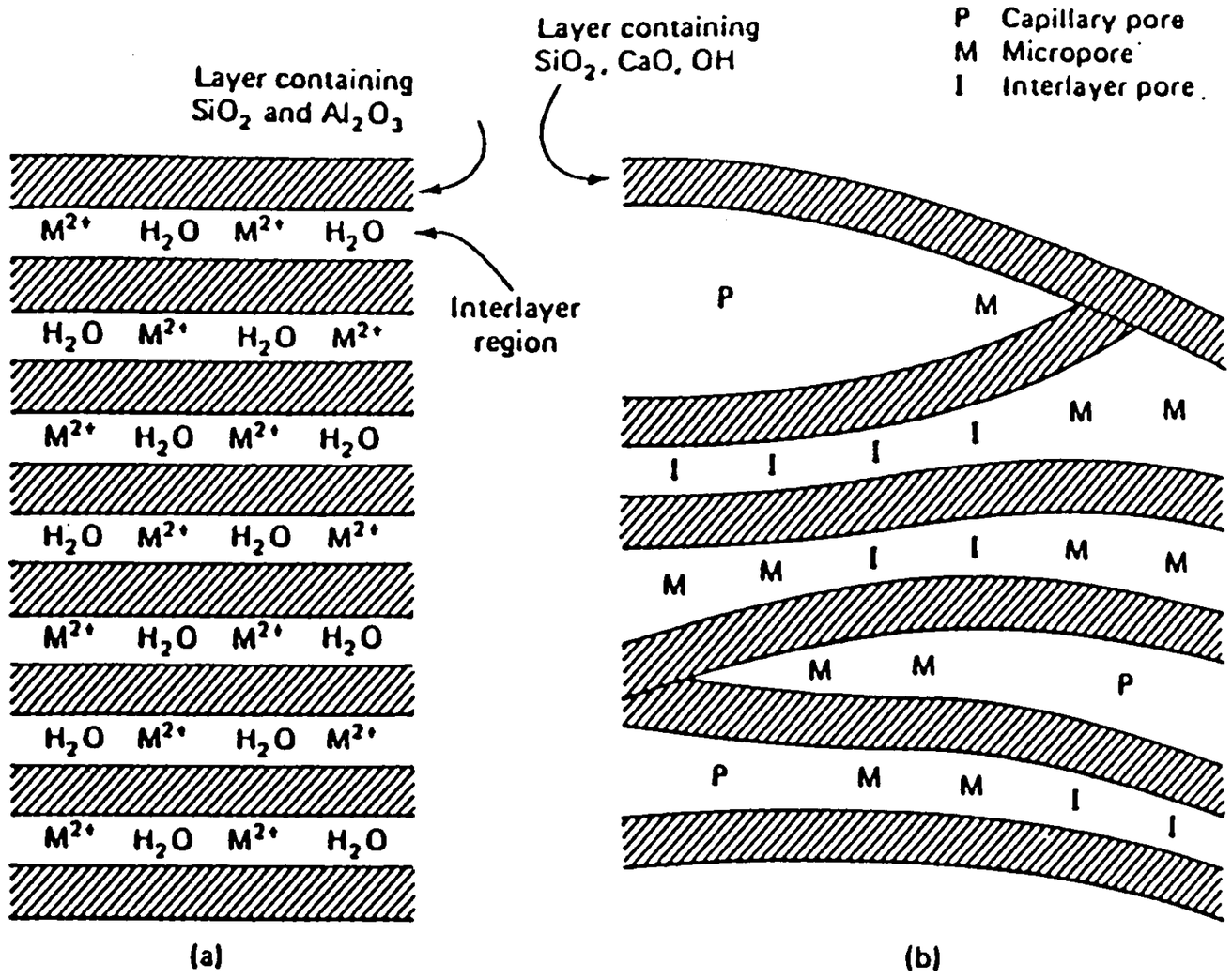

Figure 6: Schematic model of C-S-H in cement paste. (a) Well crystallised clay mineral. (b)Poorly crystallised C-S-H. (Mindess and Young 1981, p.89)

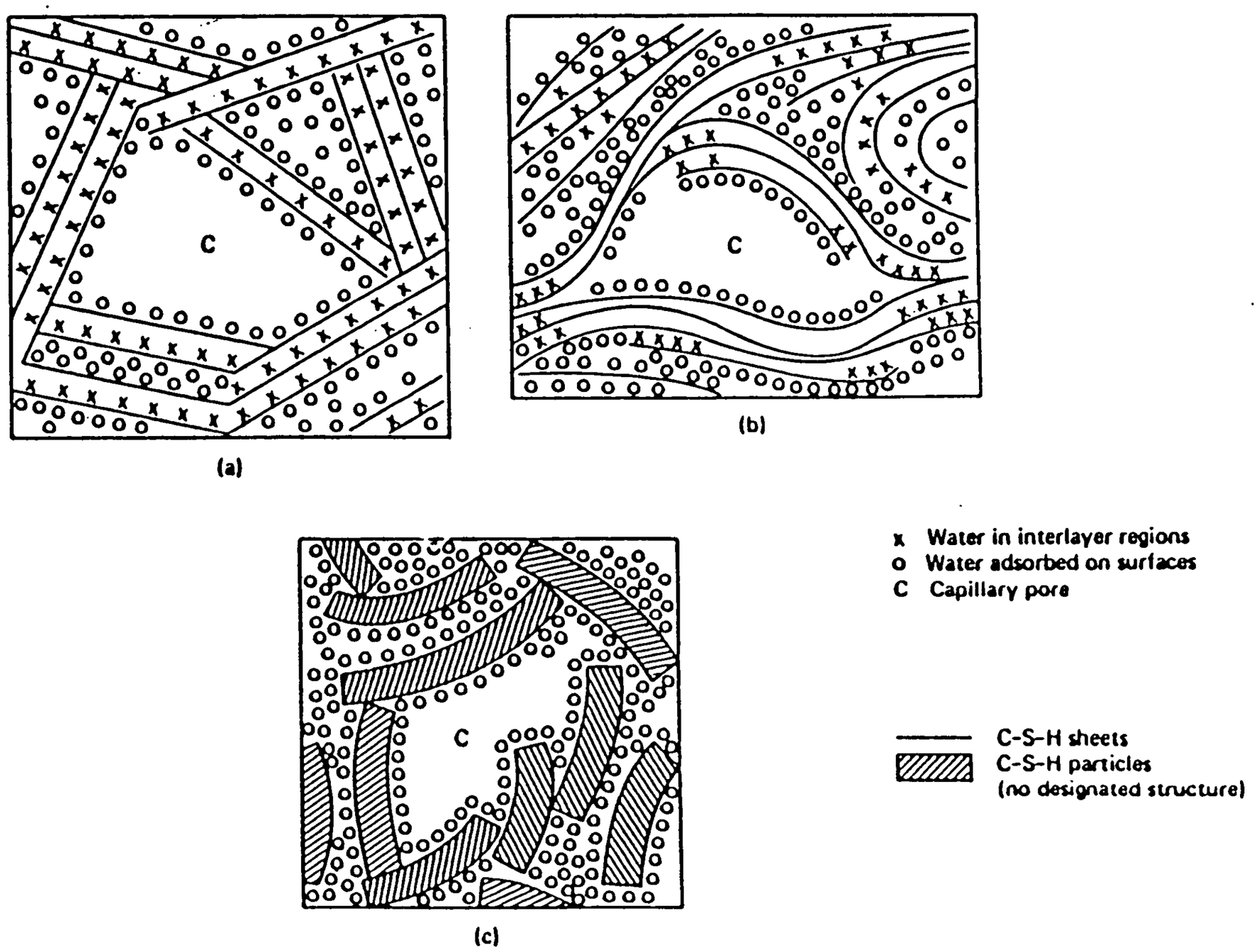

Figure 7: Schematic representation of calcium silicon hydrate
(a) Powers-Brunauer, adapted from T.C. Powers, *The Physical Structure and Engineering Properties of Concrete*, Bulletin No. 90, Portland Cement Association, Sokie, Ill., 1958, and S. Brunauer, *American Scientist*, Vol. 50, No. 1, 1962, pp.210-229. (b) Feldman-Sereda, from R. F. Feldman and P. J. Sereda, *Engineering Journal (Canada)*, Vol. 53, No. 8/9, 1970, pp.53-59. (c) Munich, adapted from F. H. Whittman, *Cement Production and Use*, Publication No. 79-08, Engineering Foundation, New York, 1979, pp.143-161.
(Mindess and Young 1981, p.91)

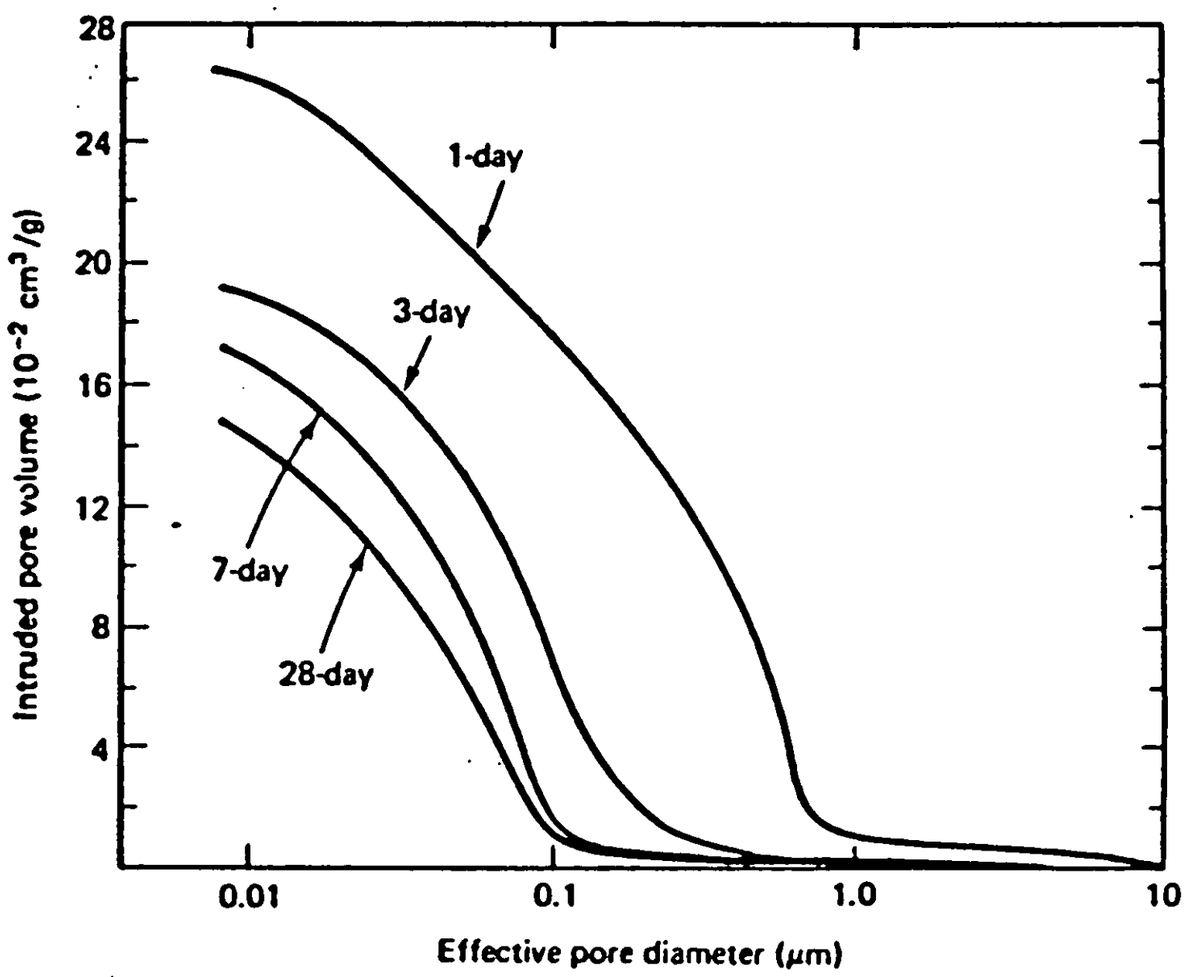

Figure 8: Shift in pore size distribution as hydration continues
(from Mindess and Young 1981, p.101) Mercury intrusion porosimetry curves for Portland cement pastes.
(originally from J. F. Young, *Powder Technology*, Vol. 9, 1974, pp.173-179.)

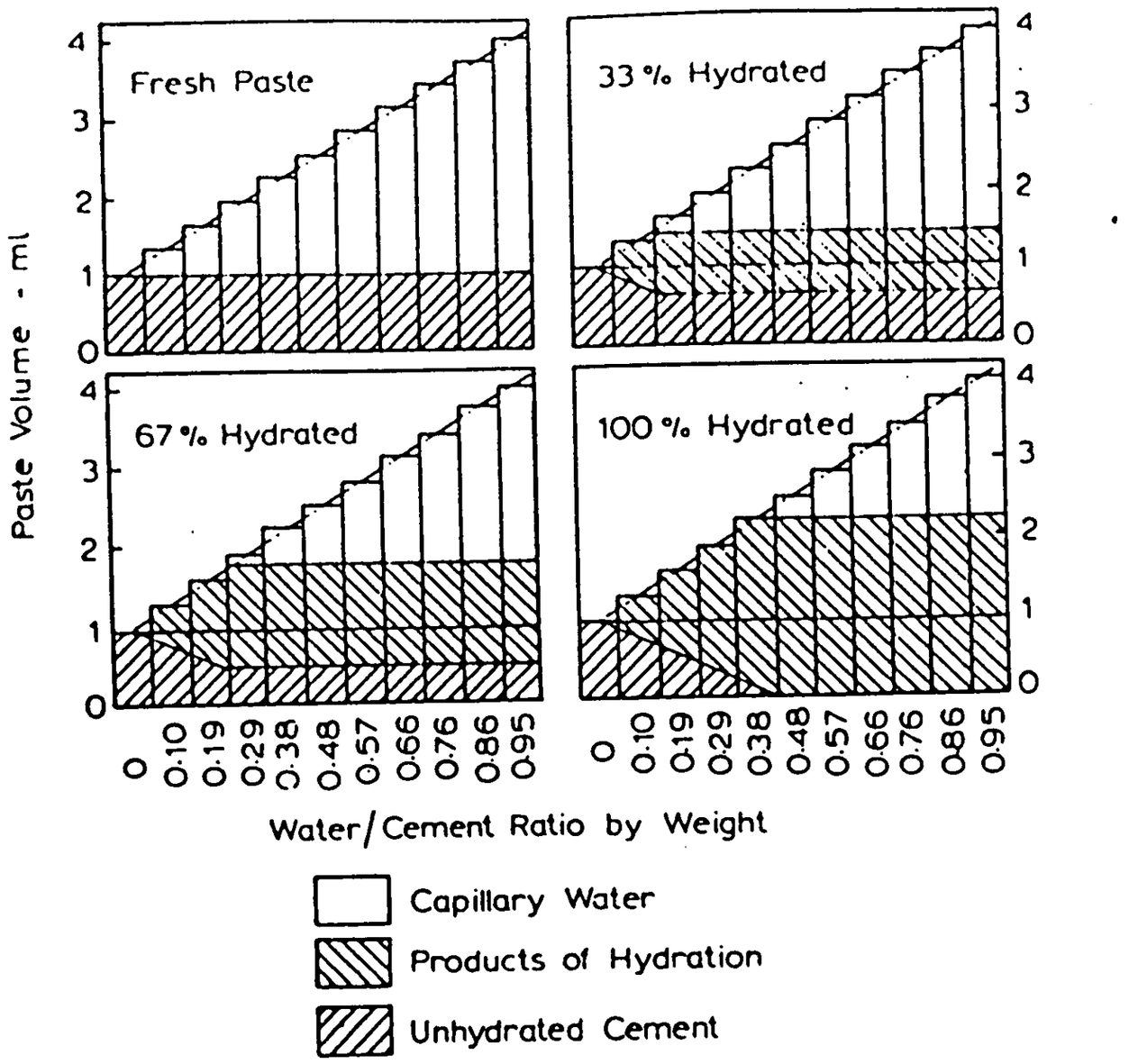

Figure 9 (a): Composition of cement paste at different stages of hydration (The percentage indicated applies only to pastes with enough water-filled space to accommodate the products at the degree of hydration indicated.)
(Neville 1981, p.30)

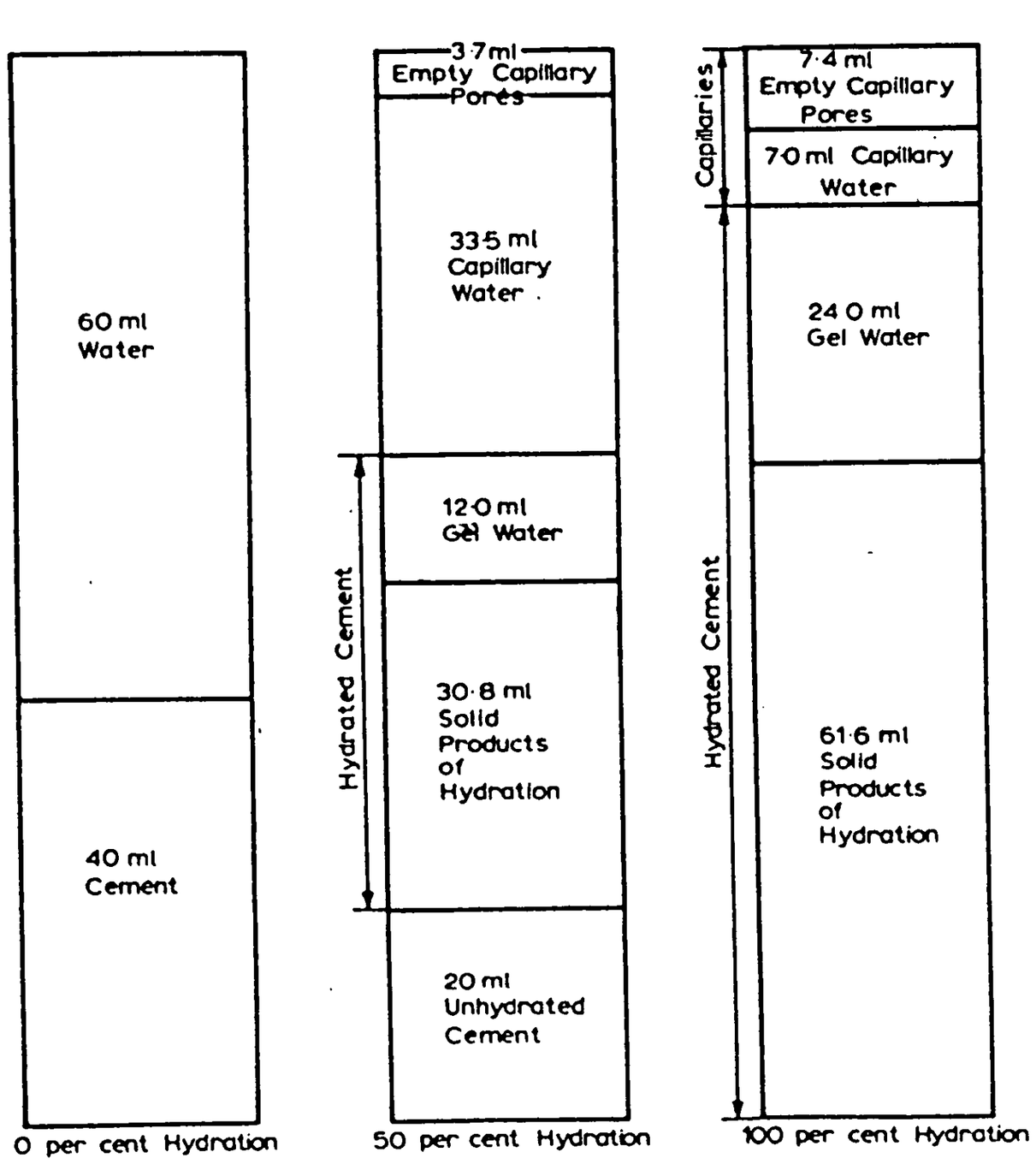

Figure 9 (b): Volumetric proportions of cement paste at different stages of hydration
(Neville 1981, p.30)

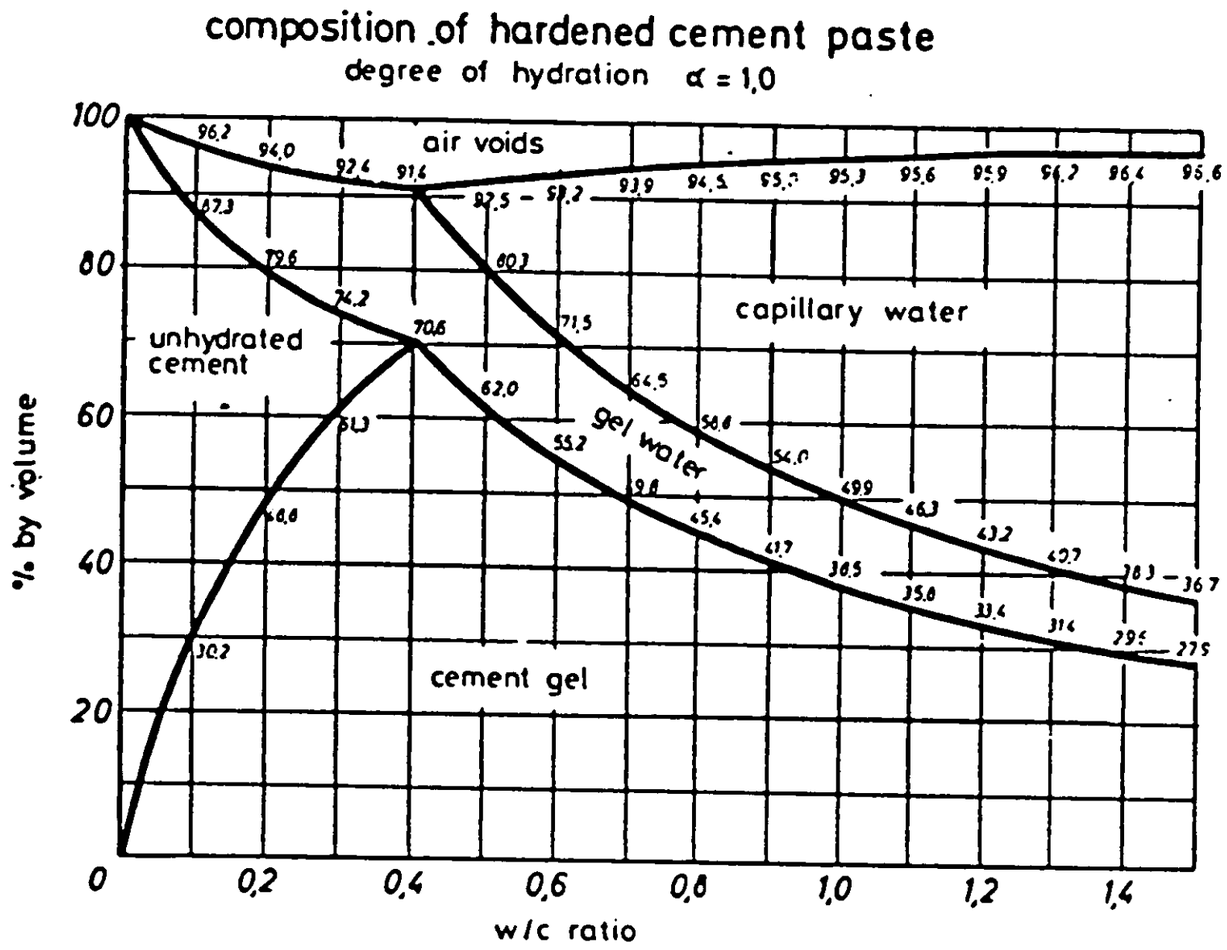

Figure 10: **Composition of fully hydrated cement paste as a function of w/c ratio, 100% hydration**
(Czernin 1980 p.63)

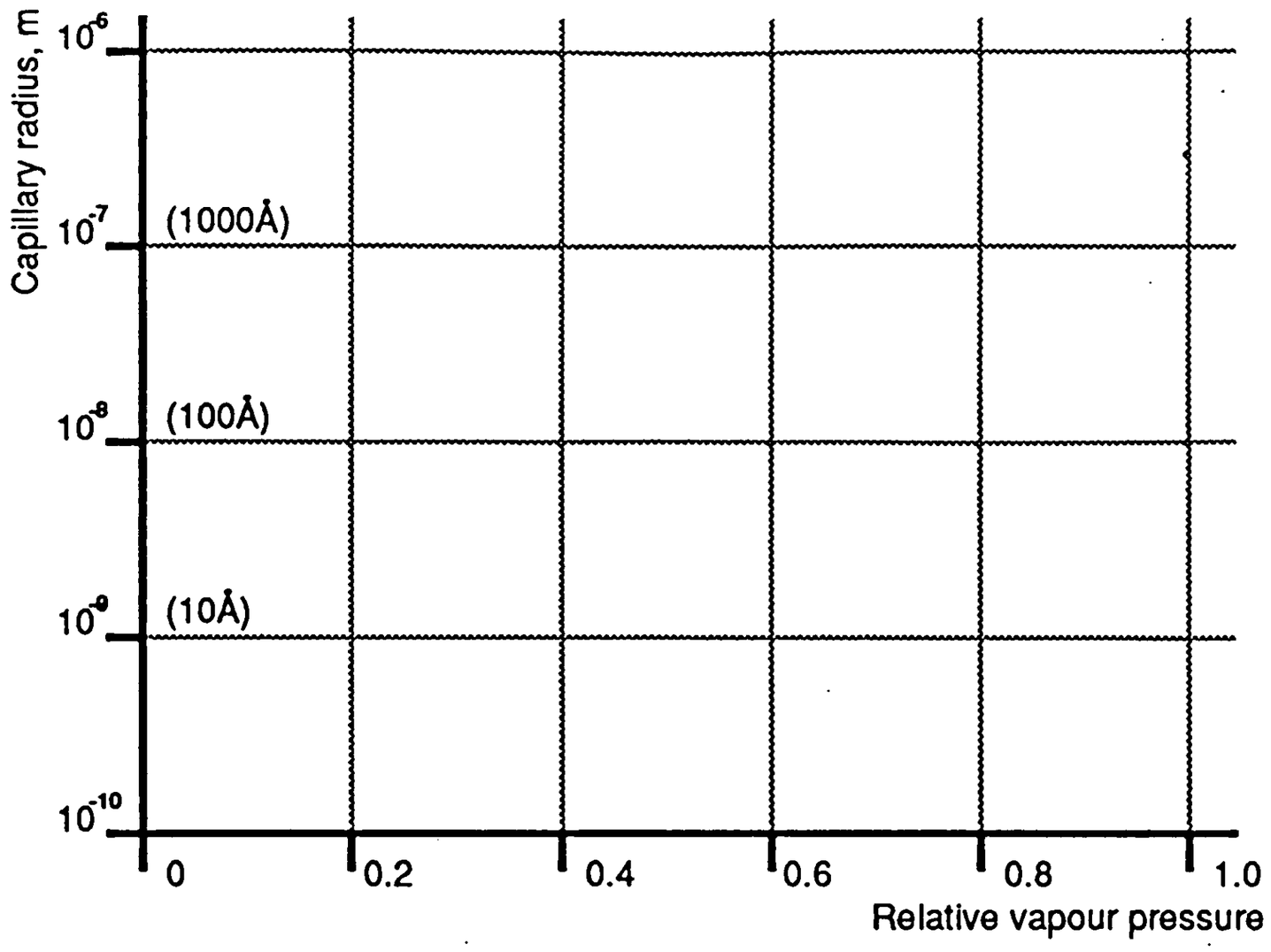

Figure 11 (a): Calculated equilibrium vapour pressures for capillaries of given radii
(McGlone 1990)

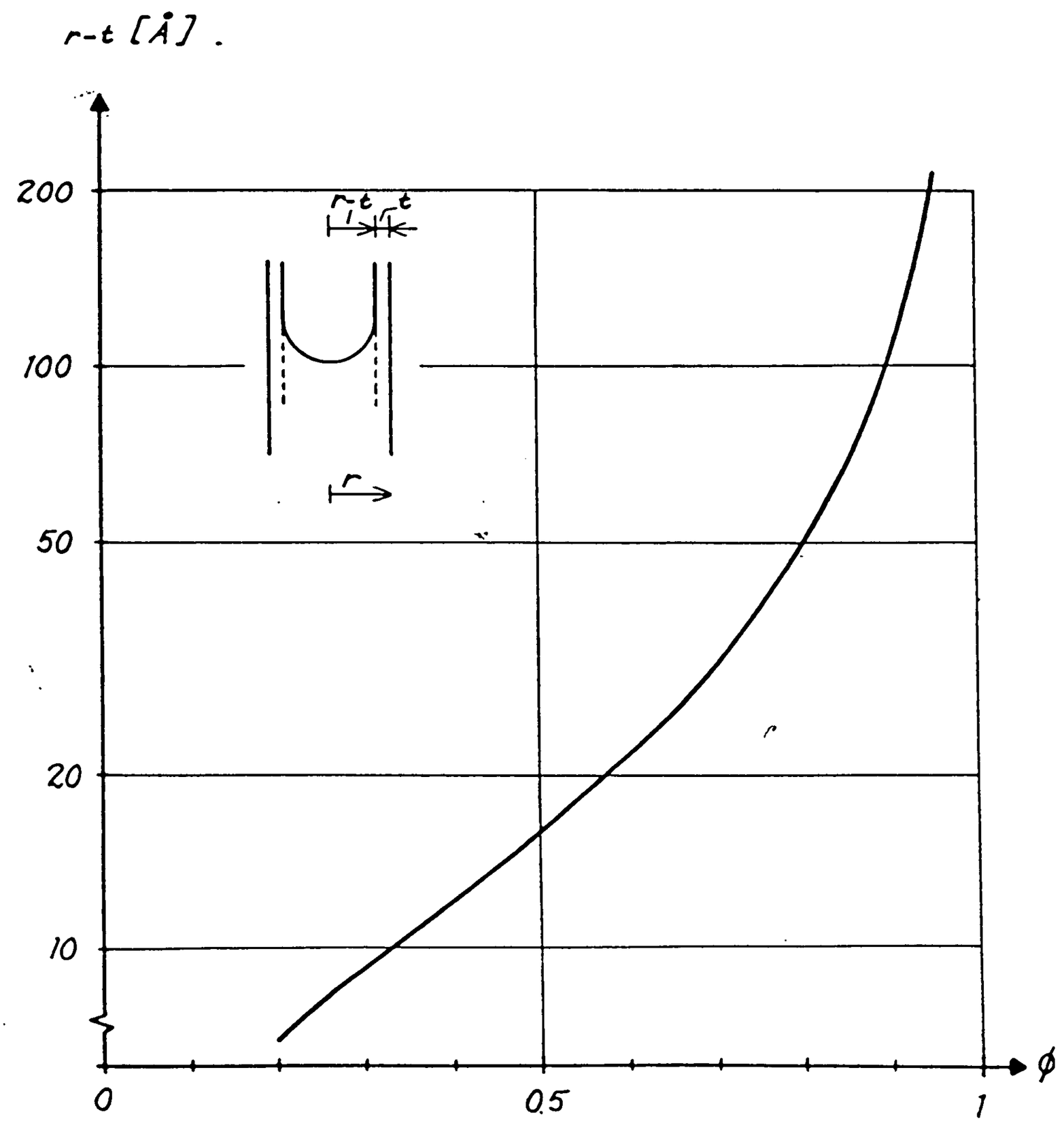

Figure 11 (b): Thickness of absorbed water film as a function of relative humidity
(Nilsson 1979 p.22)

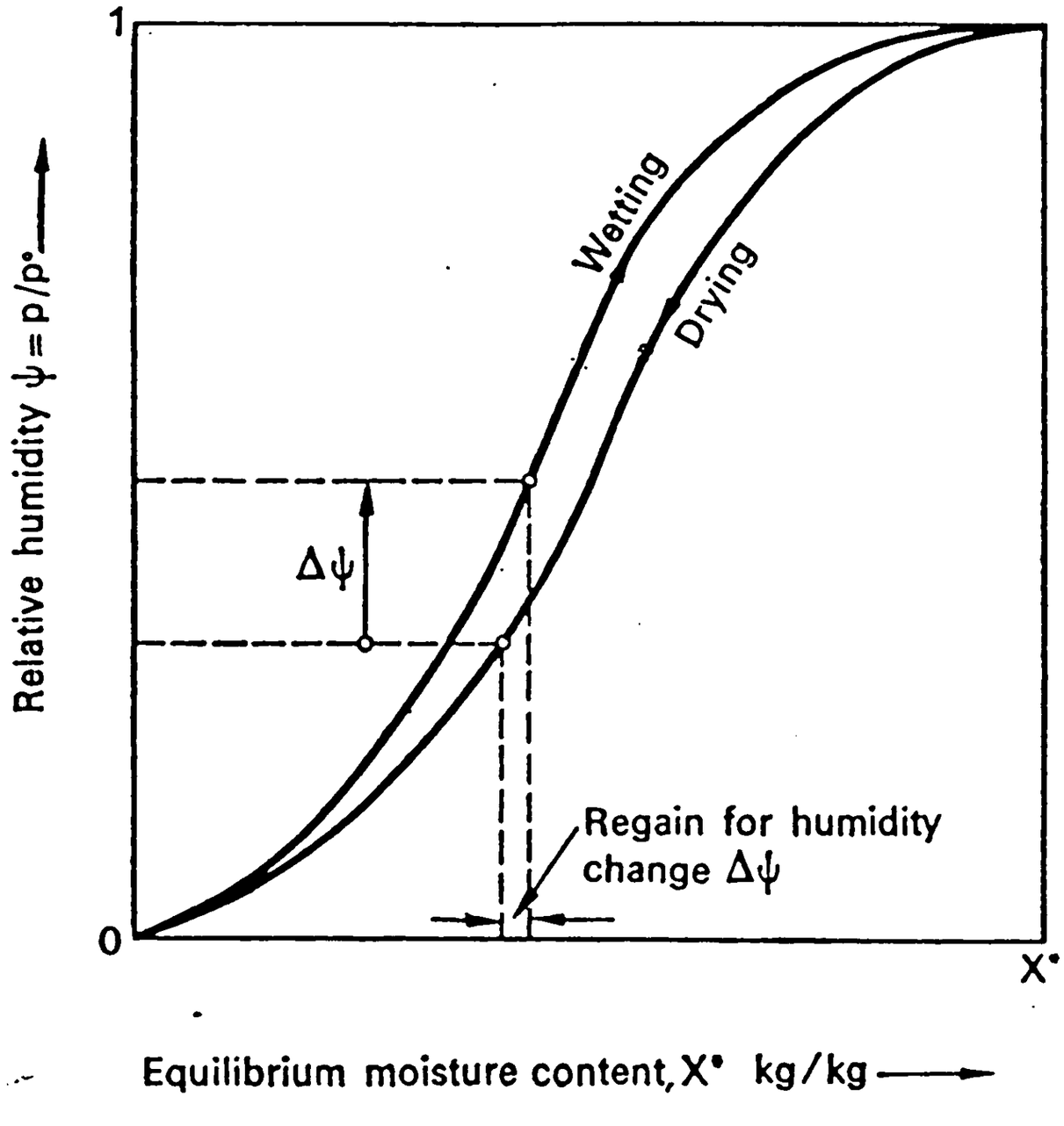

Figure 12: Sorption behaviour of a hygroscopic solid
(Keey 1972 p.24)

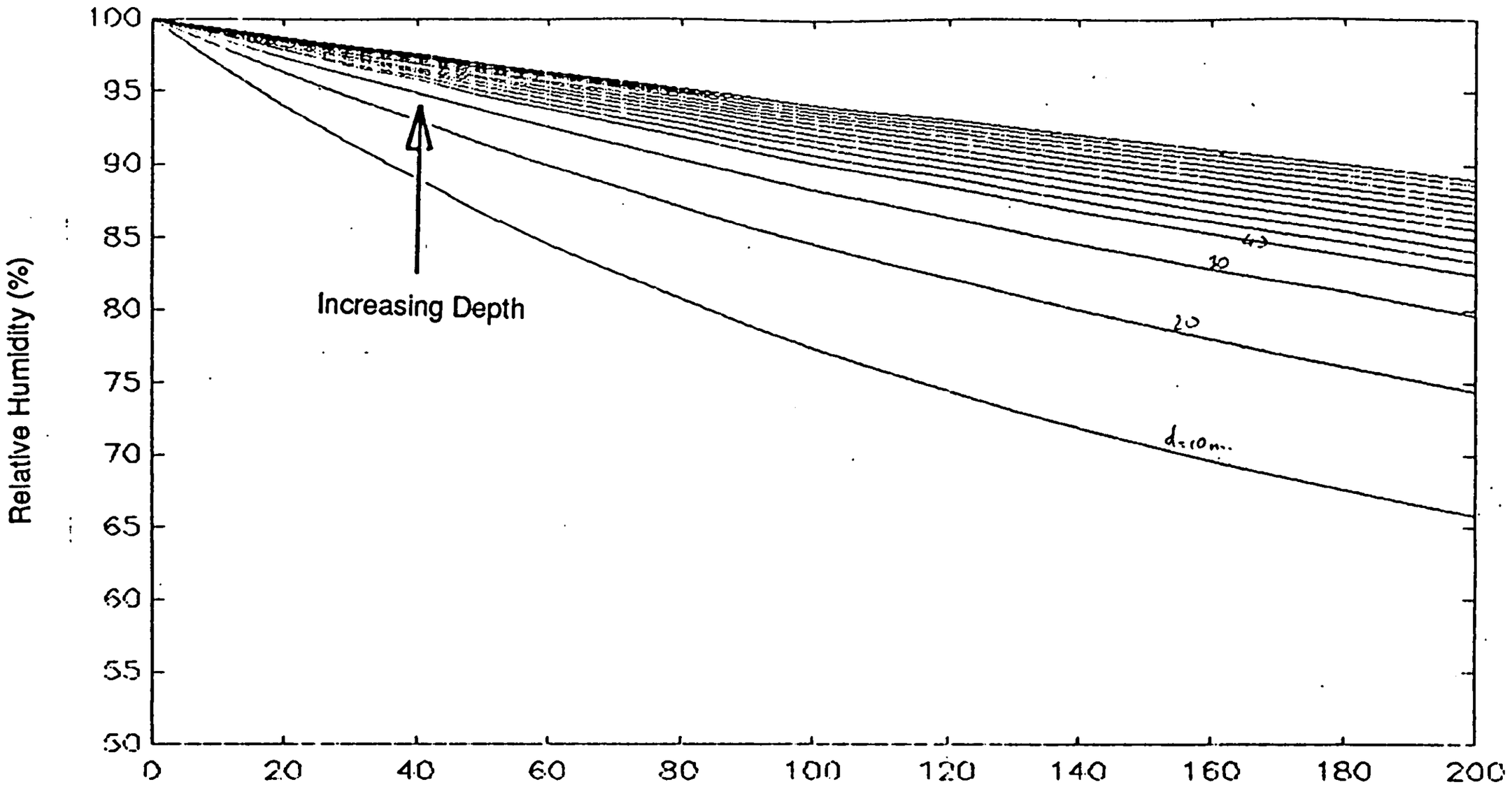

(a) Relative humidity vs time and depth, ambRH = 40%

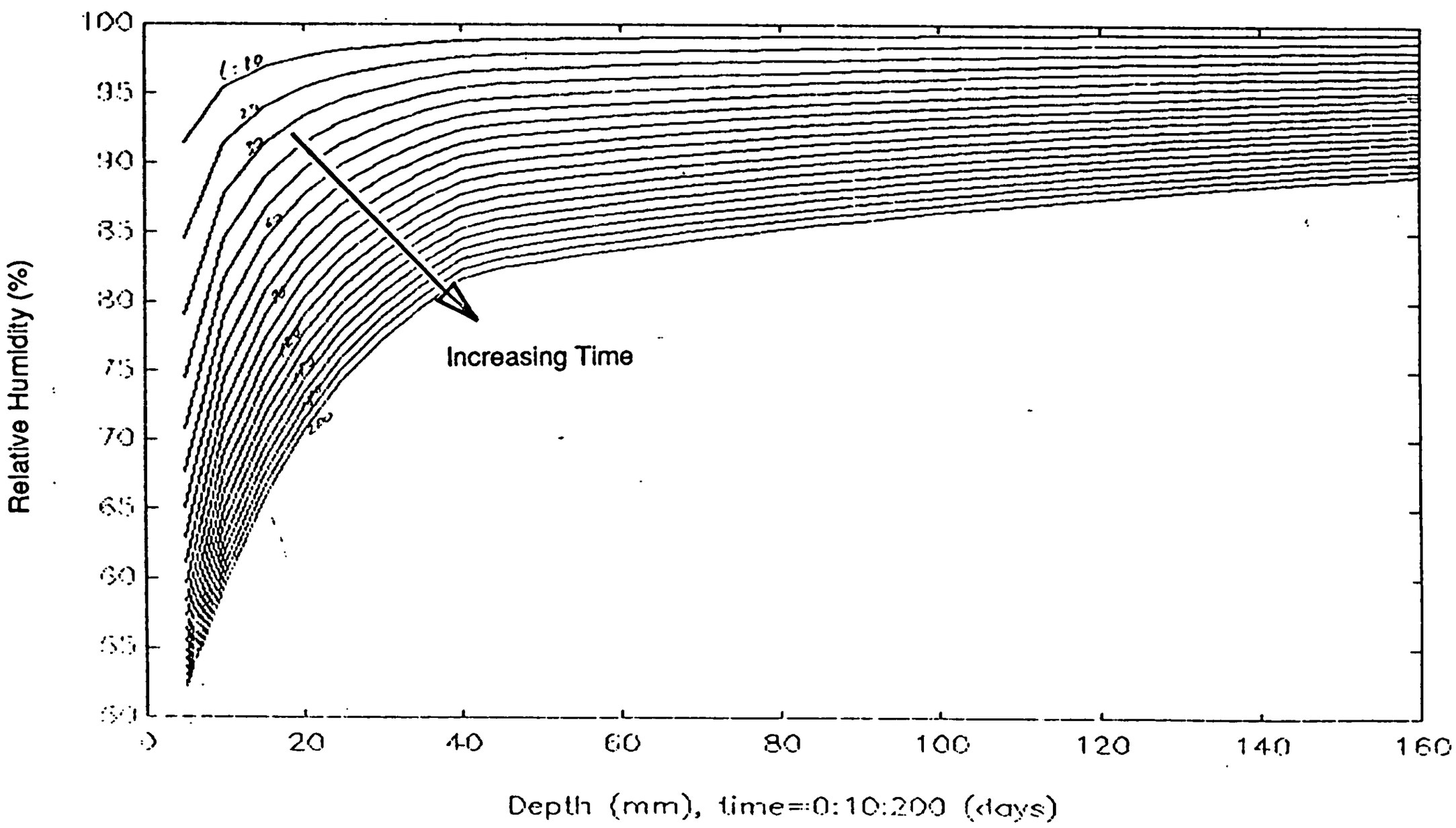

(b) Relative humidity vs depth and time, ambRH = 40%

Figure 13: Relative humidity profiles based on Parrott's (1991) formula

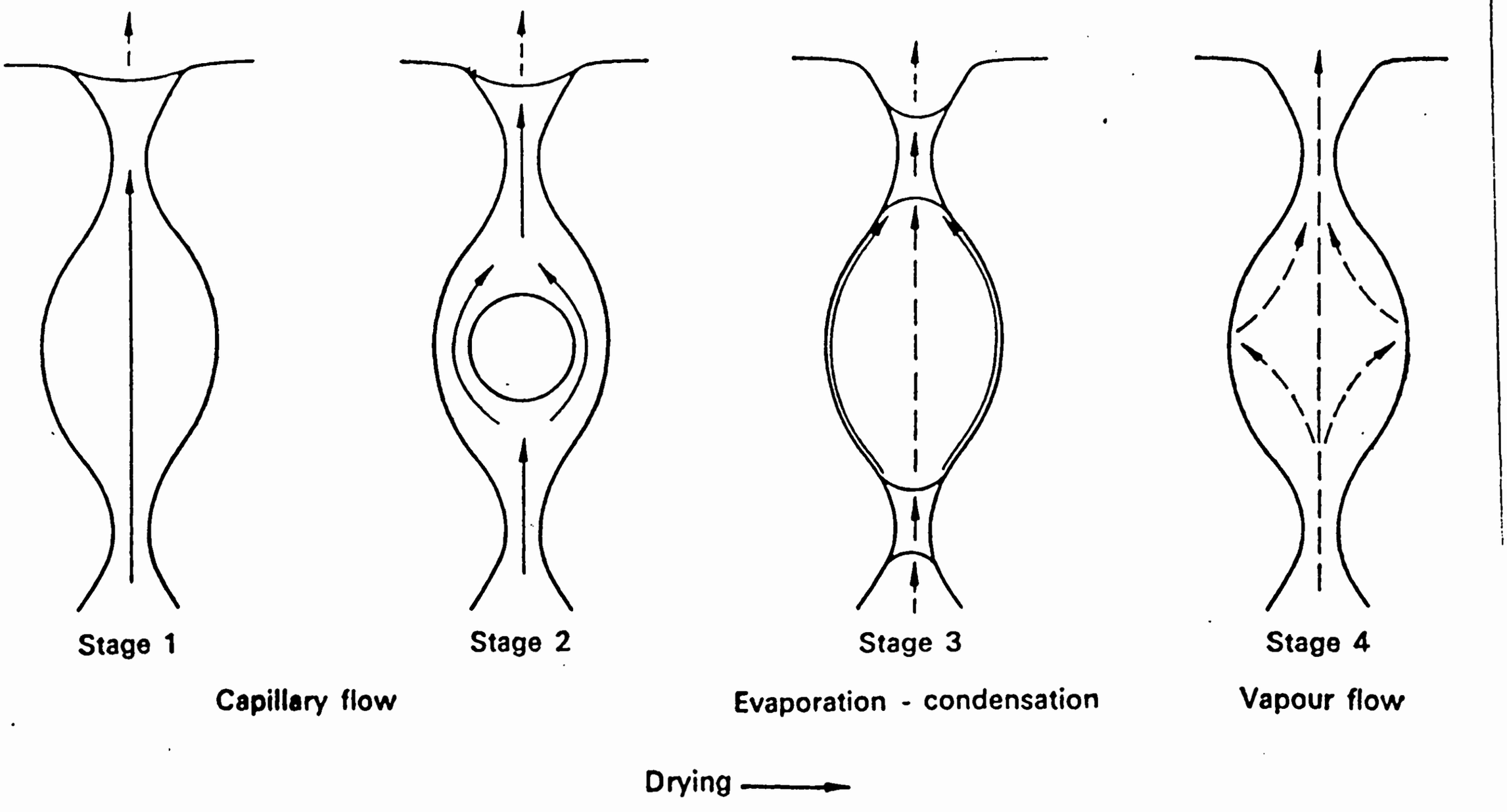

Figure 14: Four phases of moisture migration
(Keey 1972, p.127)

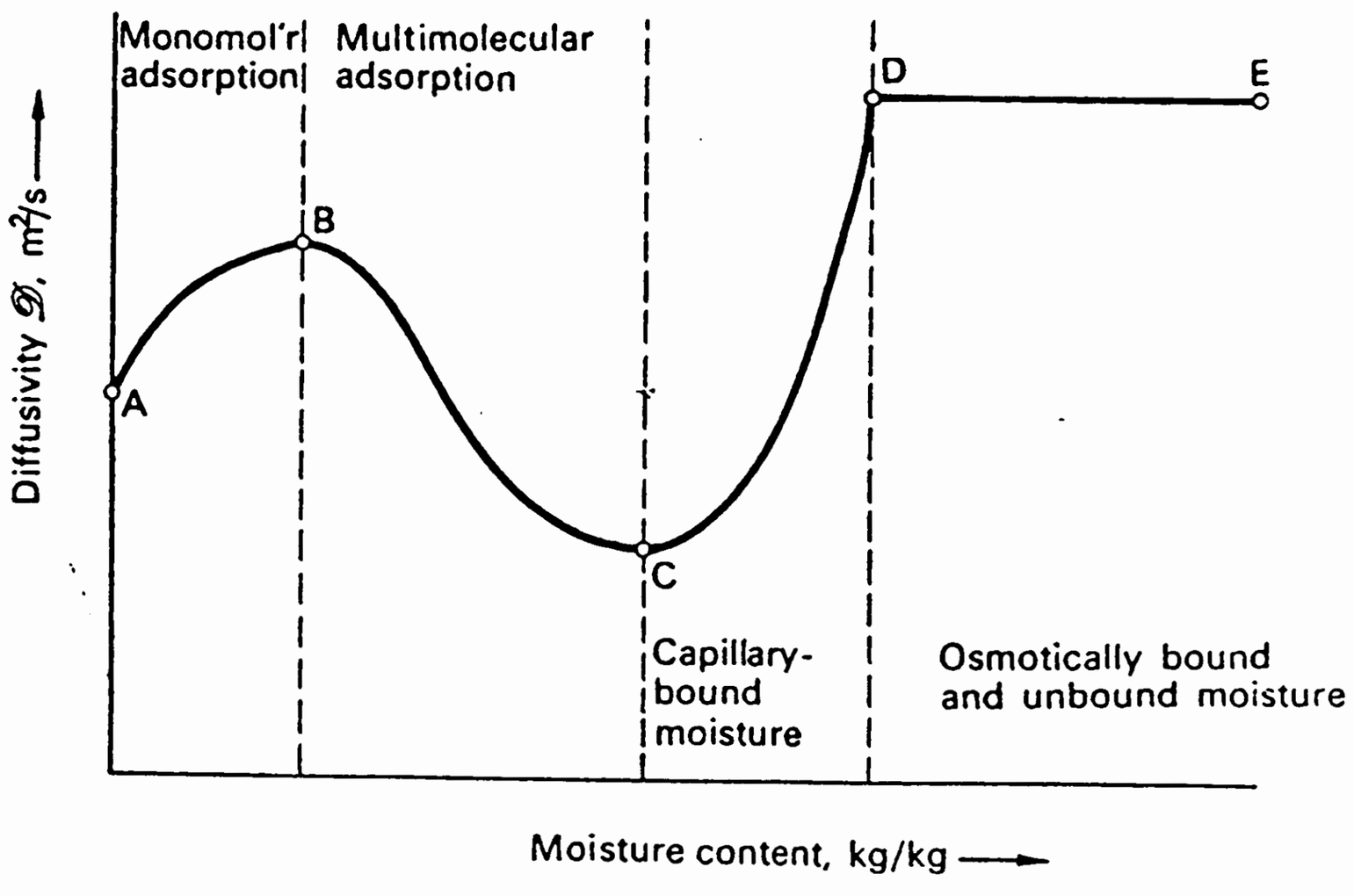

Figure 15: Variation of moisture diffusivity with moisture content
(Keey 1972, p.64)

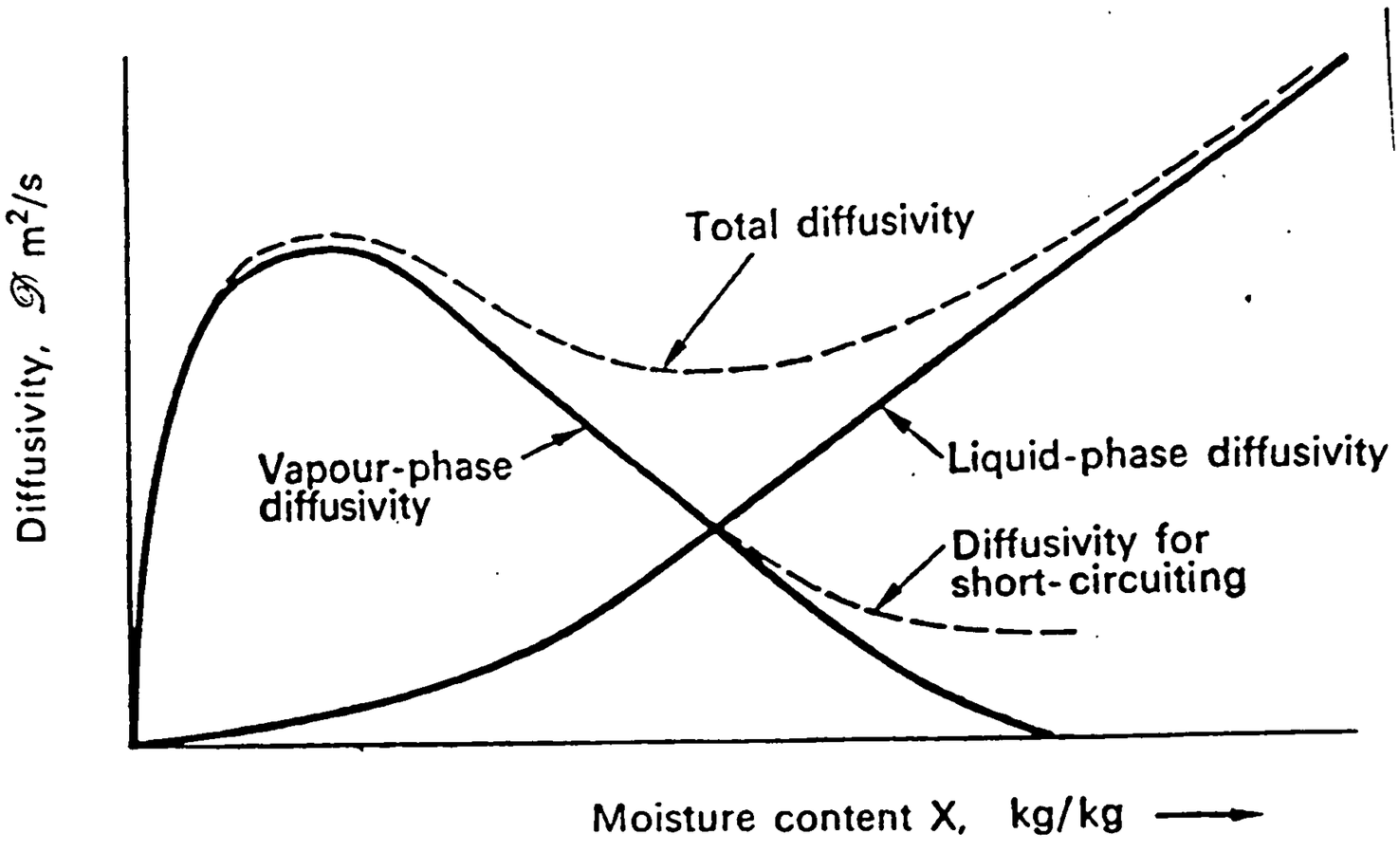

Figure 16: Two stage representation of the drying process
(Keey 1972, p.65)

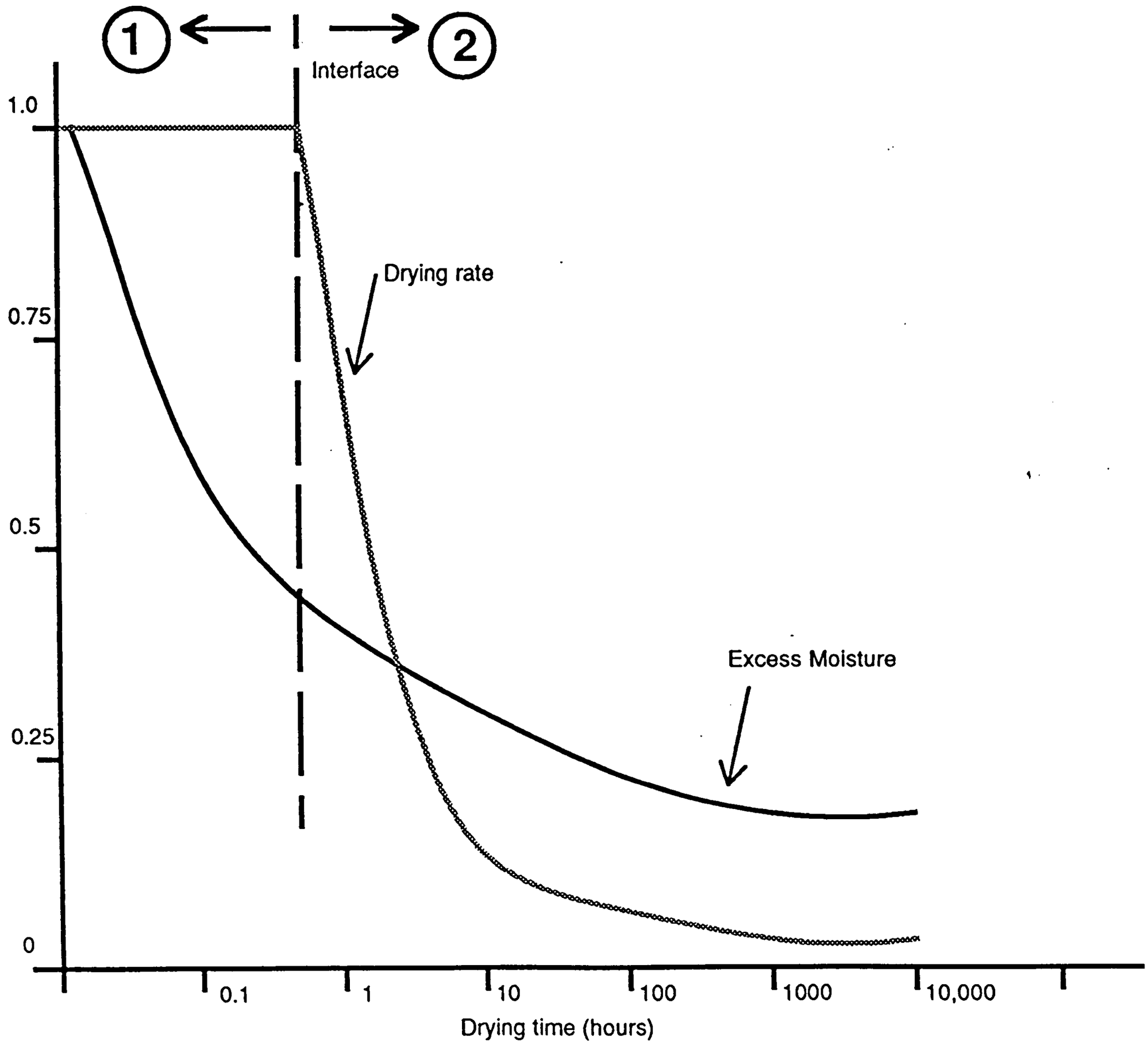

Figure 17: Wet-dry interface in drying concrete.
A representation of the two stages of drying. The ordinate axis is a relative scale for the variables plotted; excess moisture and drying rate, against their value at time zero.
(McGlone 1990)

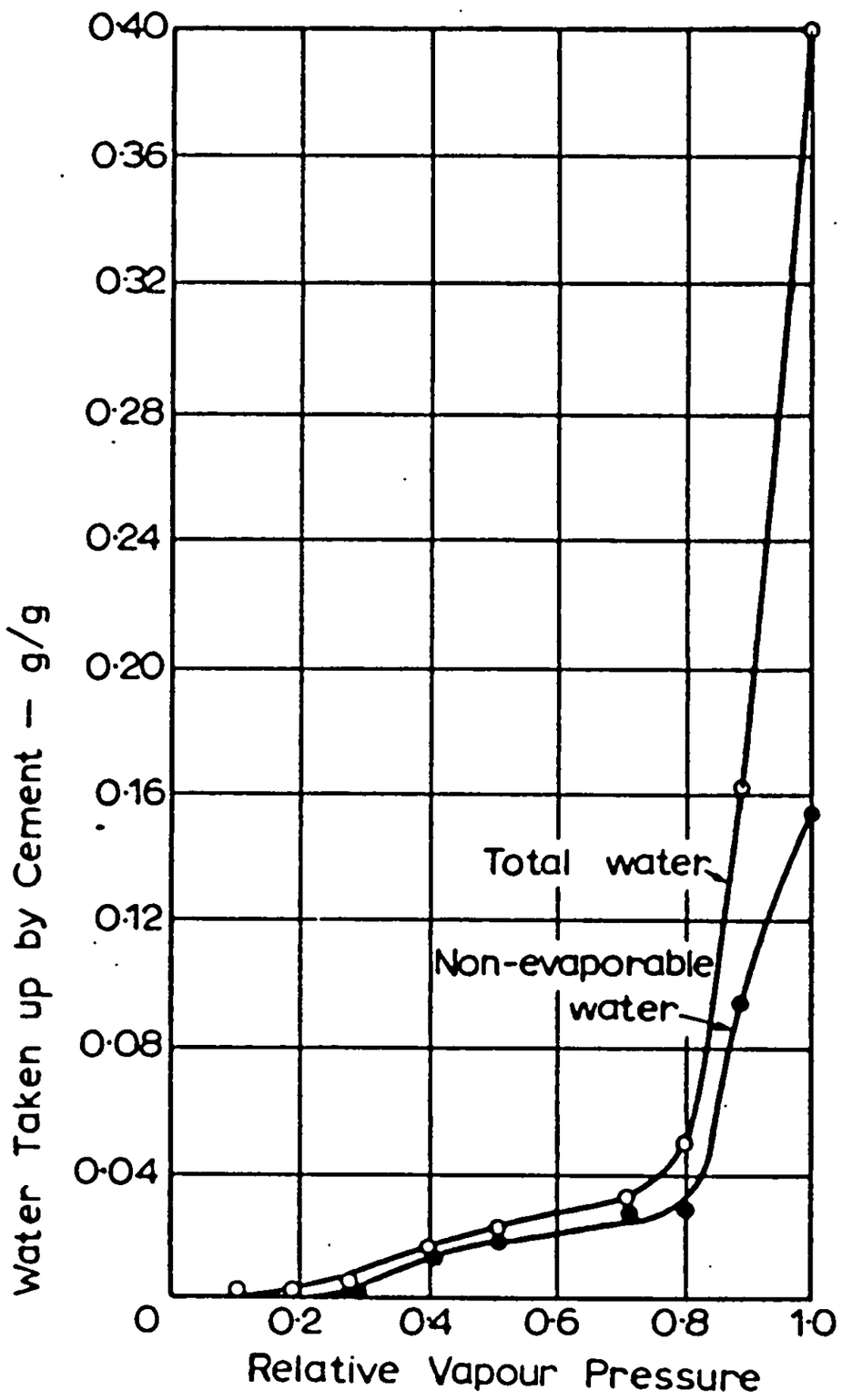

Figure 18: Water taken up by dry cement exposed to different ambient relative humidities
(Neville 1981, p.309)

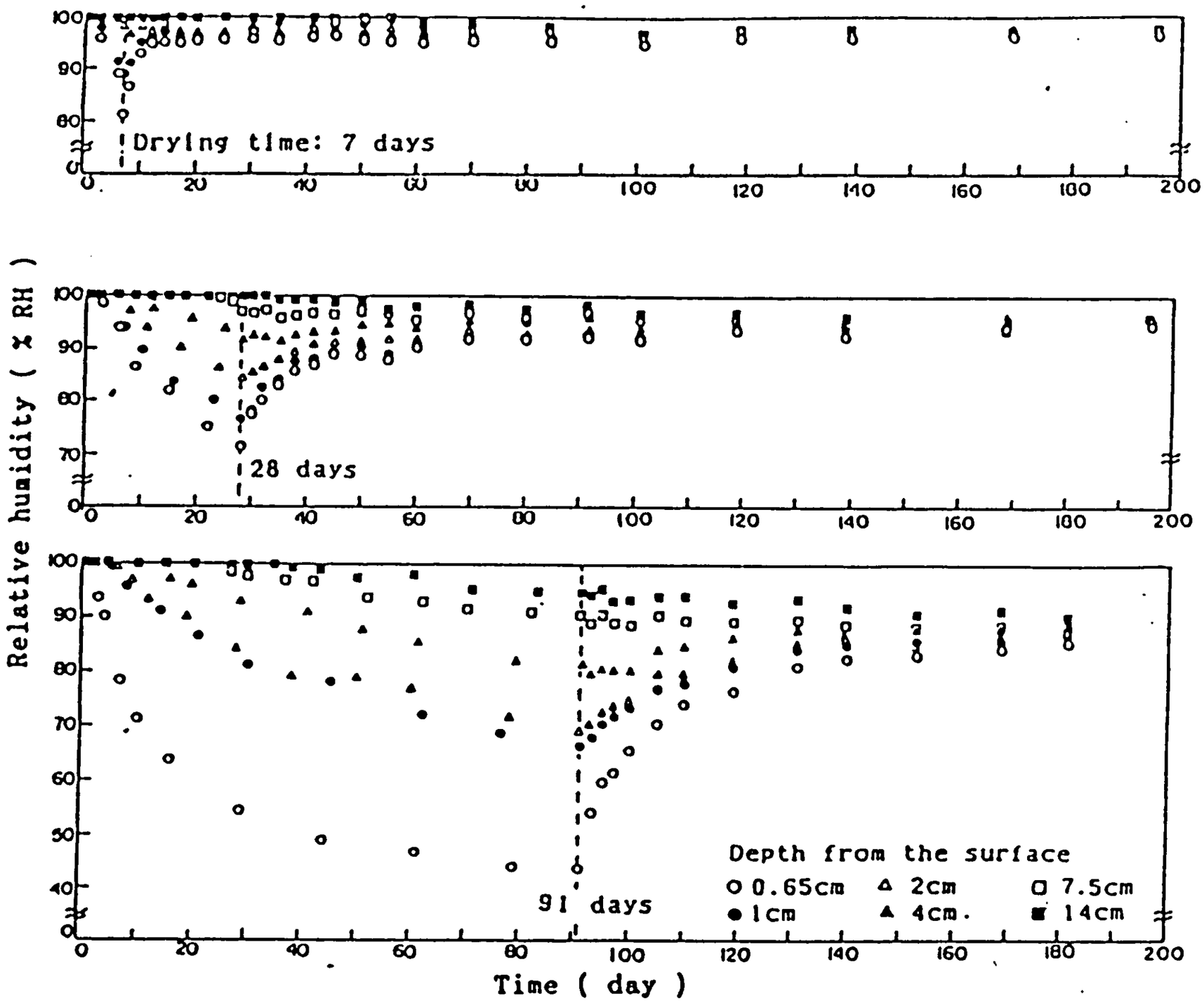

(a) Drying performed in 40% RH.

(b) Drying performed in 80% RH.

Figure 19: Changes of pore humidities in concrete before and after the drying surface is sealed
(Hashida et al. 1990, p.306)

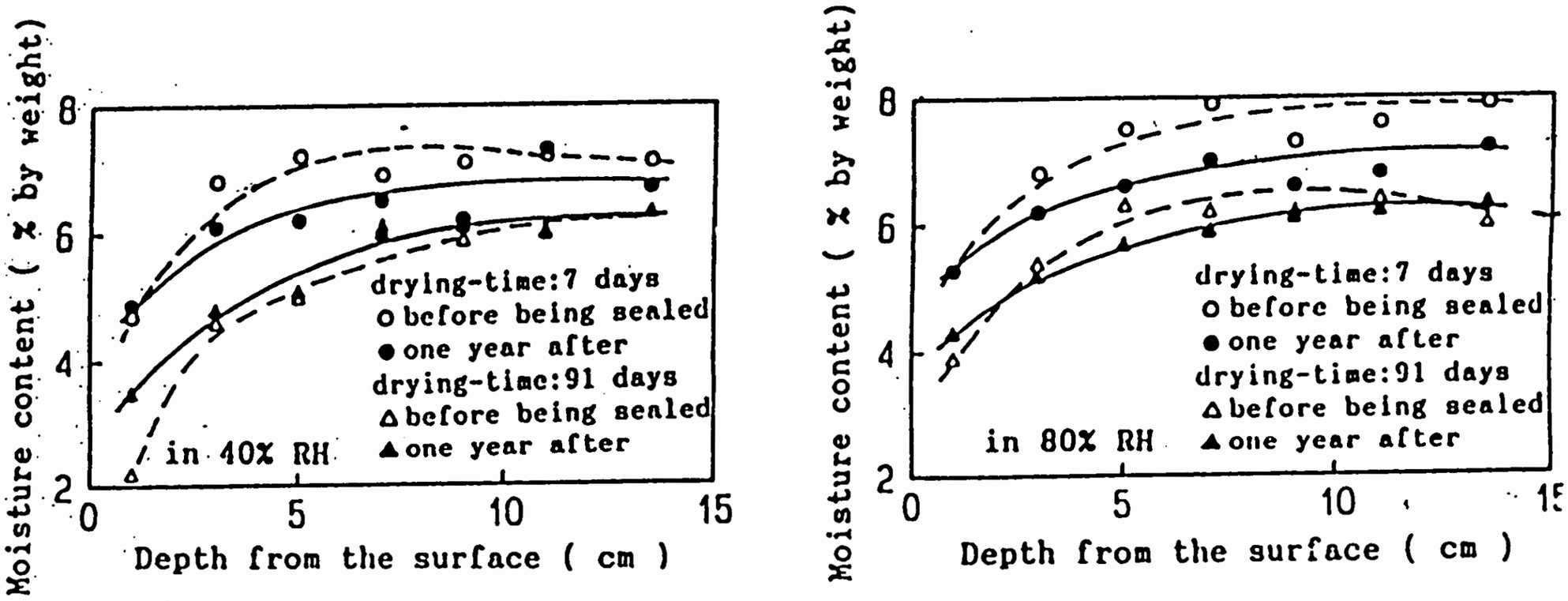

Figure 20: Distributions of the evaporable moisture content in concrete before and after the drying surface is sealed
(Hashida, et al. 1990, p.307)

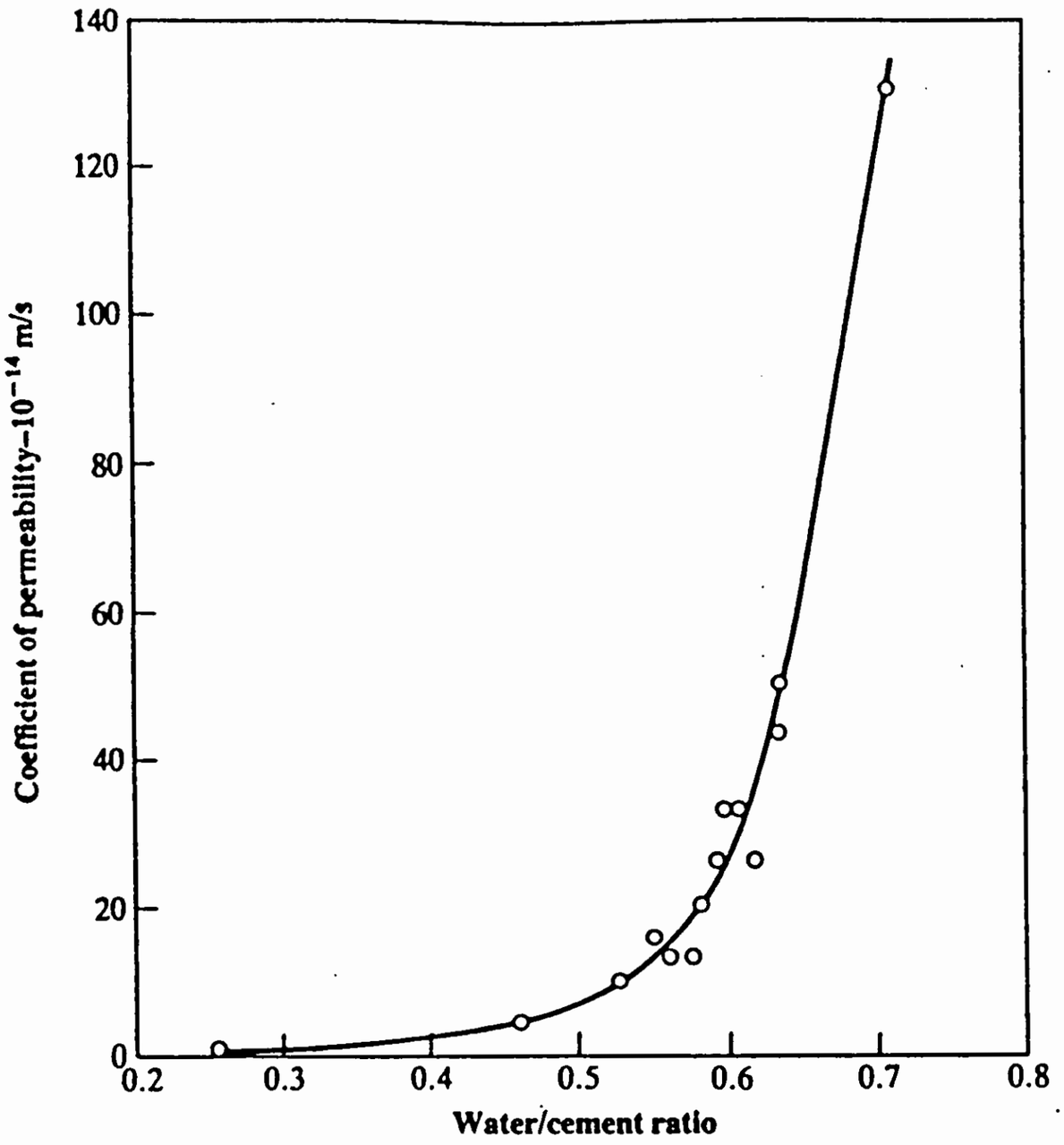

Figure 21: Relationship between permeability and w/c ratio for mature cement paste
(T. C. Powers, L. E. Copeland, J. C. Hayes and H. M. Mann, 1954 pp.285-98)

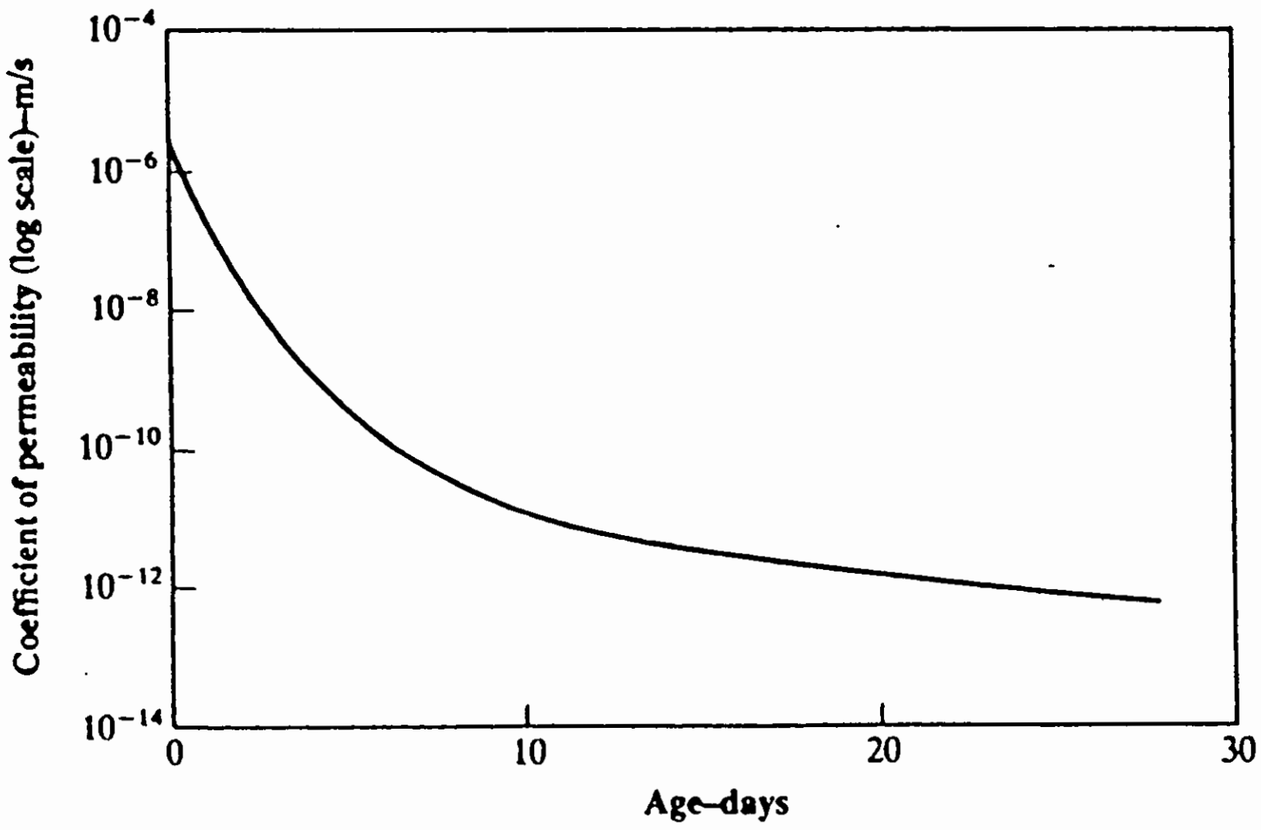

Figure 22: Reduction in permeability of cement paste with the progress of hydration; water/cement ratio = 0.7
T. C. Powers, L. E. Copeland, J. C. Hayes and H. M. Mann, *Permeability of Portland Cement Paste*, J. Amer. Conc. Inst., 51, pp.285-98, Nov. 1954.

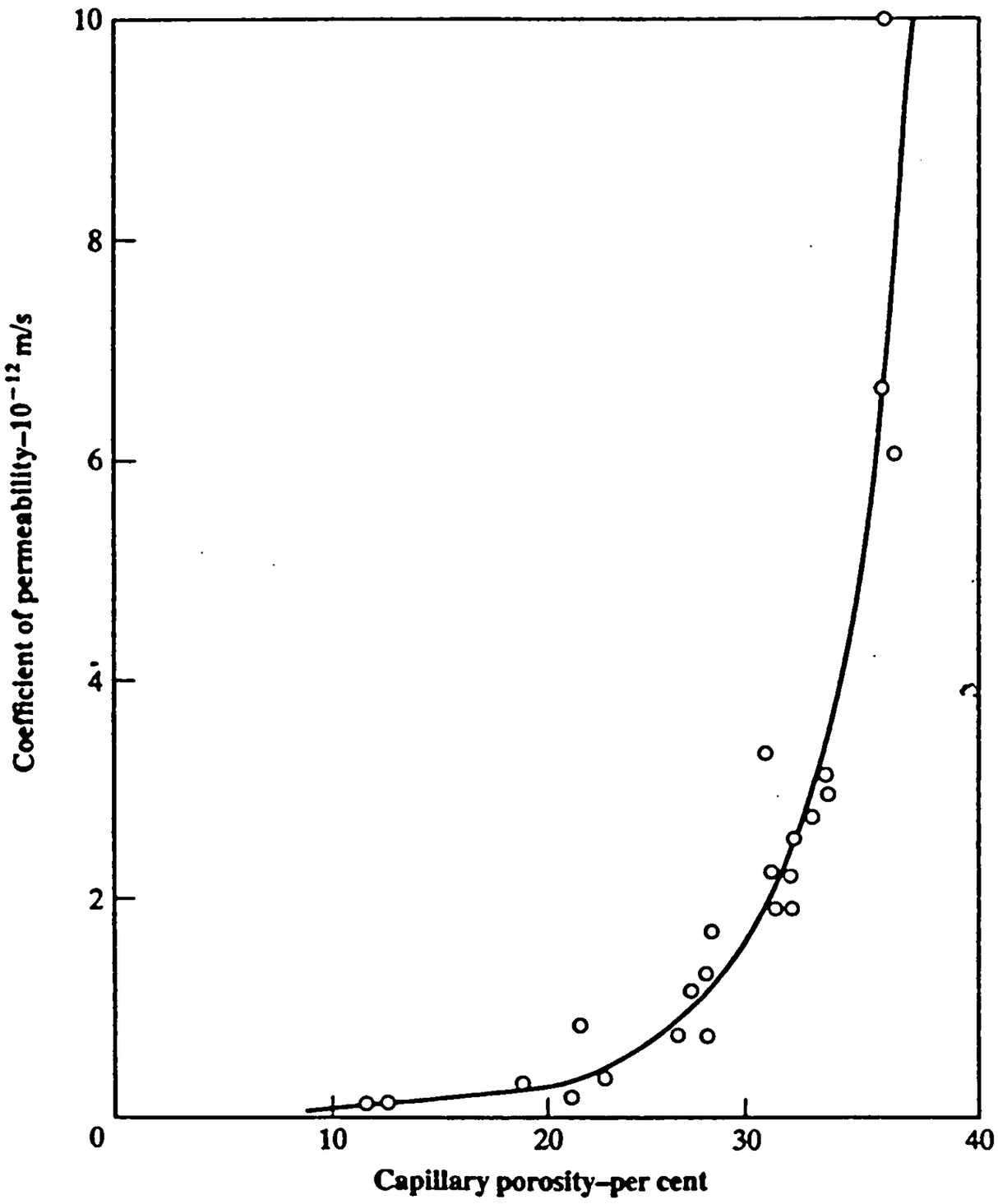

Figure 23: Relationship between permeability and capillary porosity
(Neville and Brooks 1990, p.264)

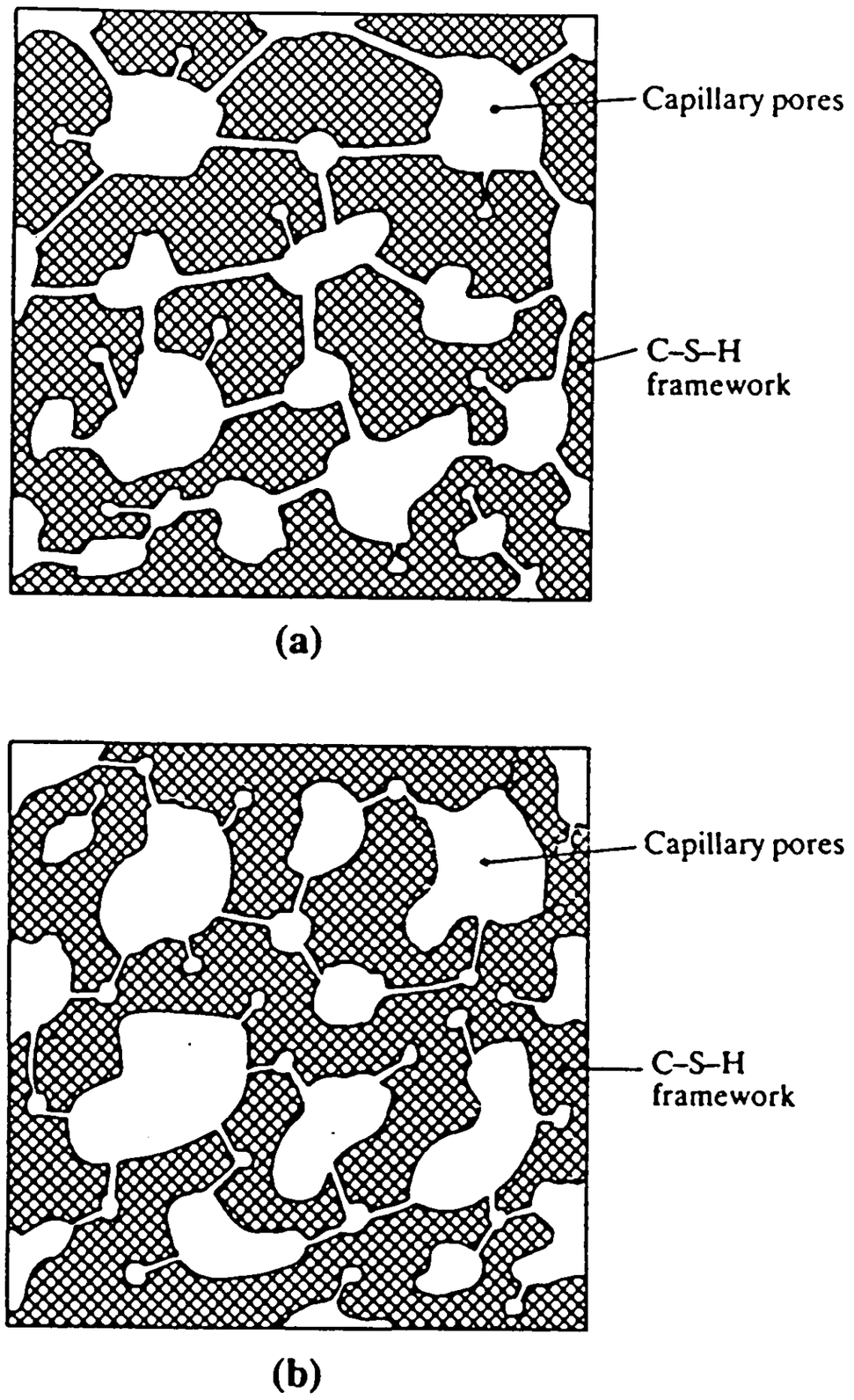

Figure 24 (a): Relationship between permeabilty and capillary porosity
Schematic representation of materials of similar porosity but: (a) High permeability - capillary pores connected by large passages (b) Low permeability - capillary pores segmented and only partly connected. (Neville and Brooks 1990, p.267)

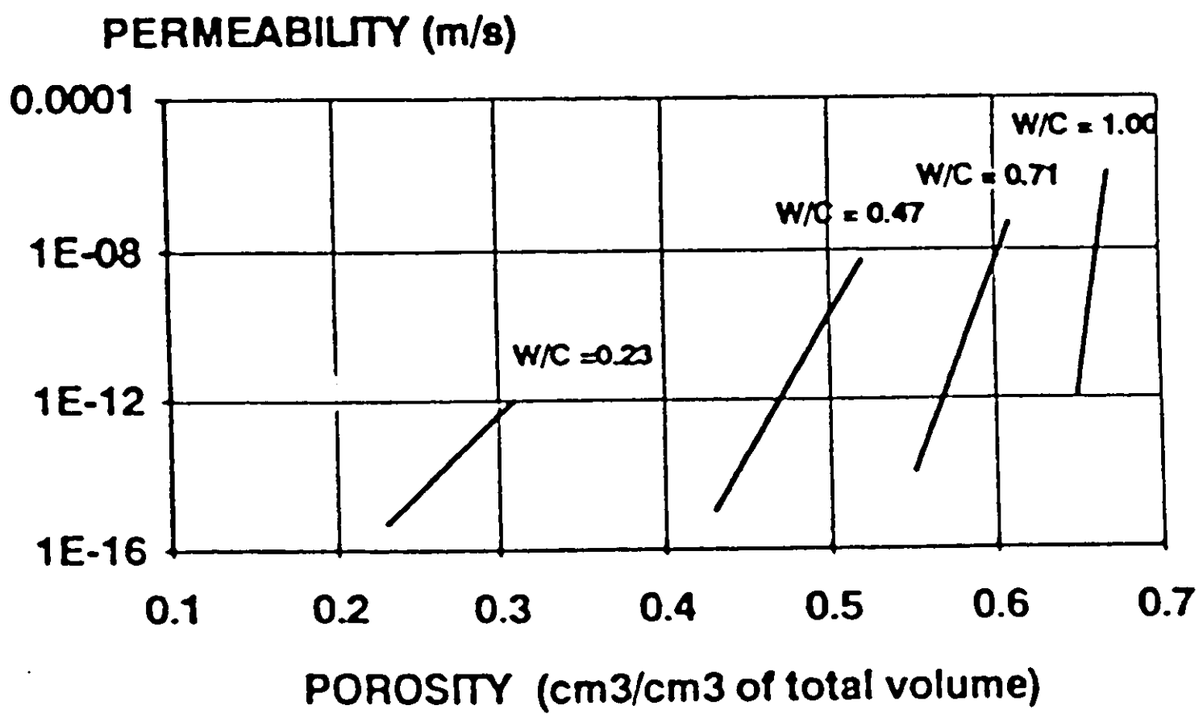

Figure 24 (a): Relationship between permeabilty, porosity, and w/c ratio
(Olliver and Massat 1992)

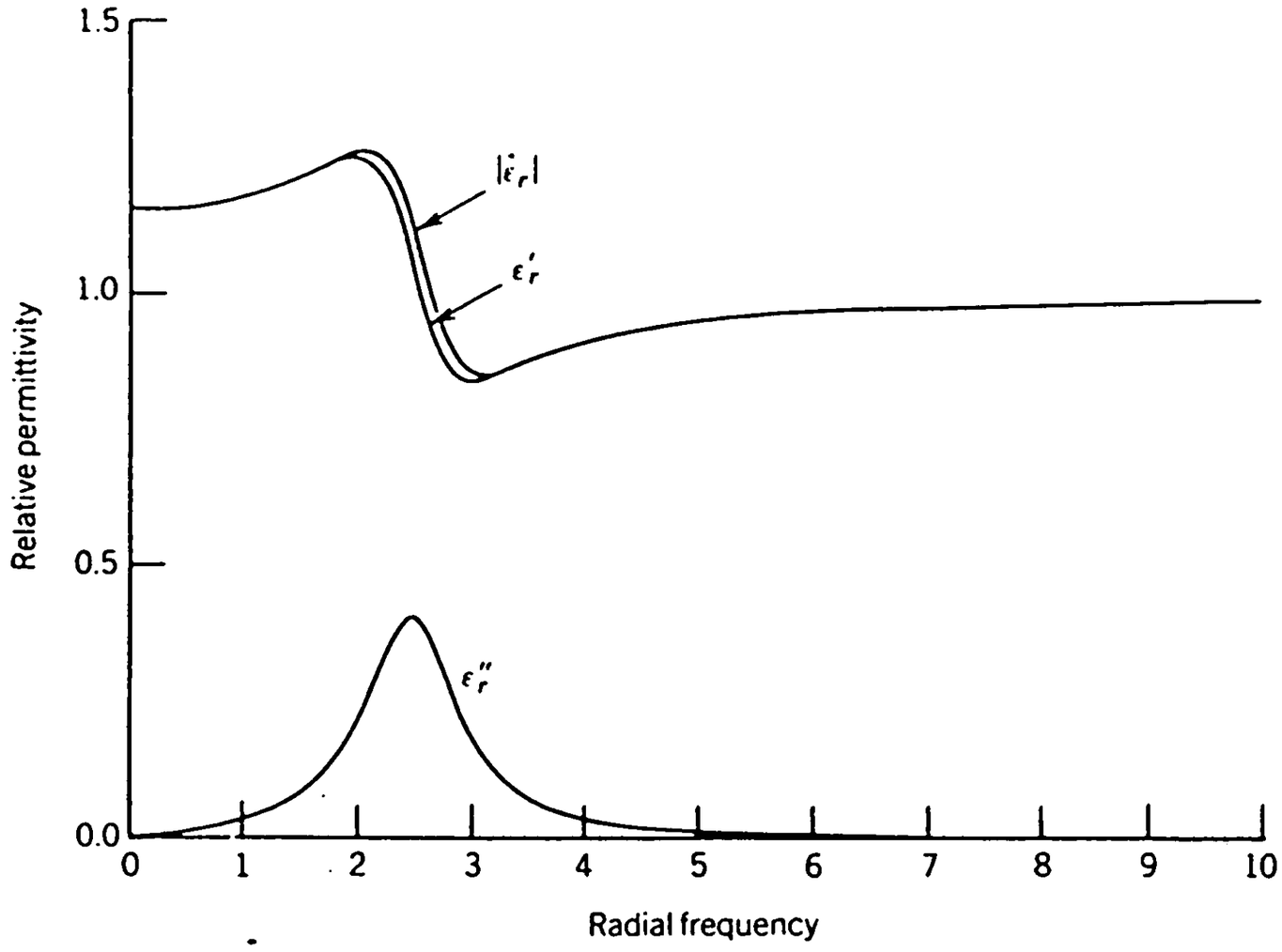

(a)

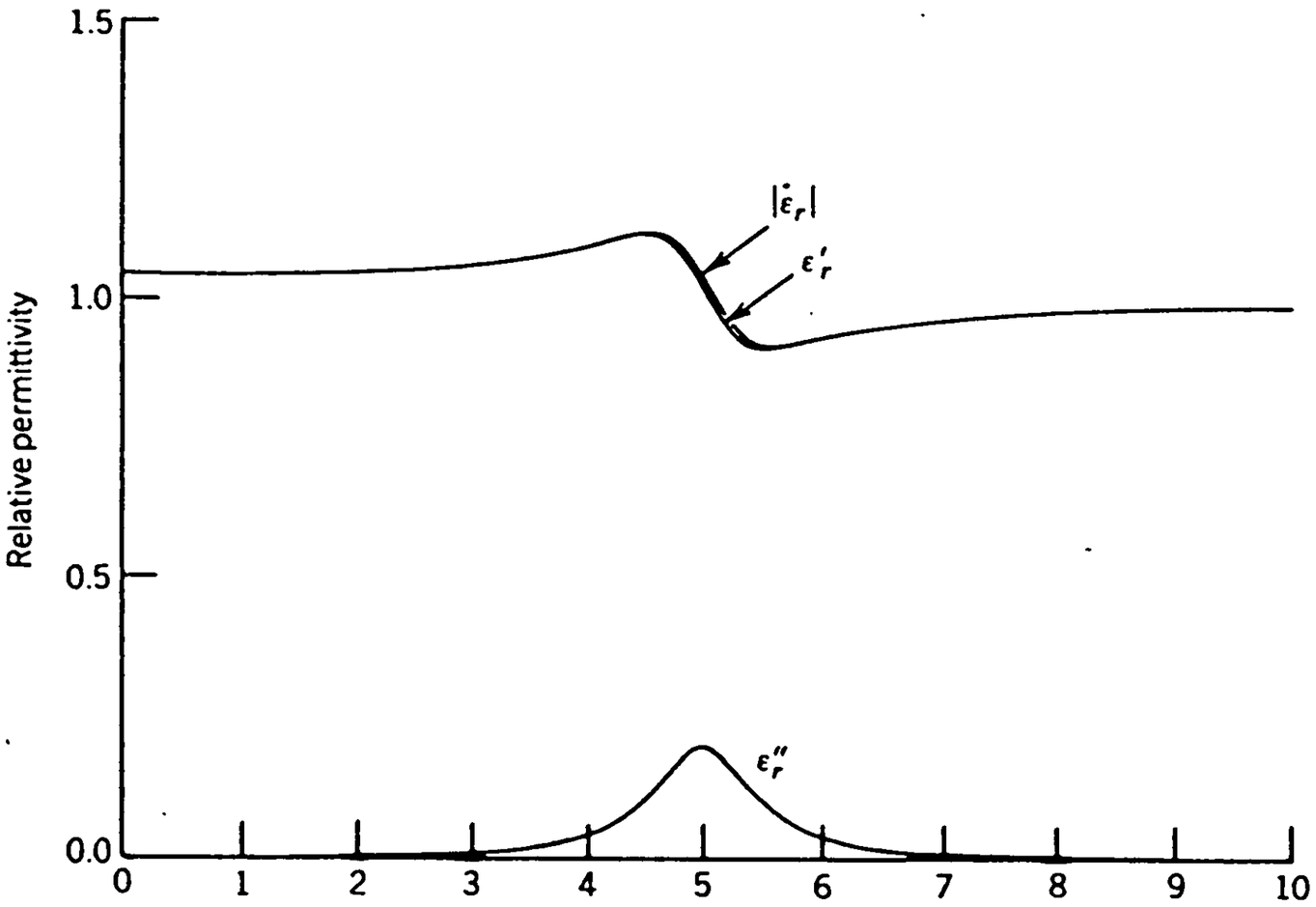

(b)

Figure 25: Theoretical variation of permittivity with frequency
Typical frequency variations of real and imaginary parts of relative permittivity of dielectrics.
(a) $N_\Theta Q^2/\varepsilon_0 m = 1$, $d/m = 1$, $\alpha/\omega = 1/5$, $\omega_0 = 2.5$
(b) $N_\Theta Q^2/\varepsilon_0 m = 1$, $d/m = 1$, $\alpha/\omega = 1/10$, $\omega_0 = 5$
(Balanis 1989, p.82)

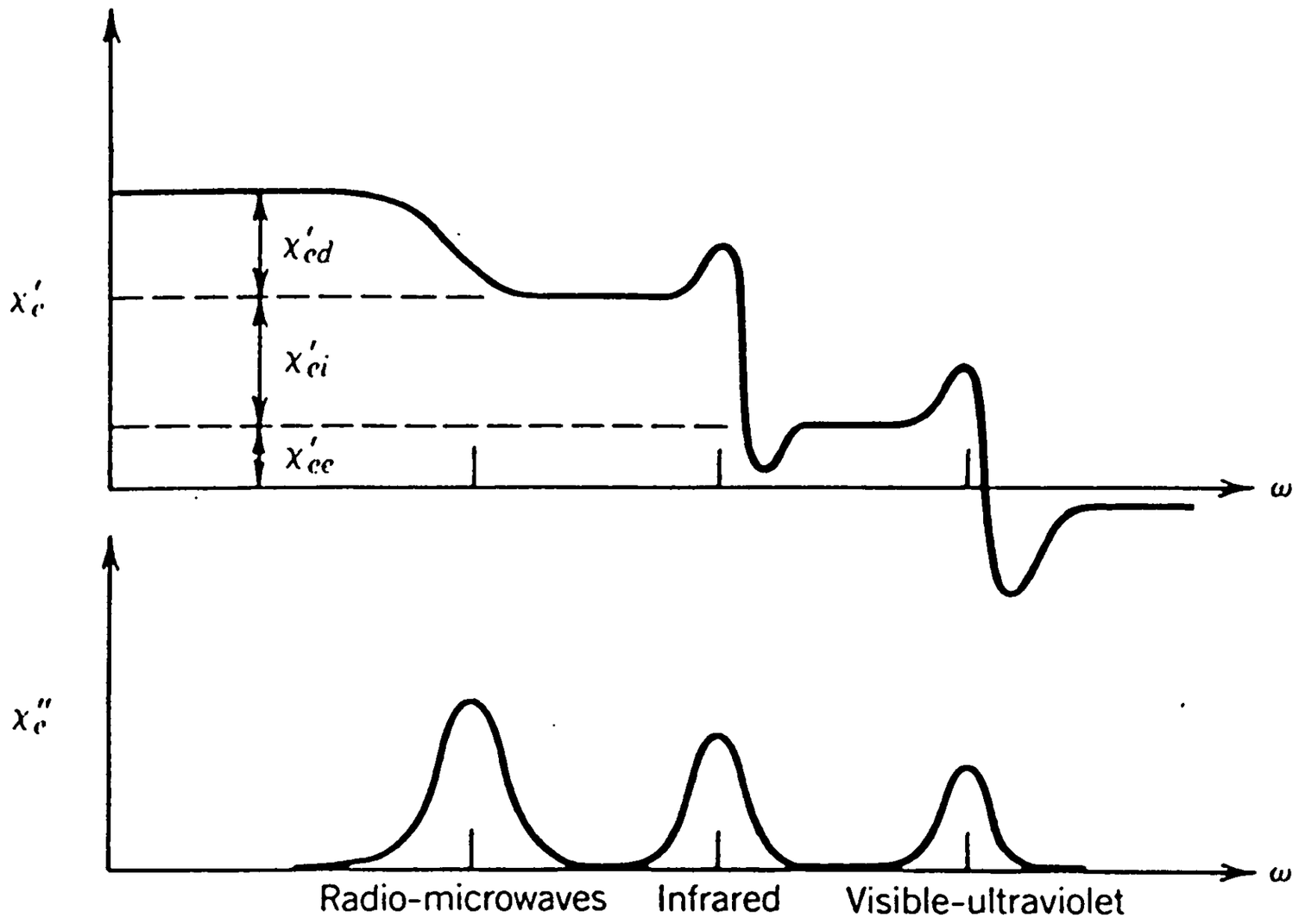

Figure 26: Variation of electric susceptability with frequency for a typical dielectric
(Balanis 1989, p.81)

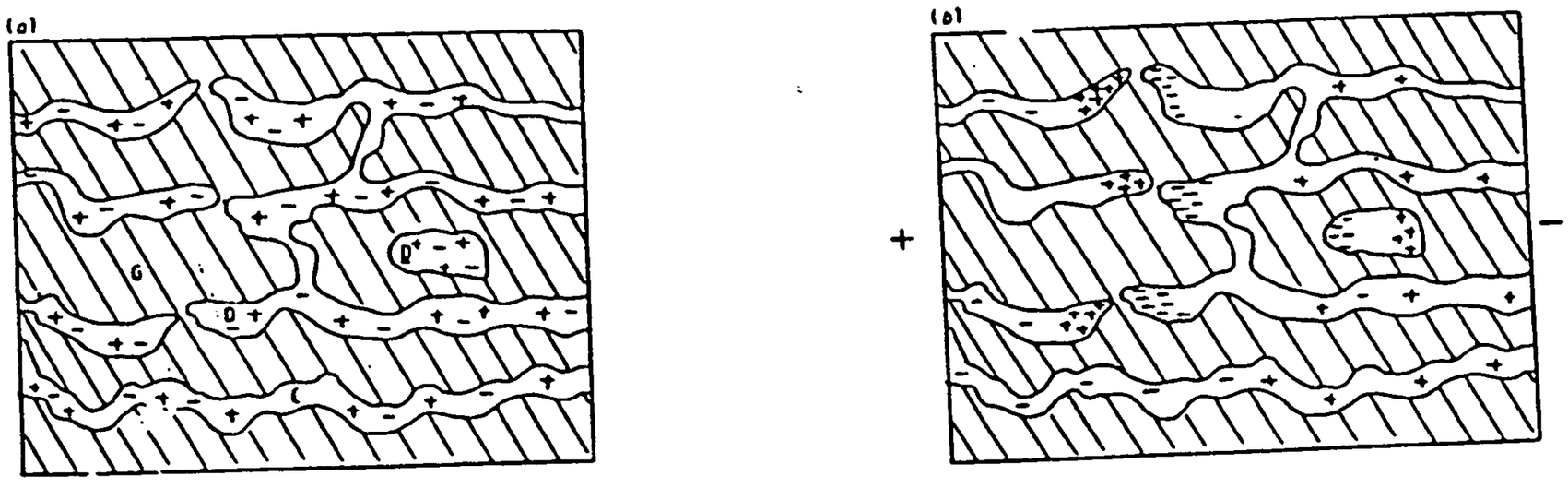

Figure 27: Interfacial polarisation
Movement of charges under an applied (alternating) electrical field during a half cycle. Changes in the (water-filled) capillaries lead to an ionic conduction effect. Charges in the closed or 'dead-end' pores give rise to interfacial polarisation.
(a) Without electric field (b) with electrical field during one half cycle.
G = gel (i.e., the products of hydration), C = continuous capillary, D = 'dead-end' or closed capillary cavities. Water will also be absorbed onto the gel exposed to the capillary pores.
(McCarter and Curran 1984)

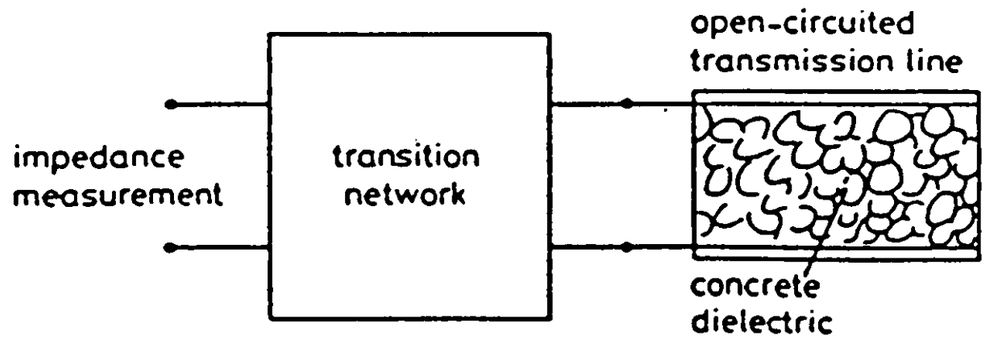

(a) Electrical model.

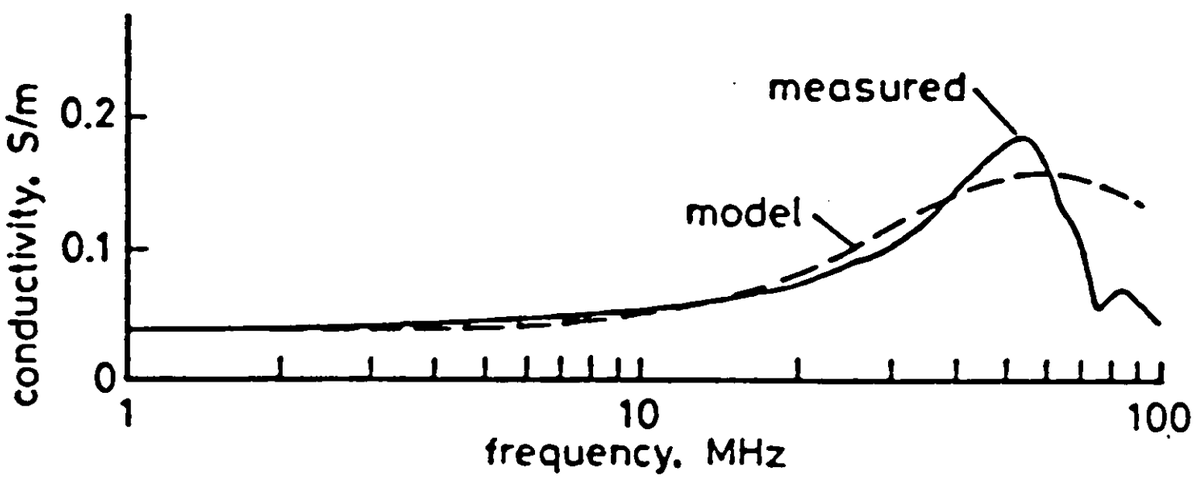

(b) Conductivity comparison at one day.

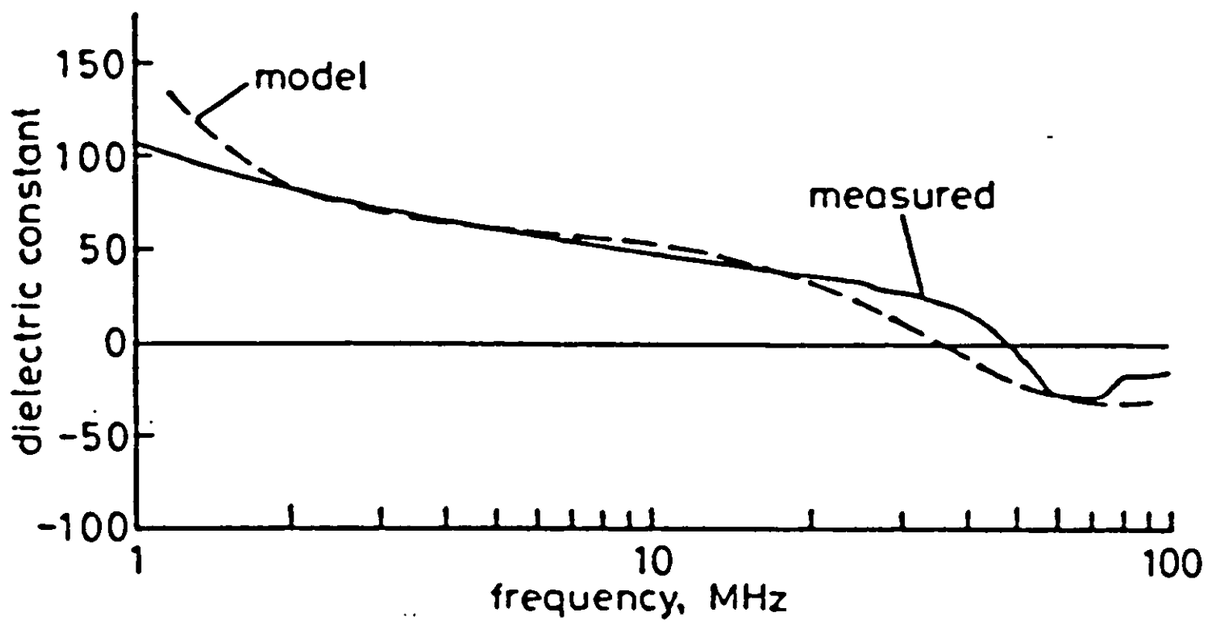

(c) Dielectric constant comparison at 1 day.

Figure 28: Dielectric constant and conductivity of fresh concrete
(Wilson and Whittington 1990)

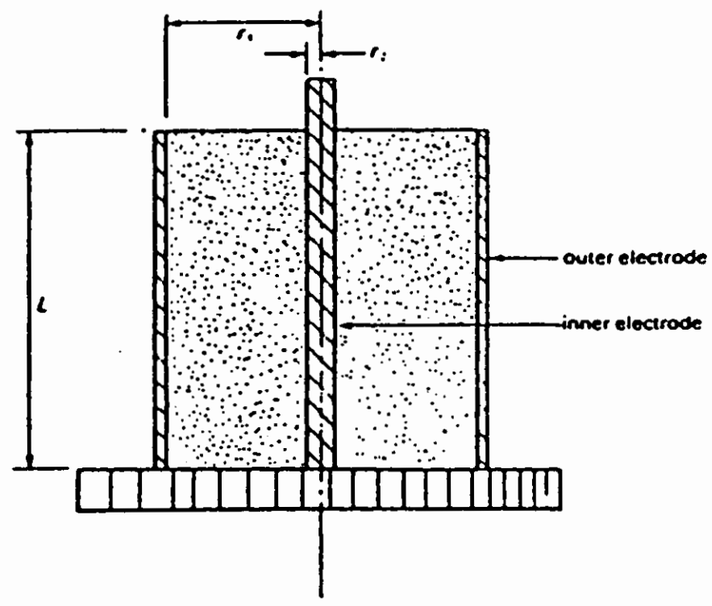

Figure 29 (a): Schematic diagram of test cell
(McCarter and Curran 1984)

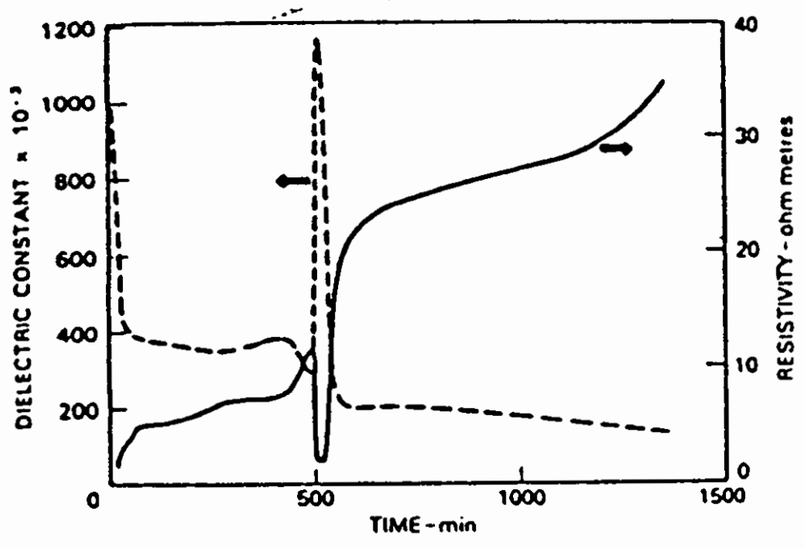

(i) Dielectric constant and electrical resistivity.

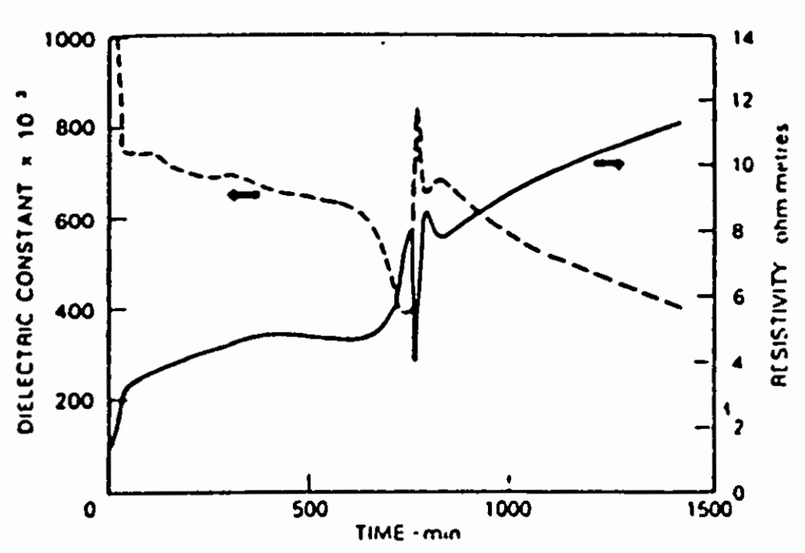

(ii) Dielectric constant and electrical resistivity.

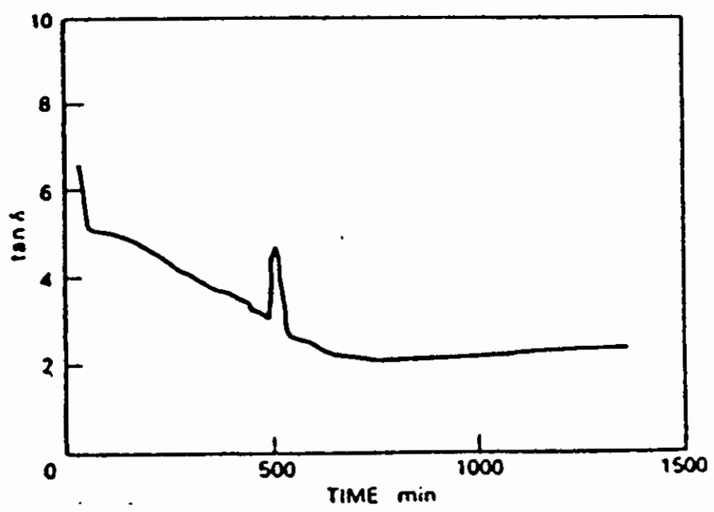

(iii) Tan δ

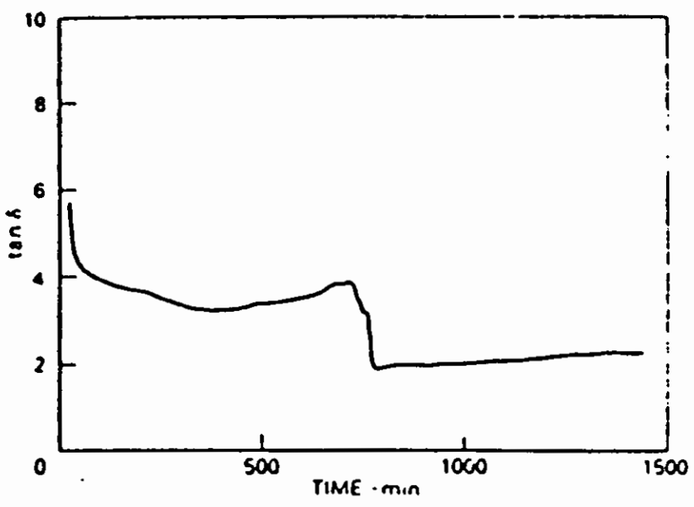

(iv) Tan δ

Figure 29 (b): Dielectric constant, resistivity and loss tangent at a frequency of 1kHz
The electrical response characteristics of setting cement paste.
(i) and (ii) giving the variation in measured parameters for paste P4 to get P4 (paste 4, wc = 0.4) (iii) and (iv) giving the variation in measured parameters for paste P5 to get P5 (paste 5 wc = 0.5)
(McCarter and Curran 1984)

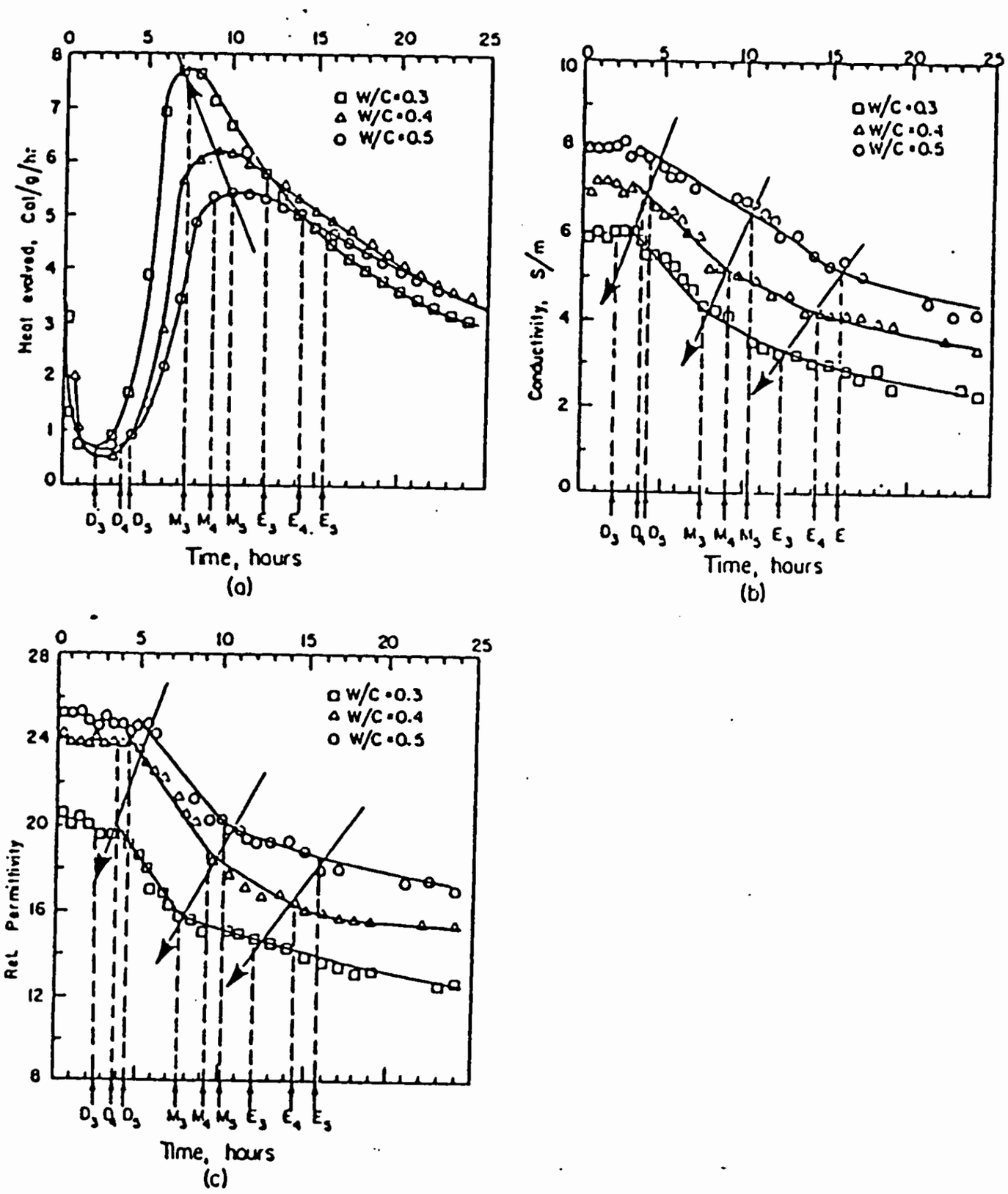

Figure 30: Effect of water/cement ratio on the heat of hydration, conductivity and relative permittivity at a frequency of 10GHz
(Moukawa et al. 1991)

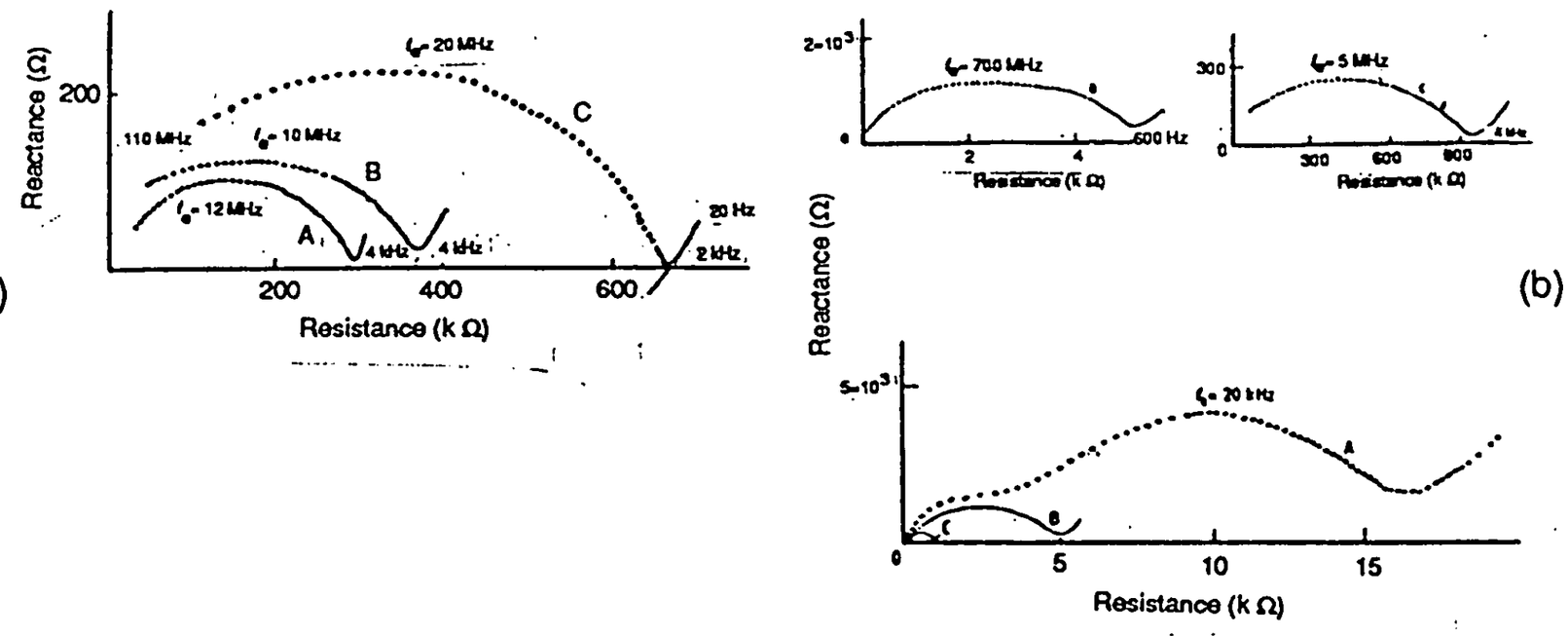

Figure 31: Characteristic impedence plots for cement pastes and mortars at different times. (a) Impedance plots for cement paste and mortar prisms. Curve A, cement paste after 28 days moist curing. Curve B, cement paste after 100 days moist curing. Curve C, mortar after 100 days moist curing.
(b) Impedance plots for mortar after drying and then immersion in water. The insets show curves B and C drawn at enlarged scale. Curve A, after drying at 70°C and then cooled in laboratory atmosphere. Curve B, 10 min. immersion in water. Curve C, 24 h immersion in water.
(McCarter and Garvin 1989)

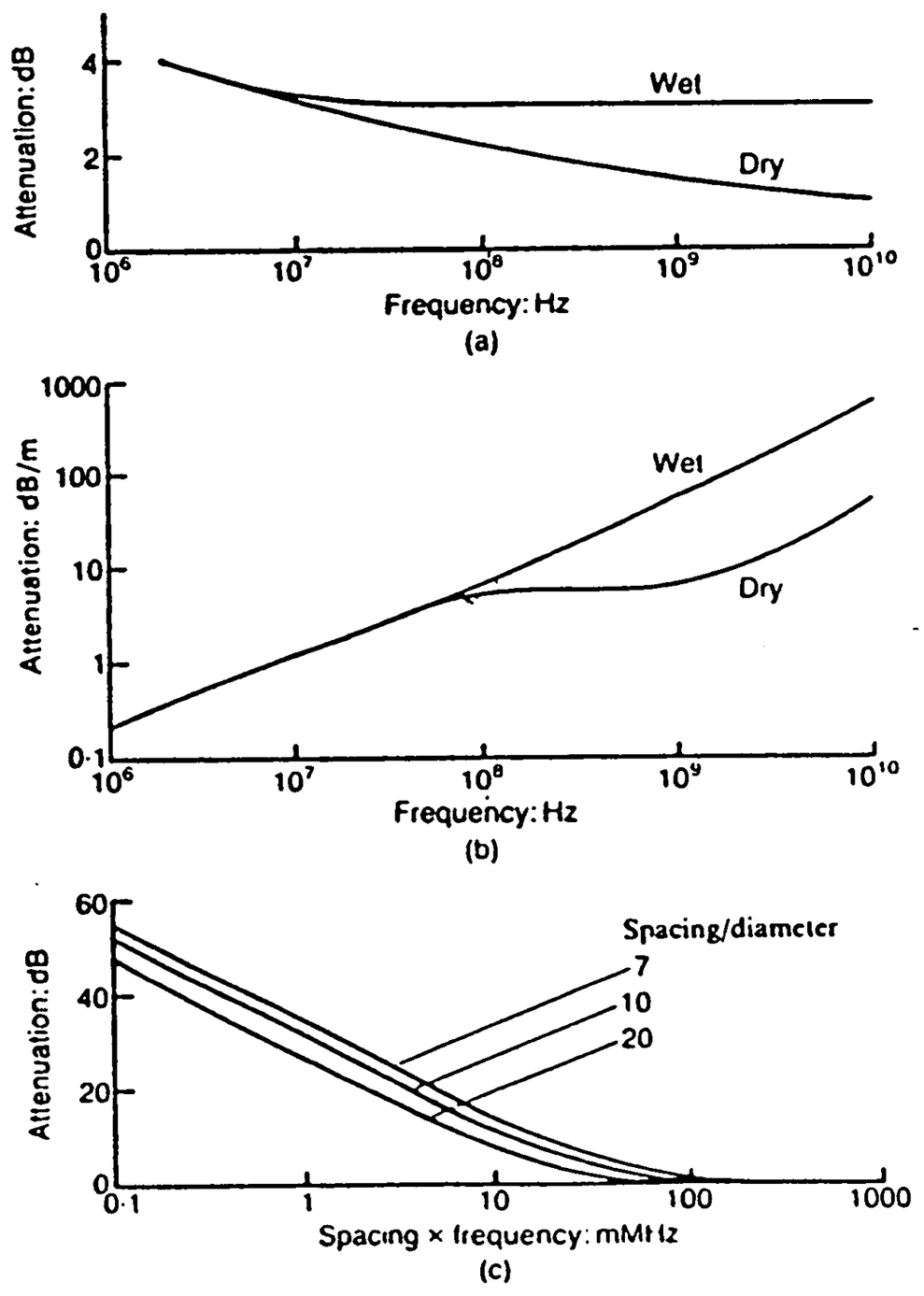

Figure 32: Contributions to the attenuation of electromagnetic waves passing through a reinforced concrete wall
(a) Reflection at the two concrete surfaces.
(b) Dissipation within the concrete.
(b) Reflection from a single layer of reinforcement.
(Battilana 1989)

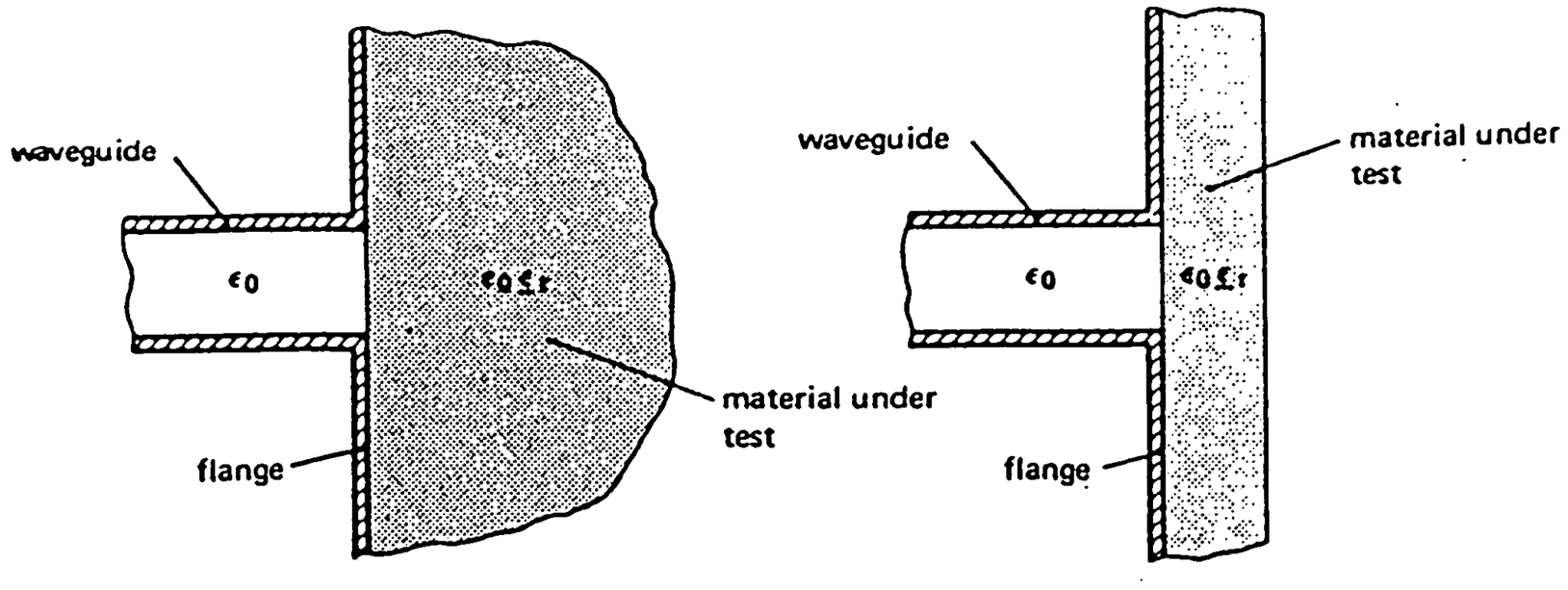

(i) Non-destructive reflection method.

(ii) Non-destructive reflection method for slabs.

Figure 33 (a): Non-destructive reflection method
(Gardiol 1984)

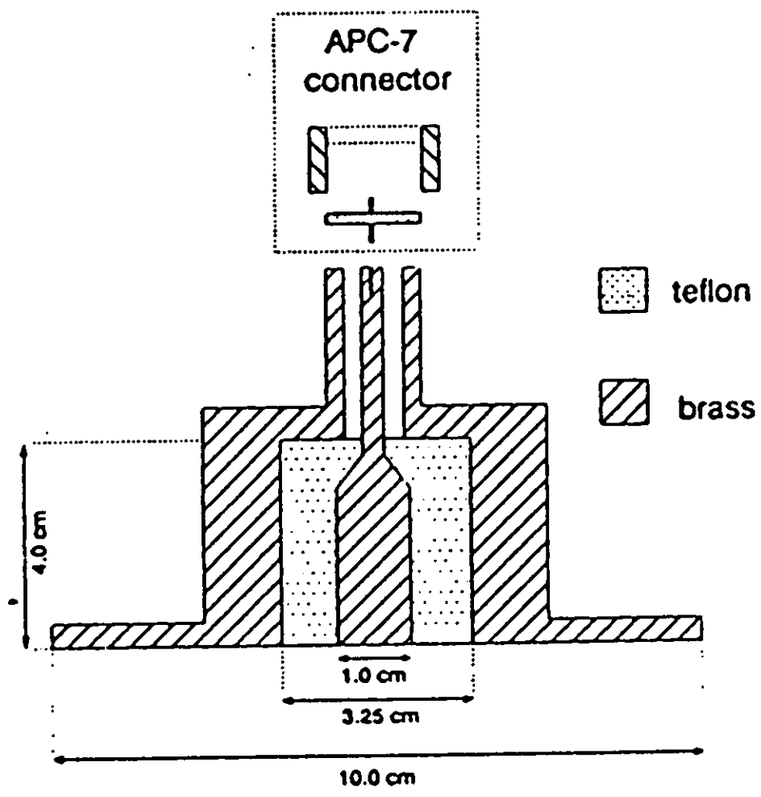

Figure 33 (b): An open-ended coaxial probe
(Otto and Chew 1991, p.743)

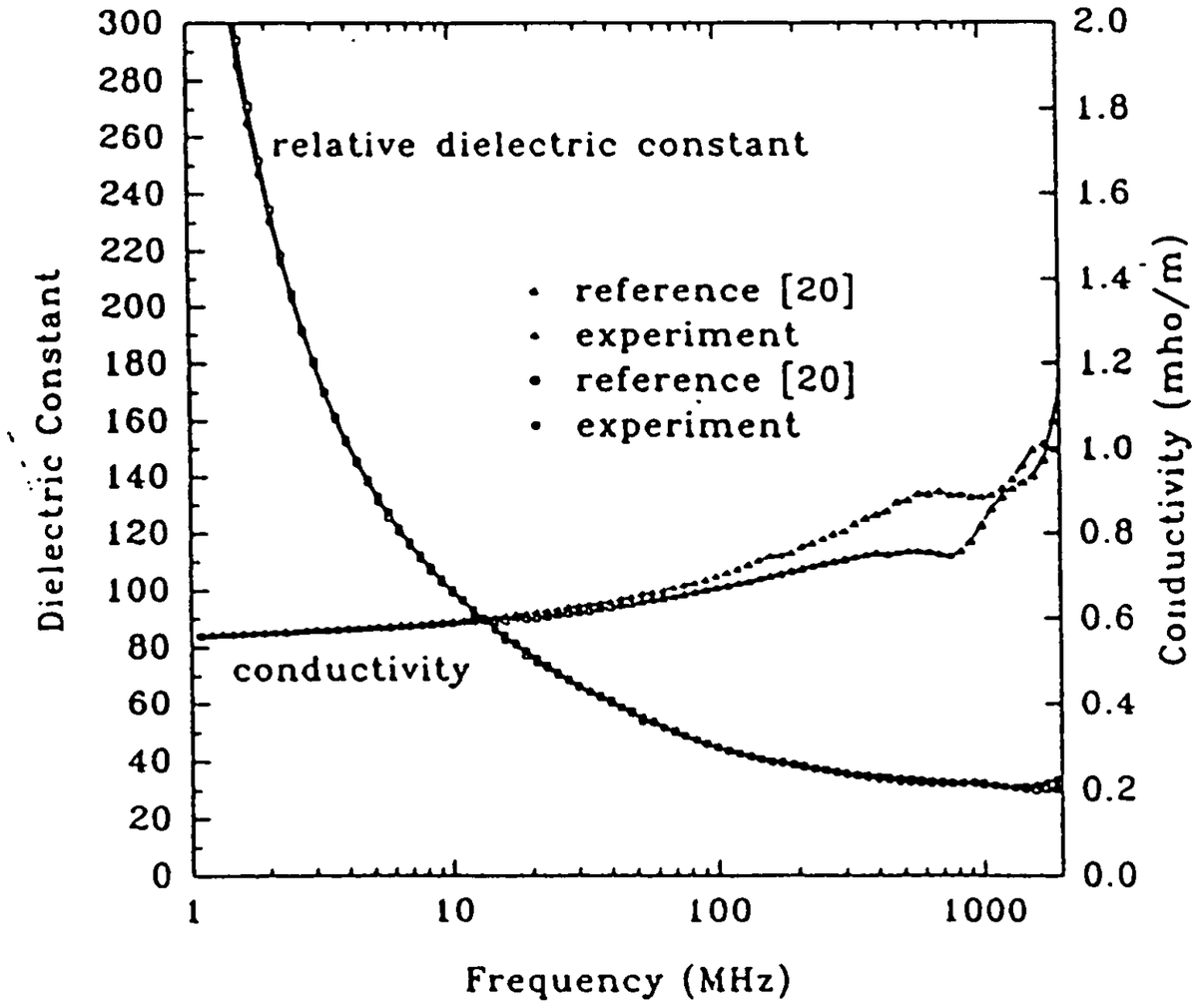

Figure 33 (c): Dielectric constant and conductivity as a function of frequency measured using a coaxial probe
(Otto and Chew 1991, p.745)

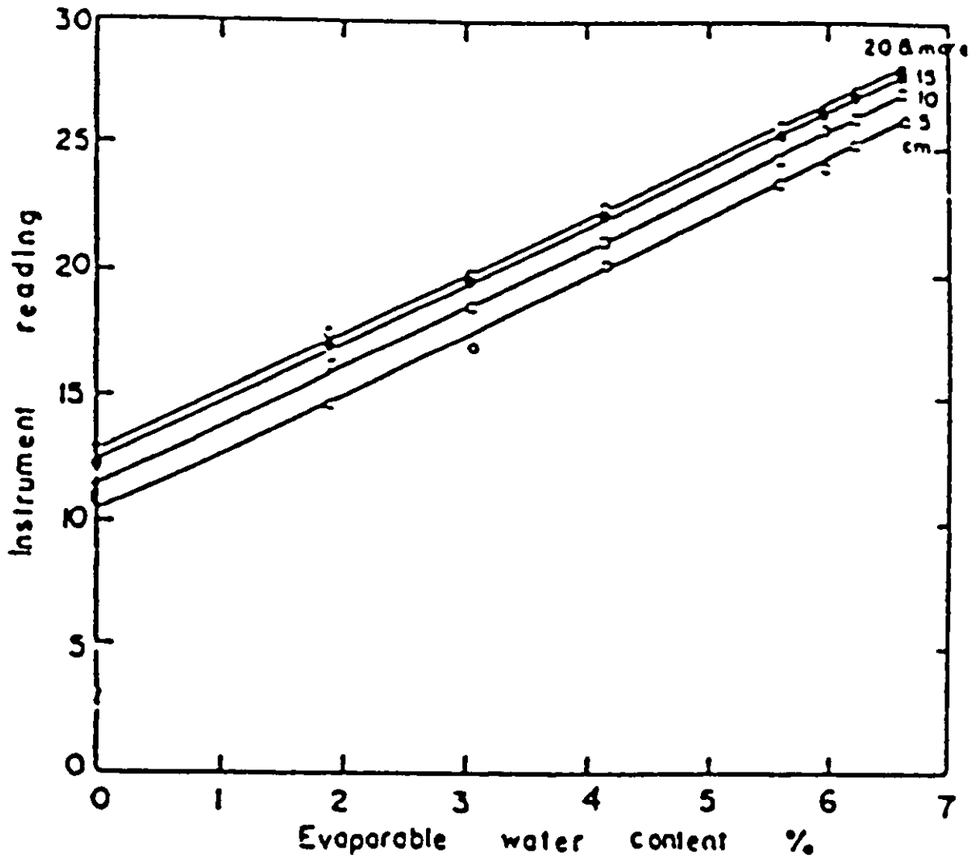

(a) At 0.3 GHz.

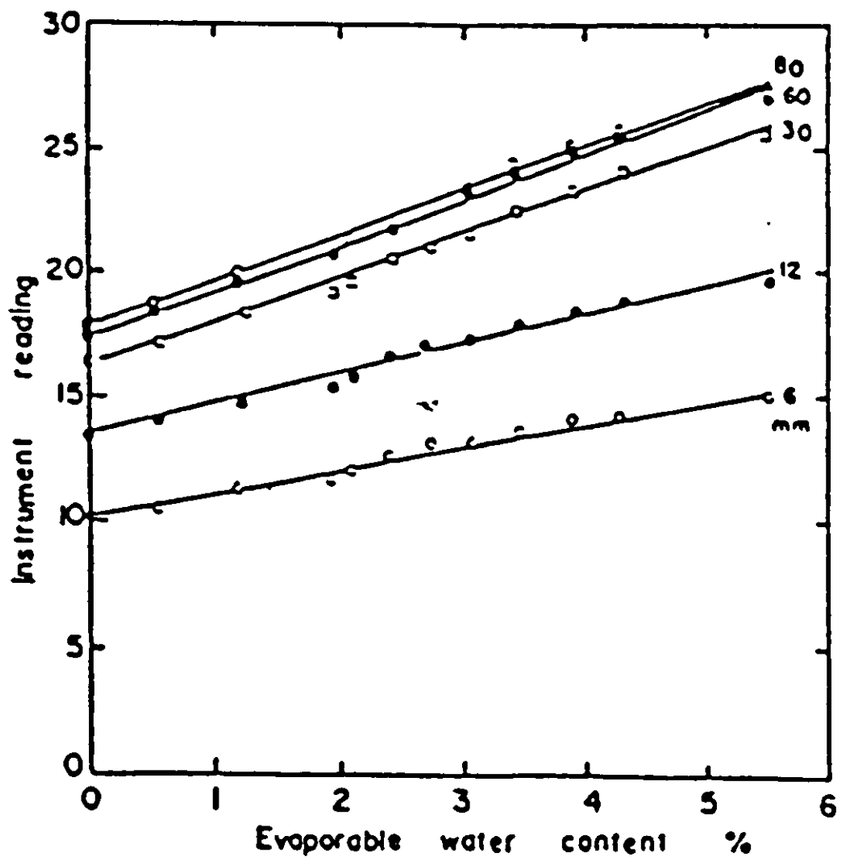

(b) At 0.8 GHz.

Figure 34: Variation of microwave resonant frequency with moisture content and sample thickness
(Bhargava and Lundberg 1972)

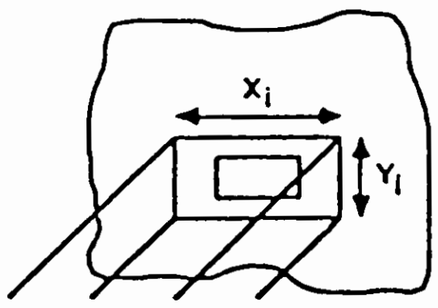

(i) 3-Dimensional view

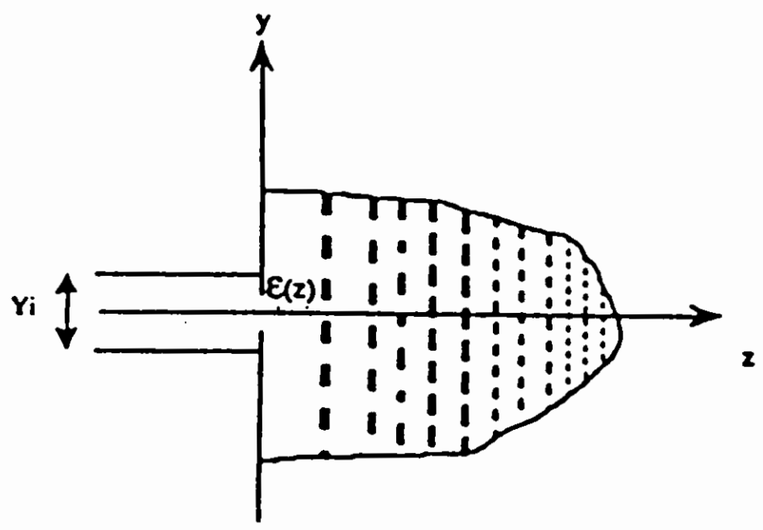

(ii) Side view

Figure 35 (a): Open-ended wave guide in contact with an inhomogenous dielectric medium
(Sanadiki and Mostafavi 1991)

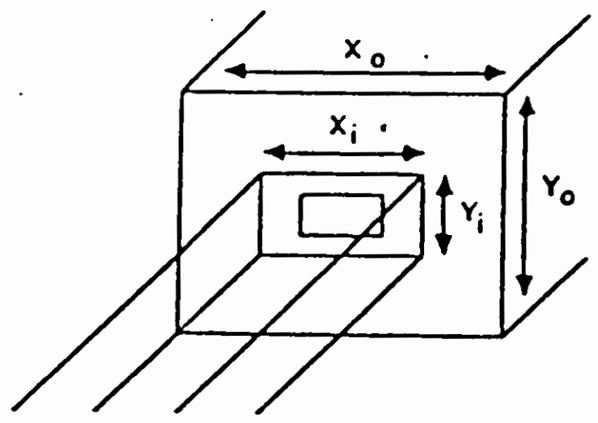

(i) 3-Dimensional view

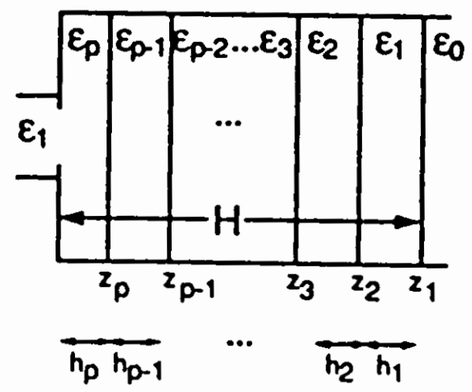

(ii) Side view

Figure 35 (b): Open-ended wave guide in contact with a stratified dielectric medium enclosed in a large waveguide
(Sanadiki and Mostafavi 1991)

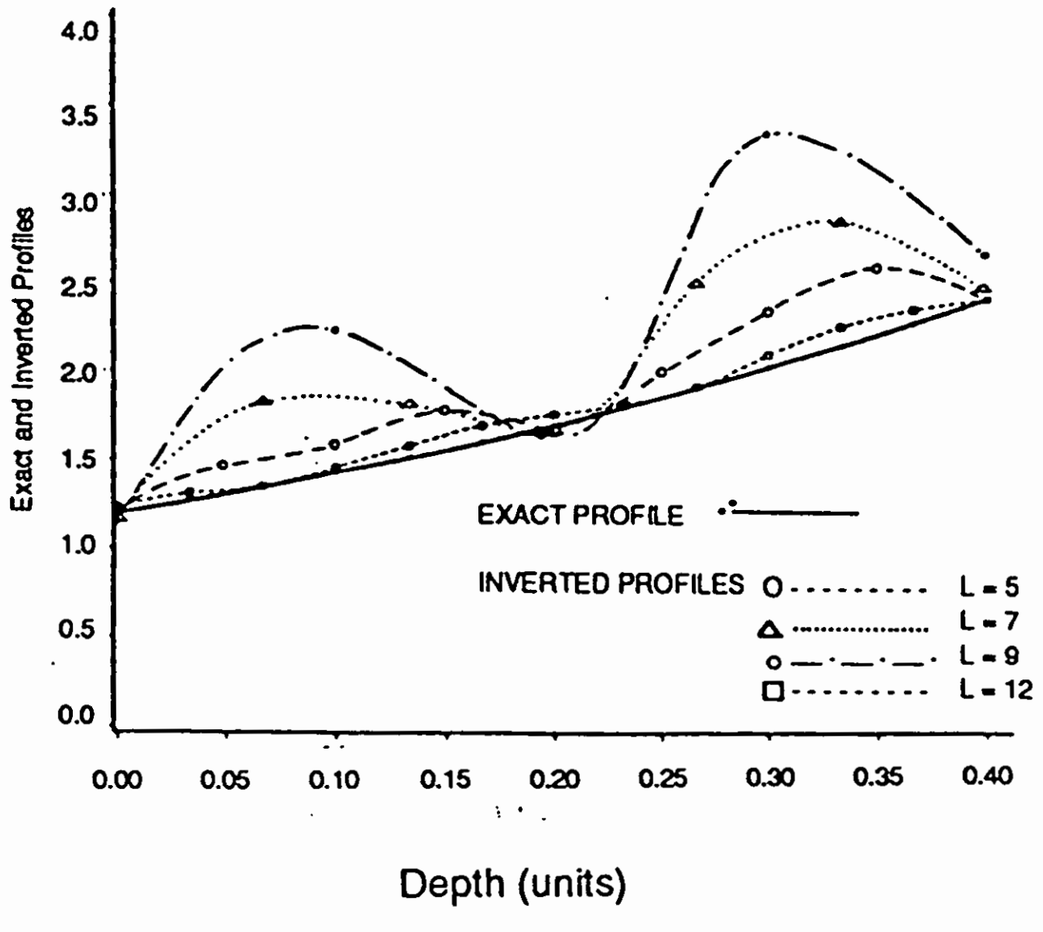

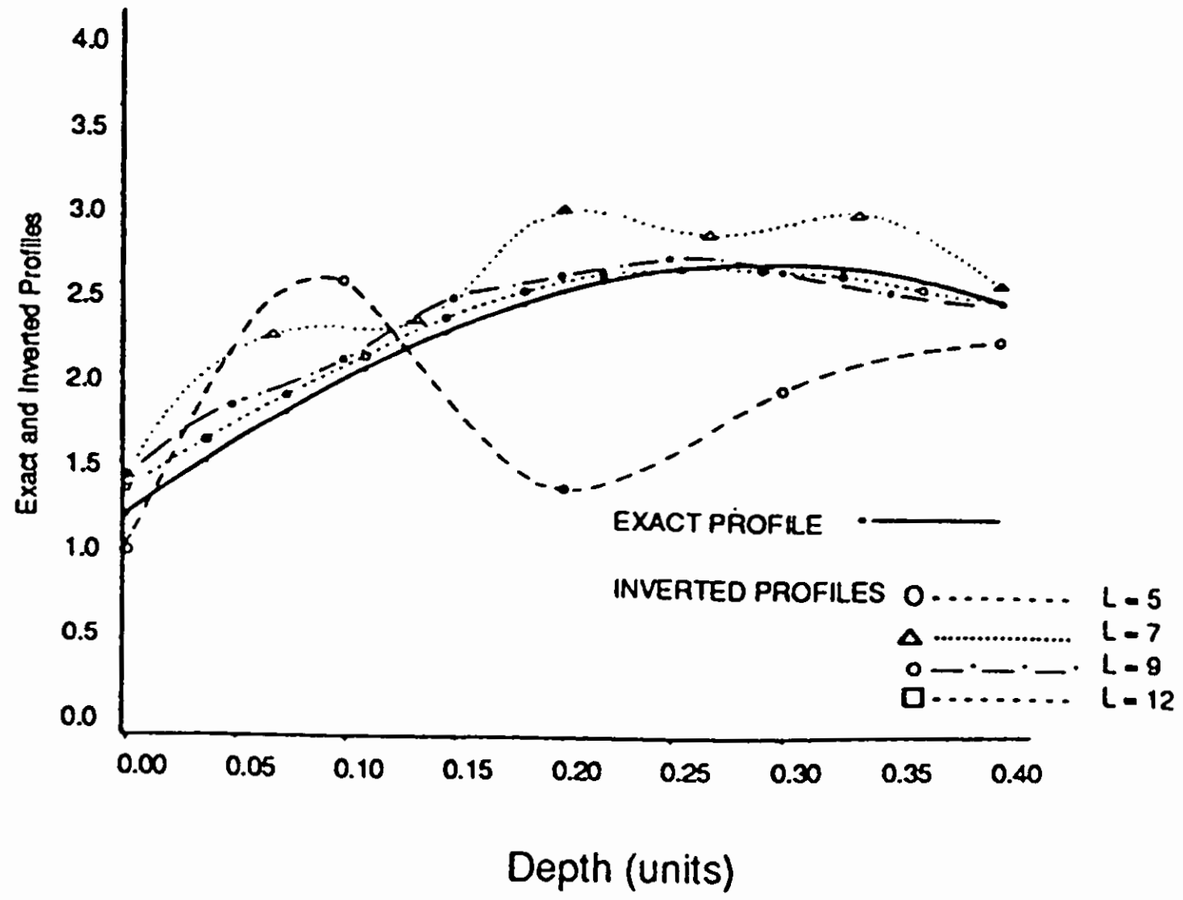

Figure 35 (c): Progress of profile inversion
(Sanadiki and Mostafavi 1991)

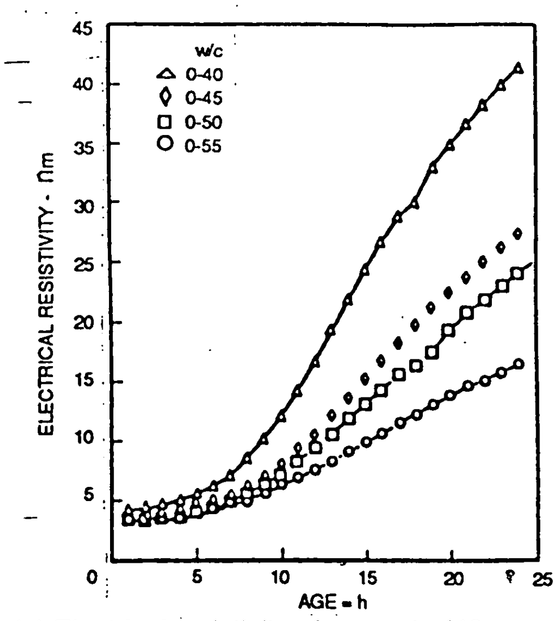

(a) Electrical resistivity of concrete (40mm gravel, 400kg/m^3 OPC) for initial period.

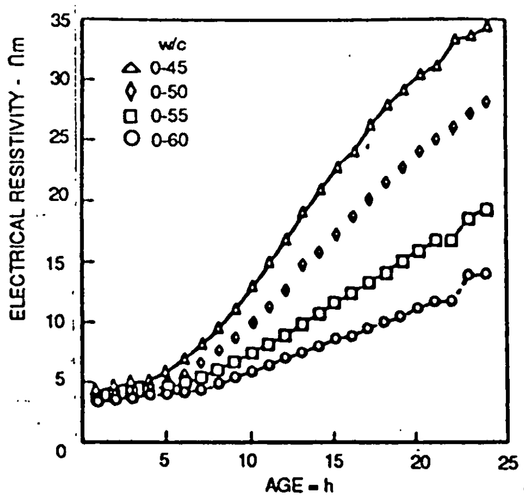

(b) Electrical resistivity of concrete (40mm gravel, 350kg/m^3 OPC) for initial period.

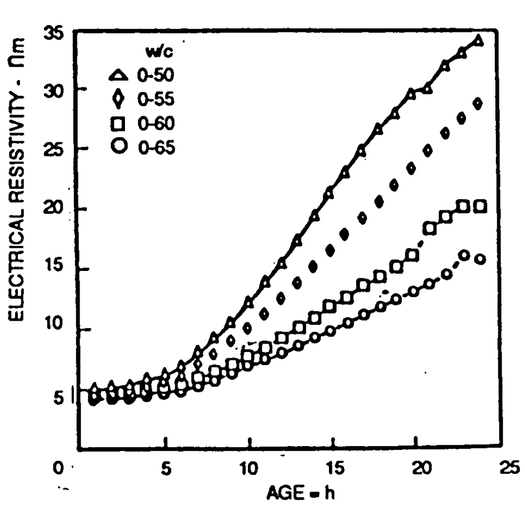

(c) Electrical resistivity of concrete (40mm gravel, 300kg/m^{3}OPC) for initial period.

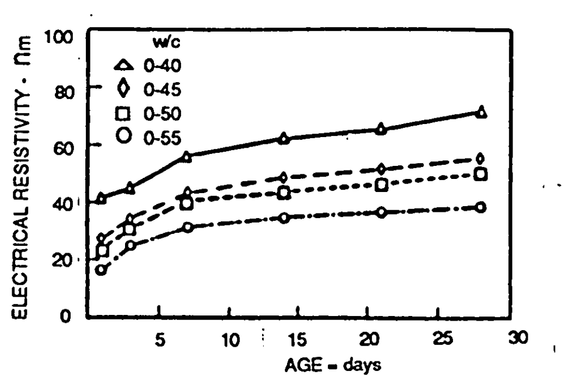

(d) Electrical resistivity of moist-cured concrete. (40mm gravel, 400kg/m^3 OPC)

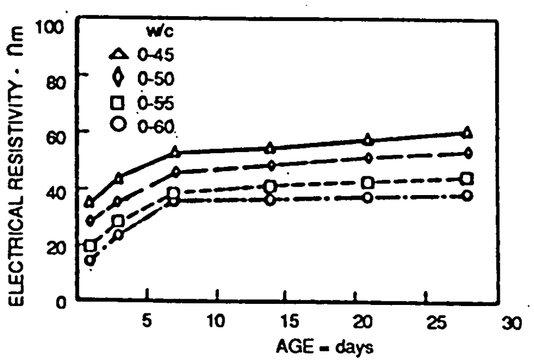

(e) Electrical resistivity of moist-cured concrete. (40mm gravel, 350kg/m^3 OPC)

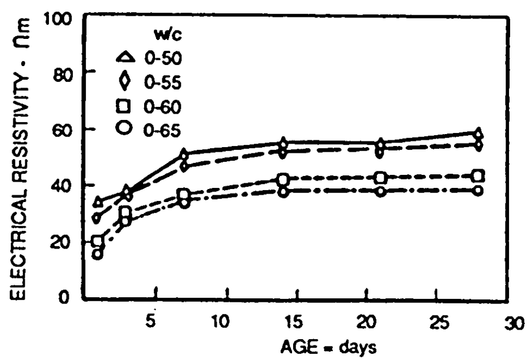

(f) Electrical resistivity of moist-cured concrete. (40mm gravel, 300kg/m^3 OPC)

Figure 36: Variation of electrical resistivity with w/c ratio, a/c ratio and time.
(Hughes et al. 1985)

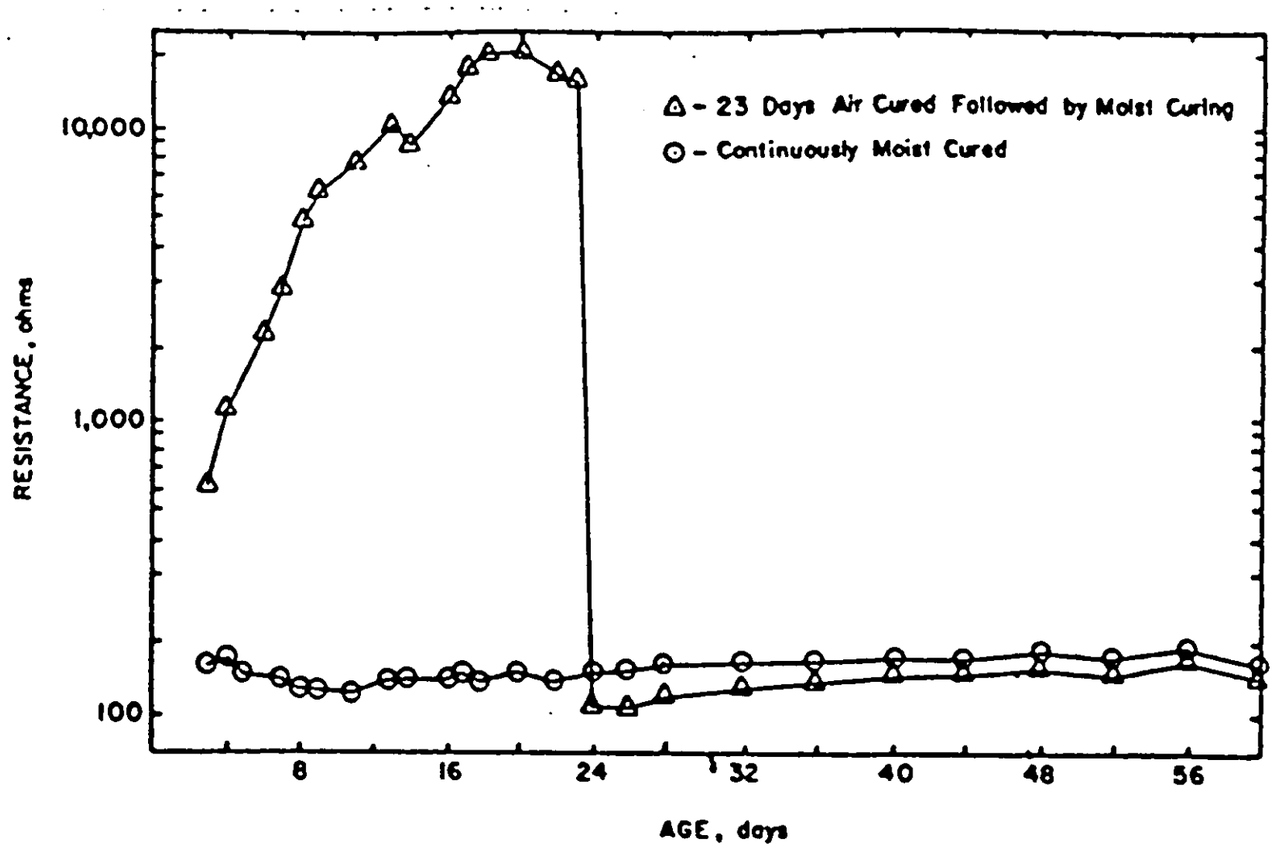

(a) Effect of age on the resistance of concrete.

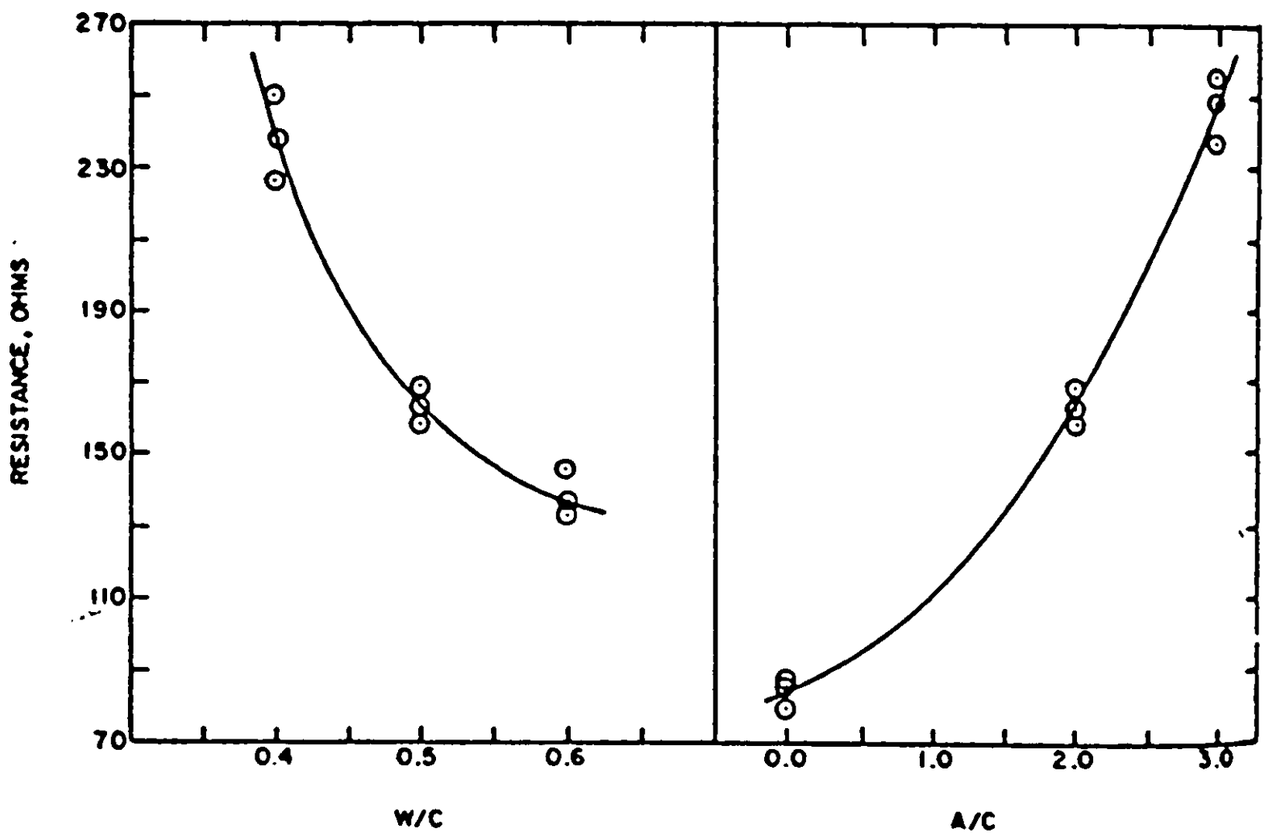

(b) Influence of W/C and A/C on the resistance of concrete.

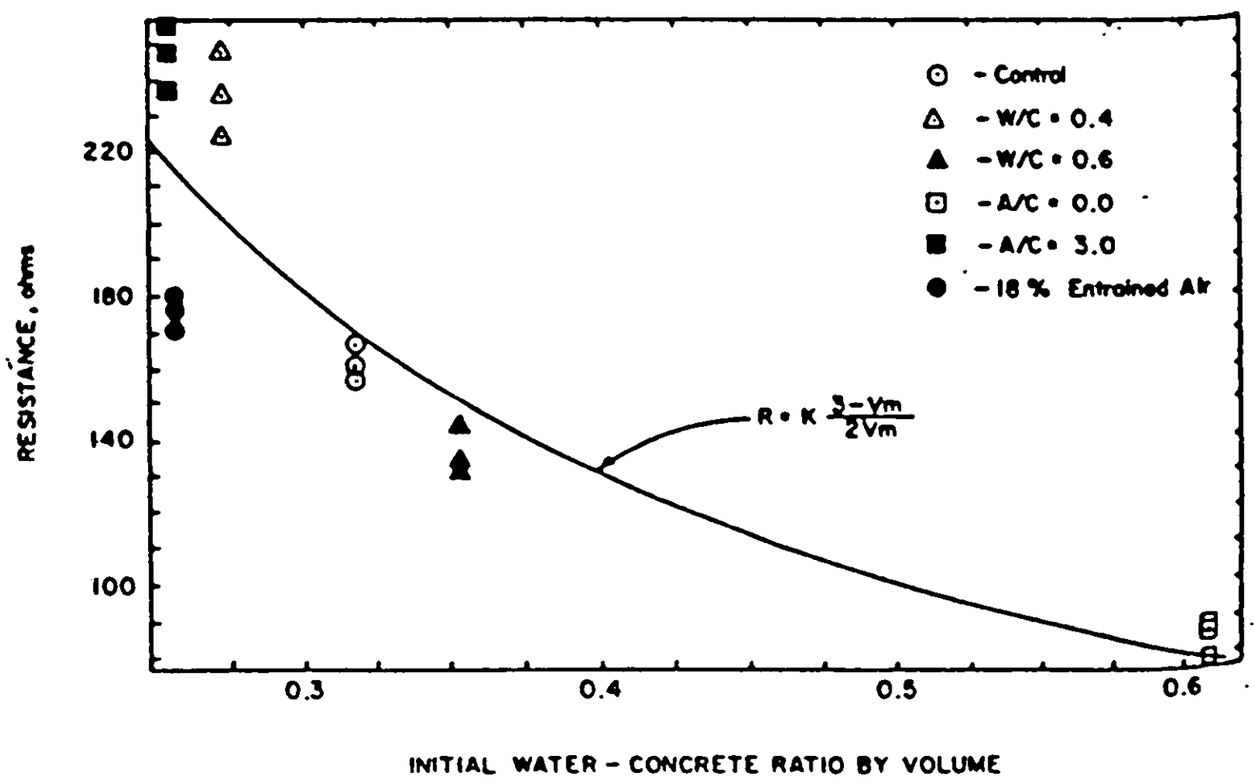

(c) Effect of water/concrete ratio on the resistance of concrete.

Figure 37: Variation of electrical resistance with w/c ratio, a/c ratio and time
(Woelfl and Lauer 1979)

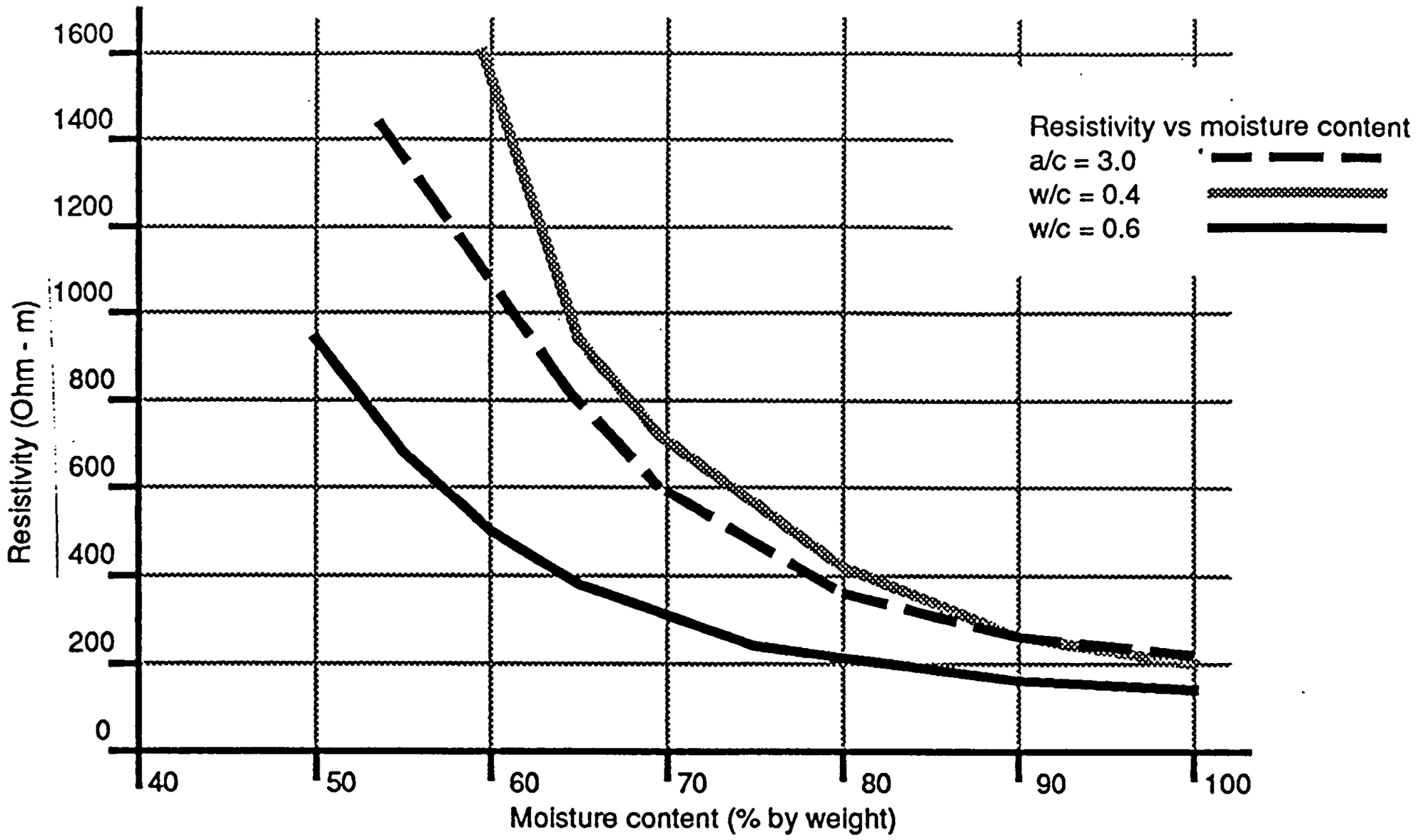

Figure 38: Variation of resistivity with moisture content
(An interpretation of data from Woelfl and Lauer 1979)

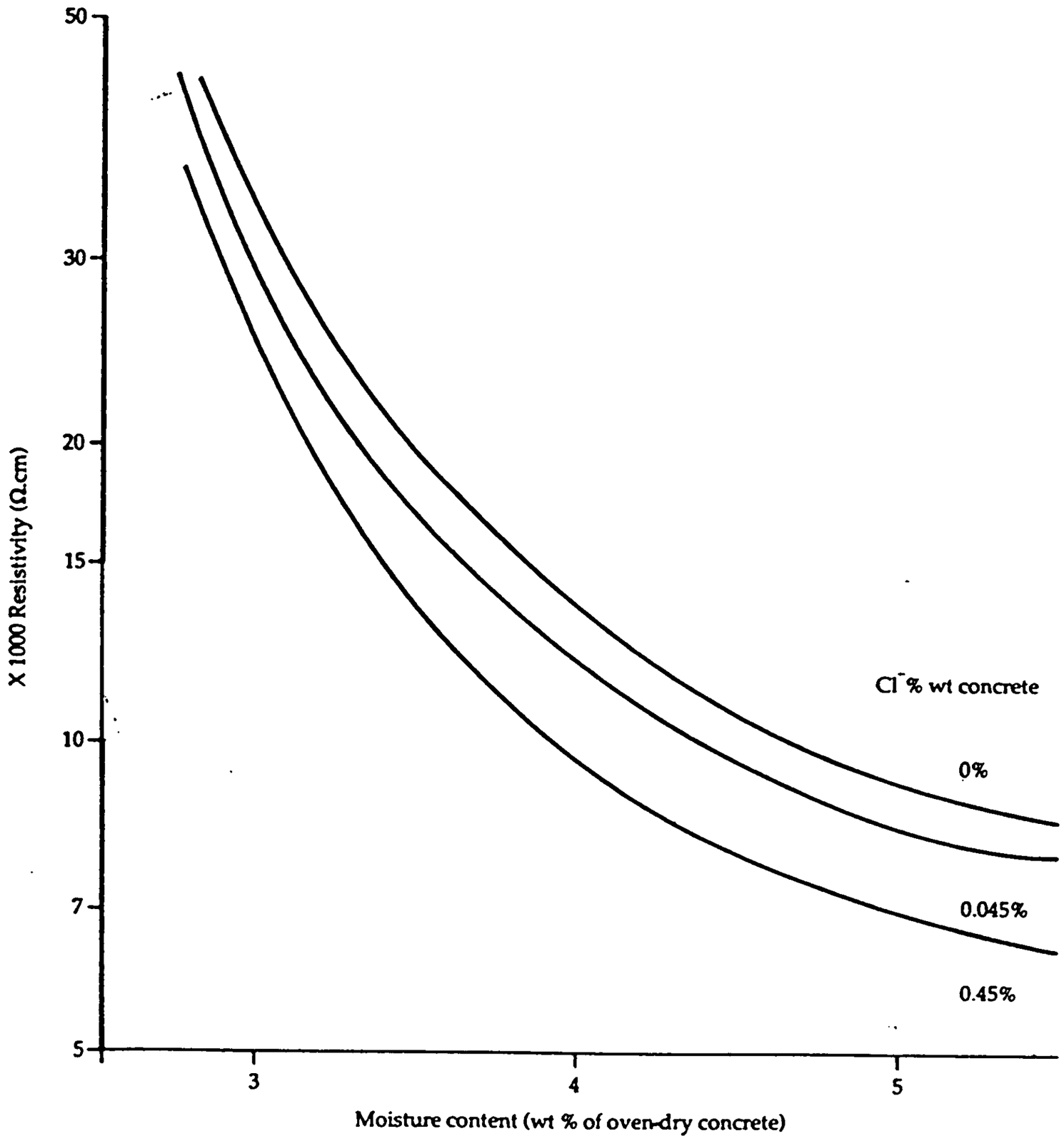

Figure 39: Variation of resistivity with moisture and chloride constant
(Heiman 1992, p.317)

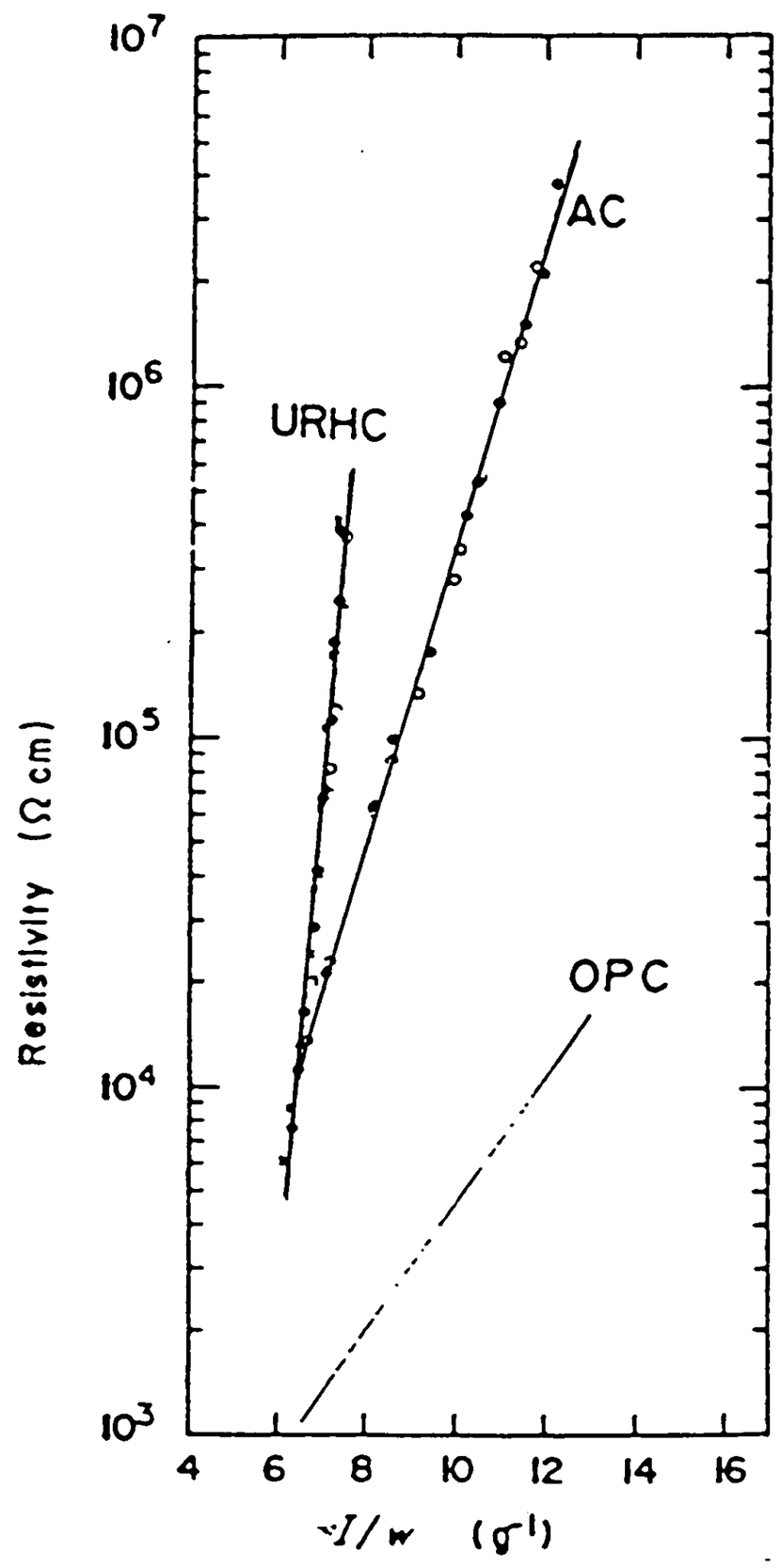

Figure 40: Variation in the electrical resistivity with the reciprocal of the evaporable water content, w, for hardened AC and URHC with a curing time of 7 days. The straight line for hardened OPC with the same curing time is also shown. (Tashiro, et al 1987)

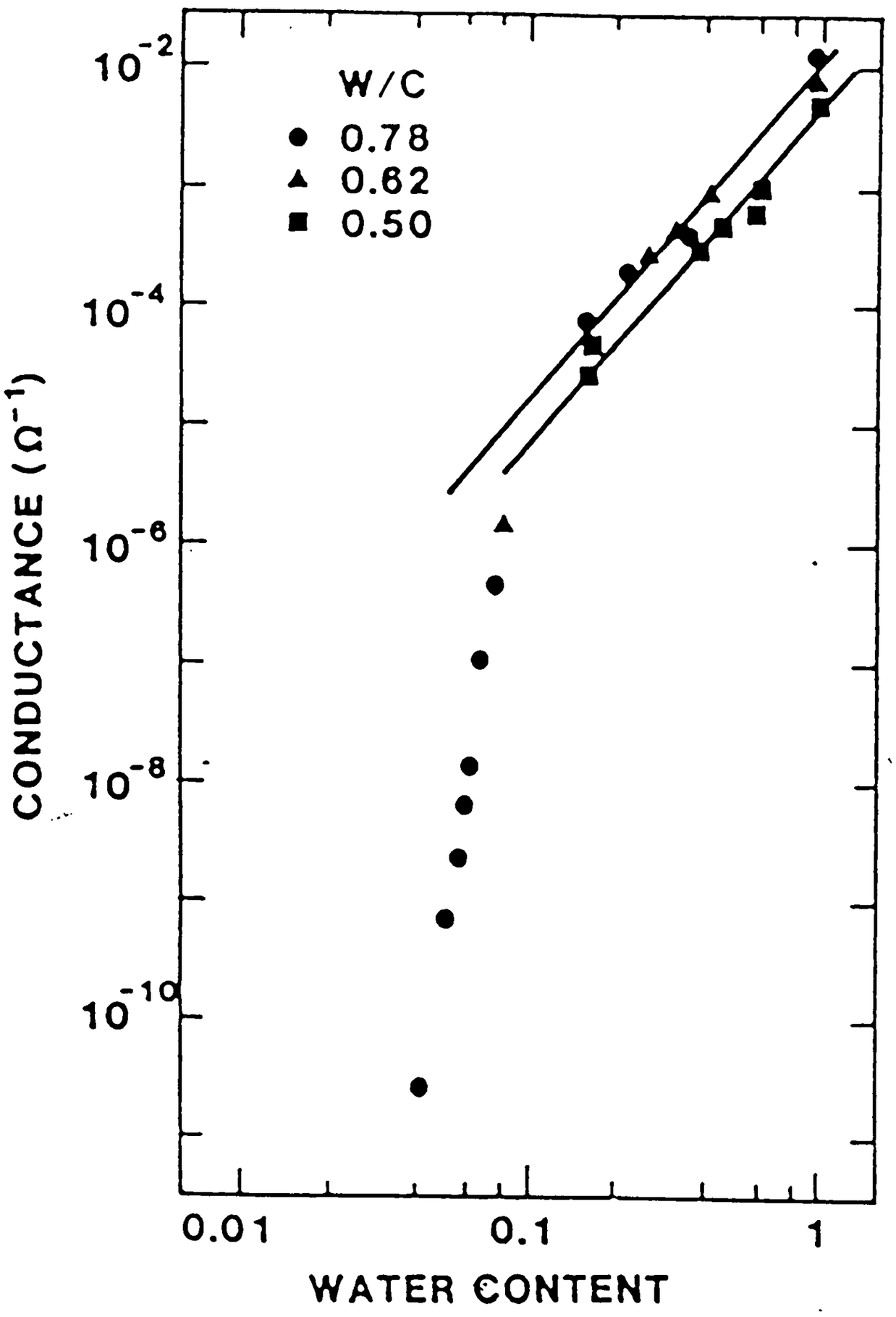

Figure 41: Variation of conductivity with moisture content.
The water content is given relative to the water that is evaporable at 378°K.
The lines show fits to the data in the power law region $t \approx 2.7$.
(Berg et al. 1992)

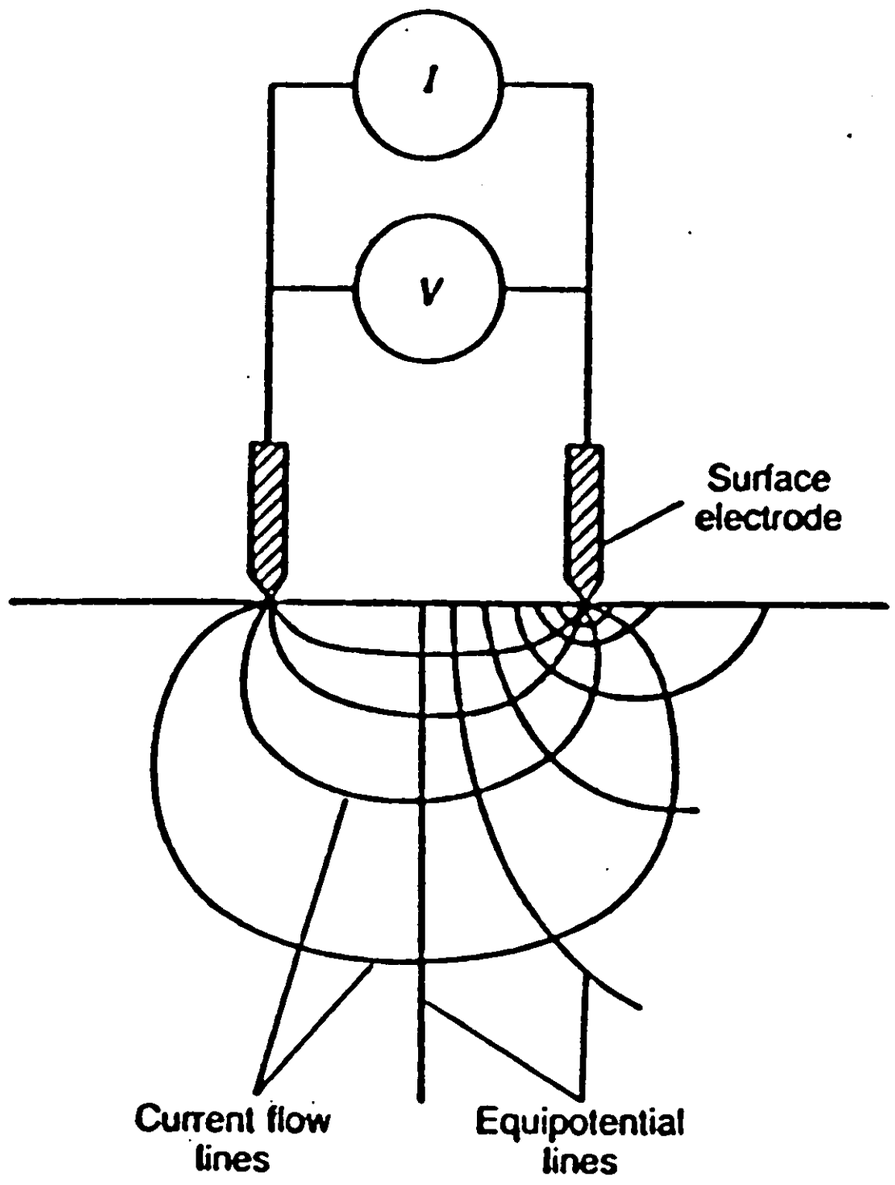

(a) Two-probe array.

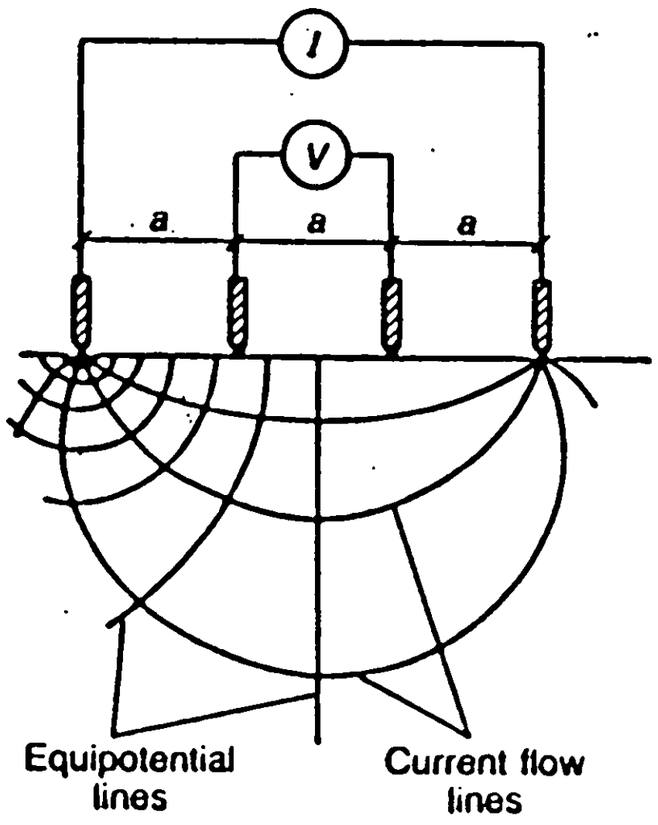

(b) Four-probe resistivity measurement, Wenner array.

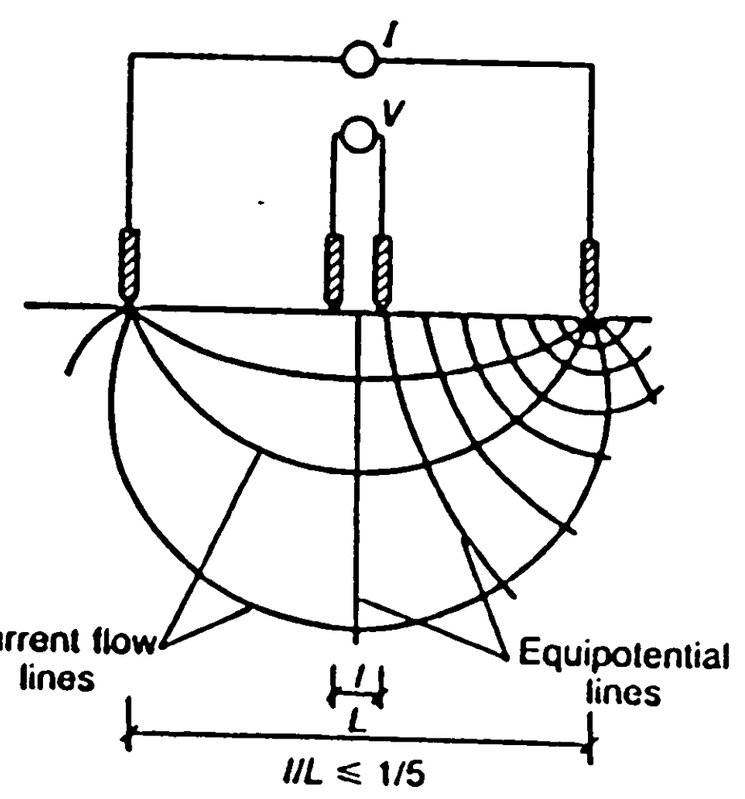

(c) Four-probe resistivity measurement, Schlumberger array.

Figure 42: Types of array used in geoelectric sounding
(Millard 1991)

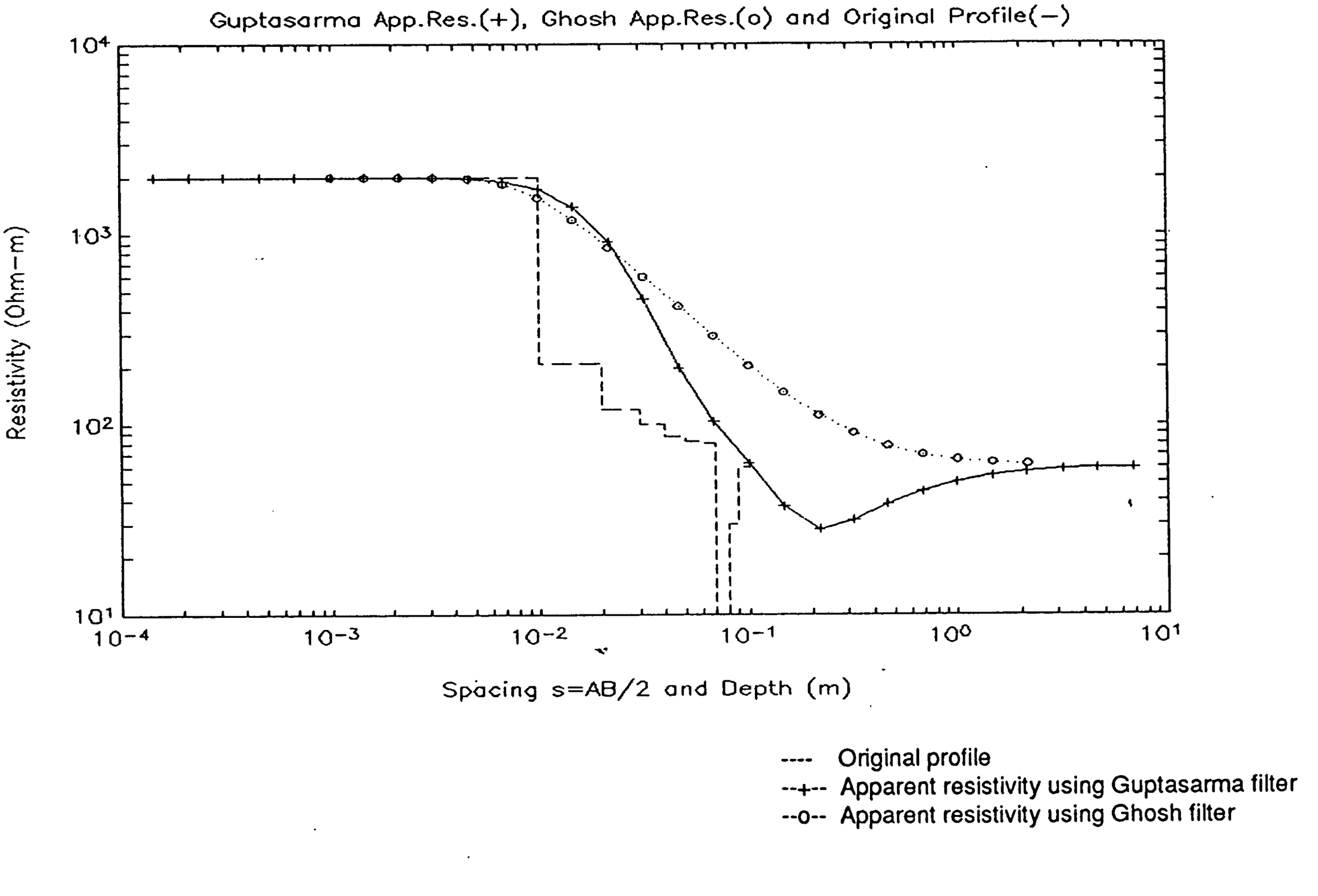

Figure 43: Apparent resisitivity curves generated by different digital filters

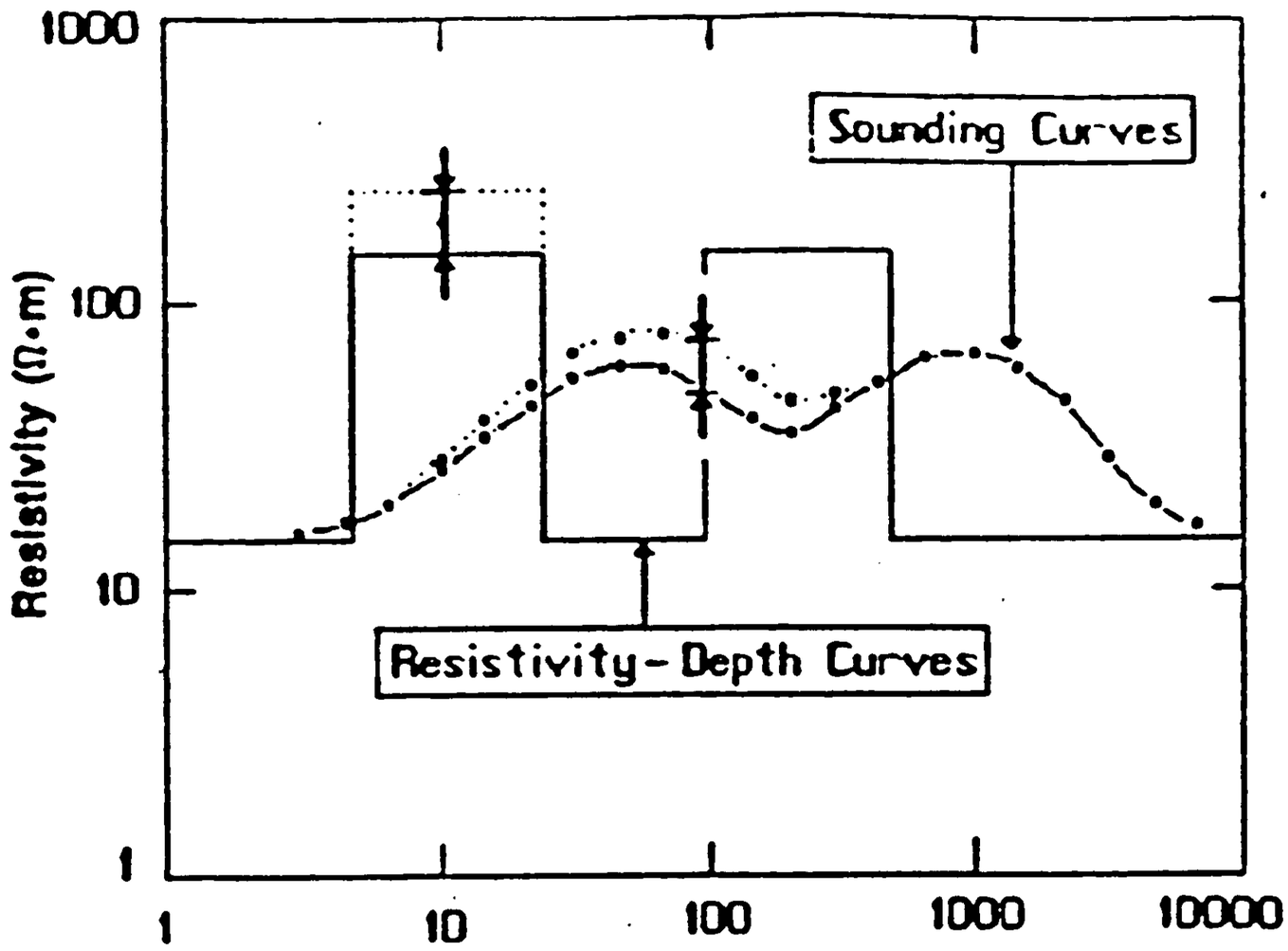

(a) Two five-layer Schlumberger sounding curves and layerings illustrating the spatial relations among electrode spacings, apparent resistivities, depths and true resistivities. Graphs also show that the maximum change in apparent resistivity is approximately equal to the maximum change in true resistivity.

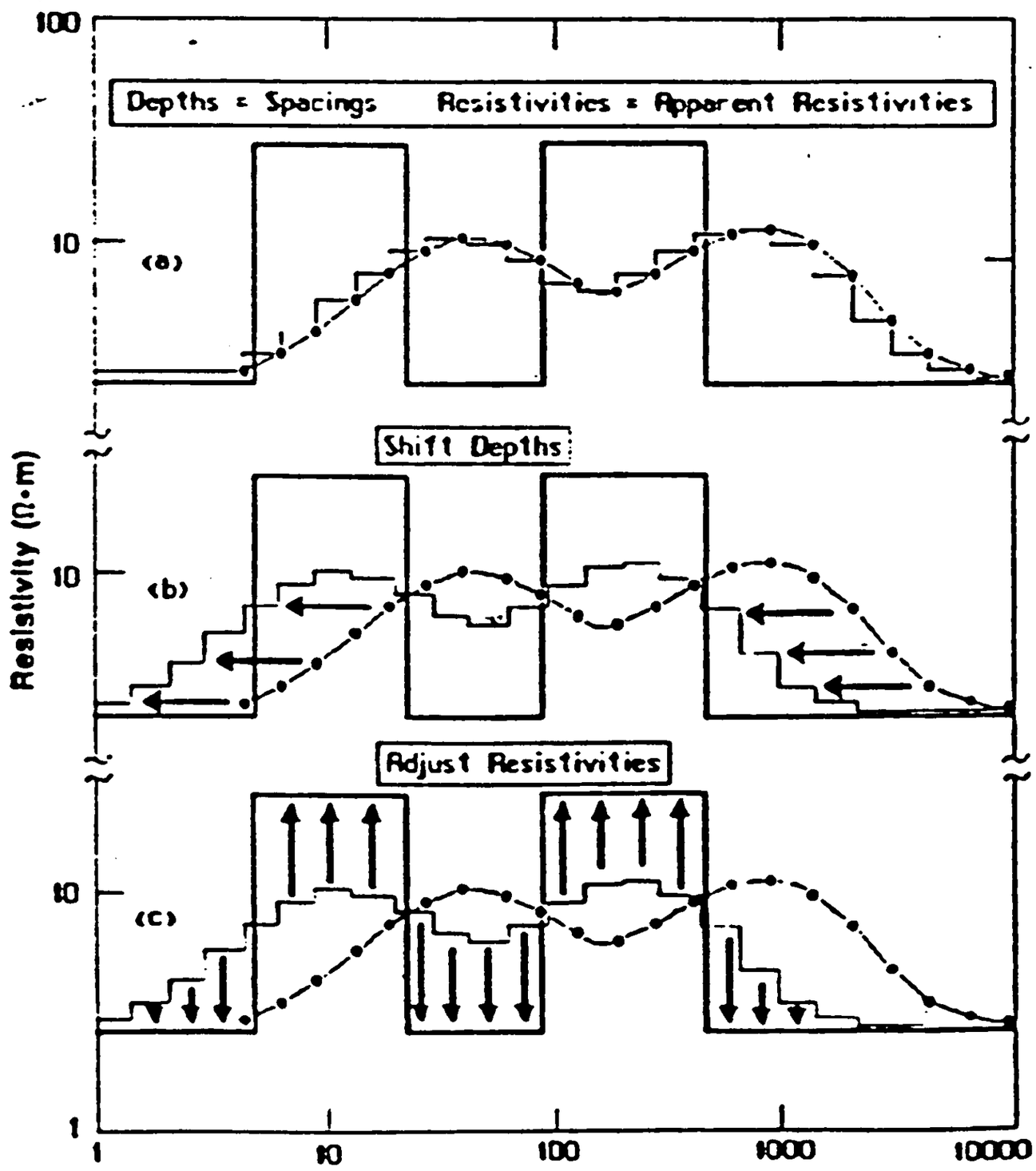

(b) Basic steps in the automatic interpretation method. 1. Assume that layer depths = electrode spacings and that apparent resistivities = true resistivities. 2. Shift assumed layer depths to the left to bring then in phase with actual layering. 3. Adjust amplitudes of assumed resistivities to those of actual layering.

Figure 44 : Principles of Zohdy's method
(Zohdy 1989)

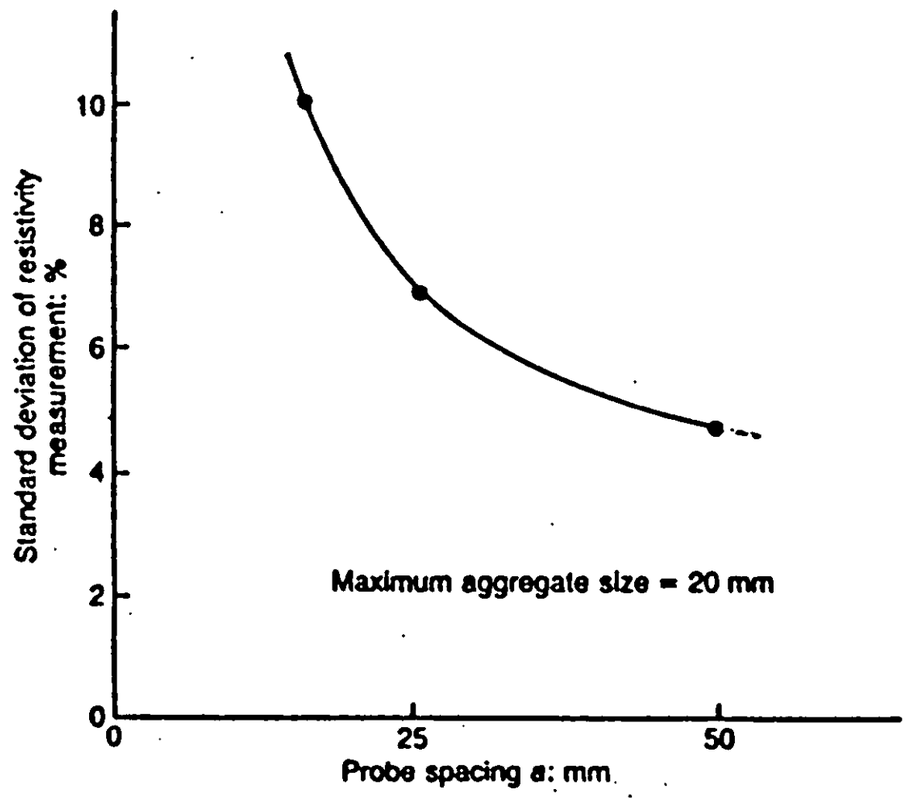

Figure 45: Influence of probe spacing on scatter in resistivity measurements
(Millard 1991)

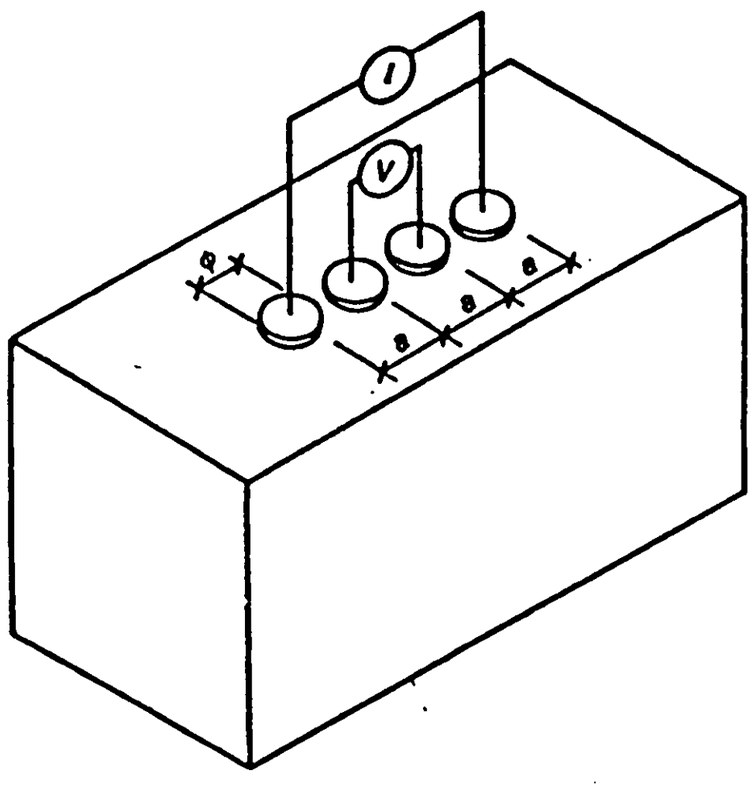

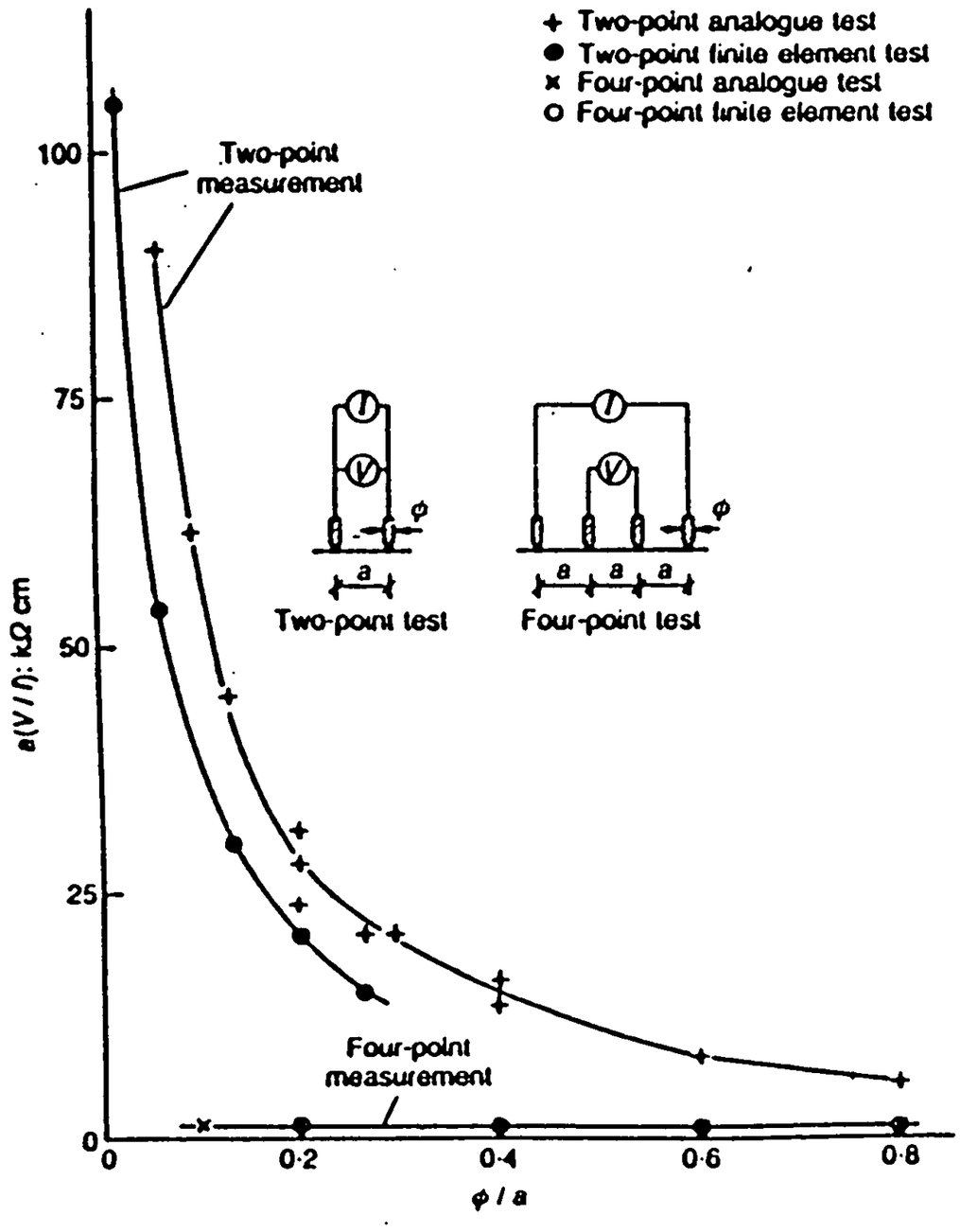

Figure 46: Influence of electrode contact area on resistivity measurements
(Millard 1991)

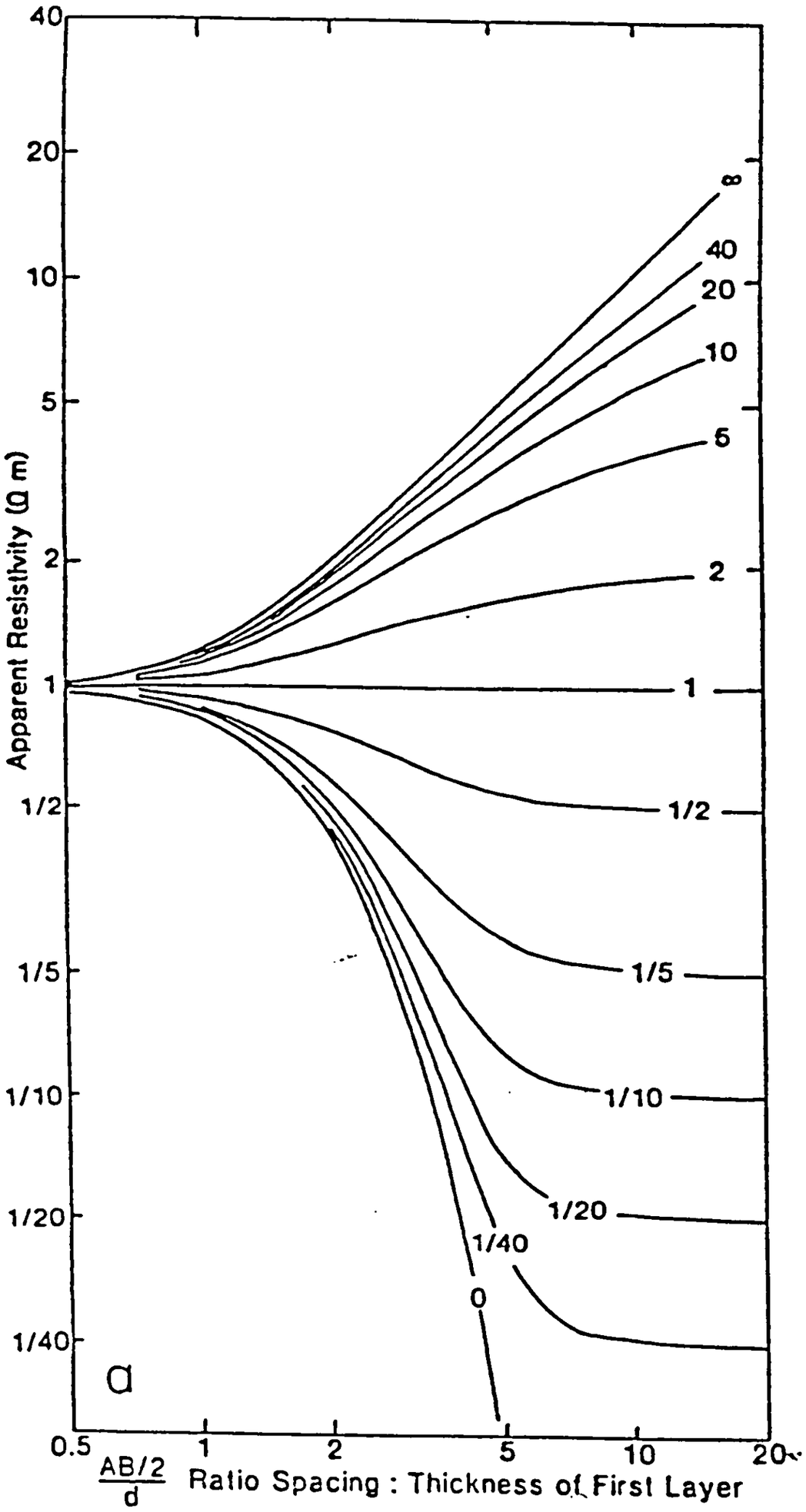

(a) Theoretical resistivity curves for 2-layered earth plotted for a selection of resistivity contrasts between the upper and lower layer.

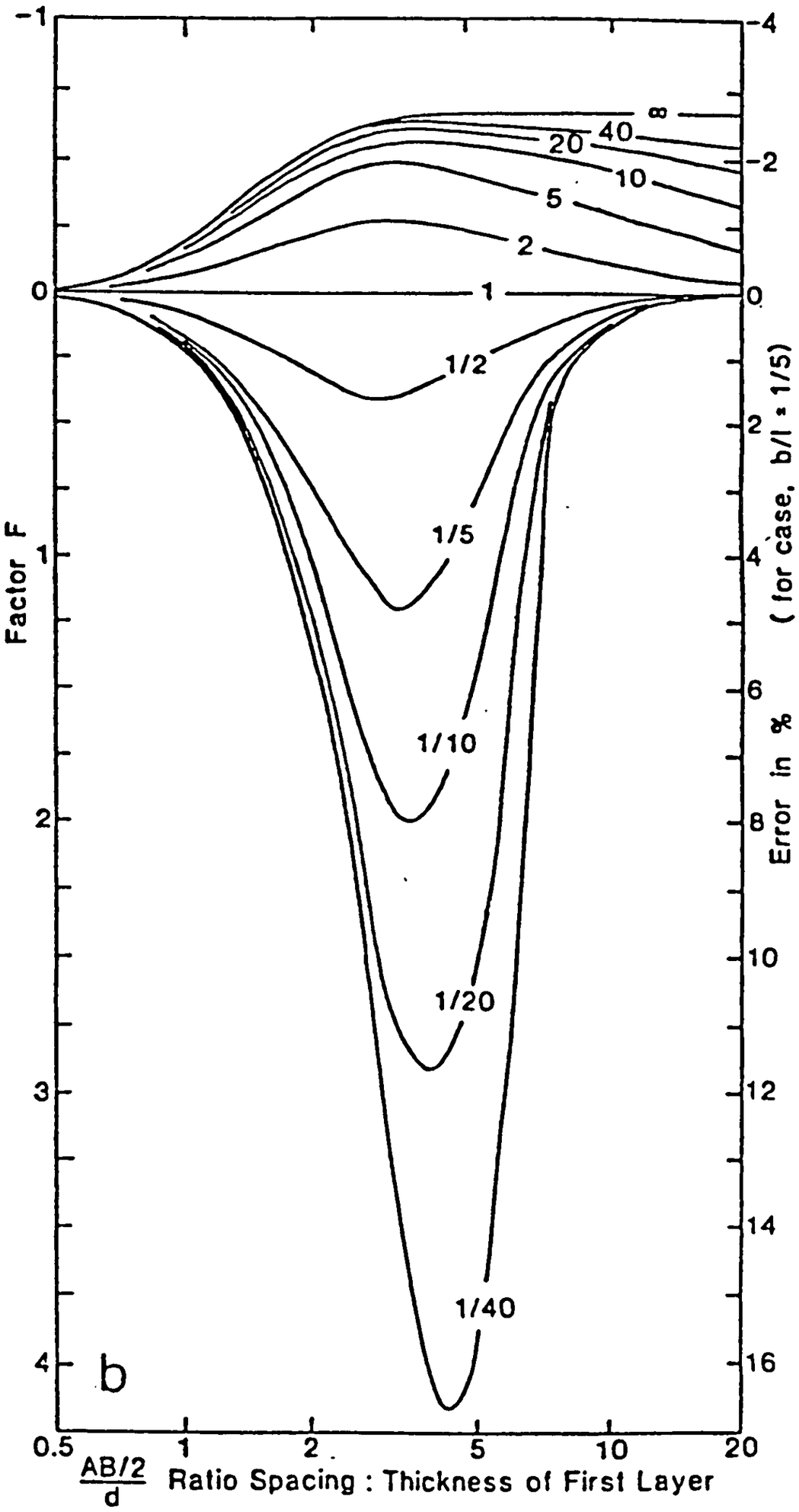

(b) Correction factor F versus ratio of spacing to first layer thickness. The right hand axis gives the size of error incurred if the correction is not made, for the case where b/l =1/5.

Figure 47 : Apparent resistivity curves and the corresponding finite-probe spacing correction factor
(Bibby and Fisk 1988)

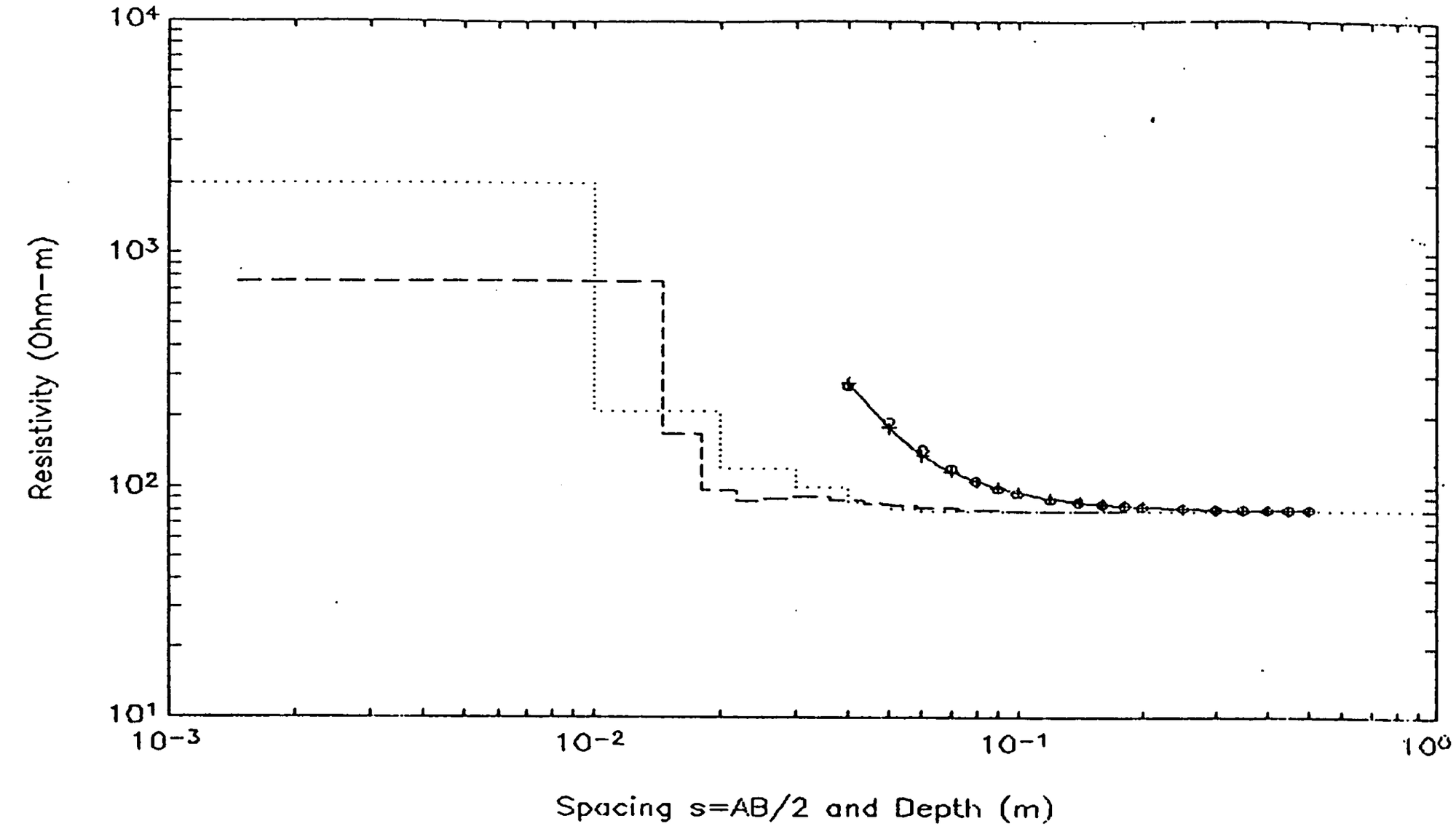

Figure 48: (a) Recovery without noise
..... original profile
-+-+- resultant 'field' apparent resistivity curve
------- recovered profile
-o-o- resultant best fit 'calculated' apparent resistivity curve

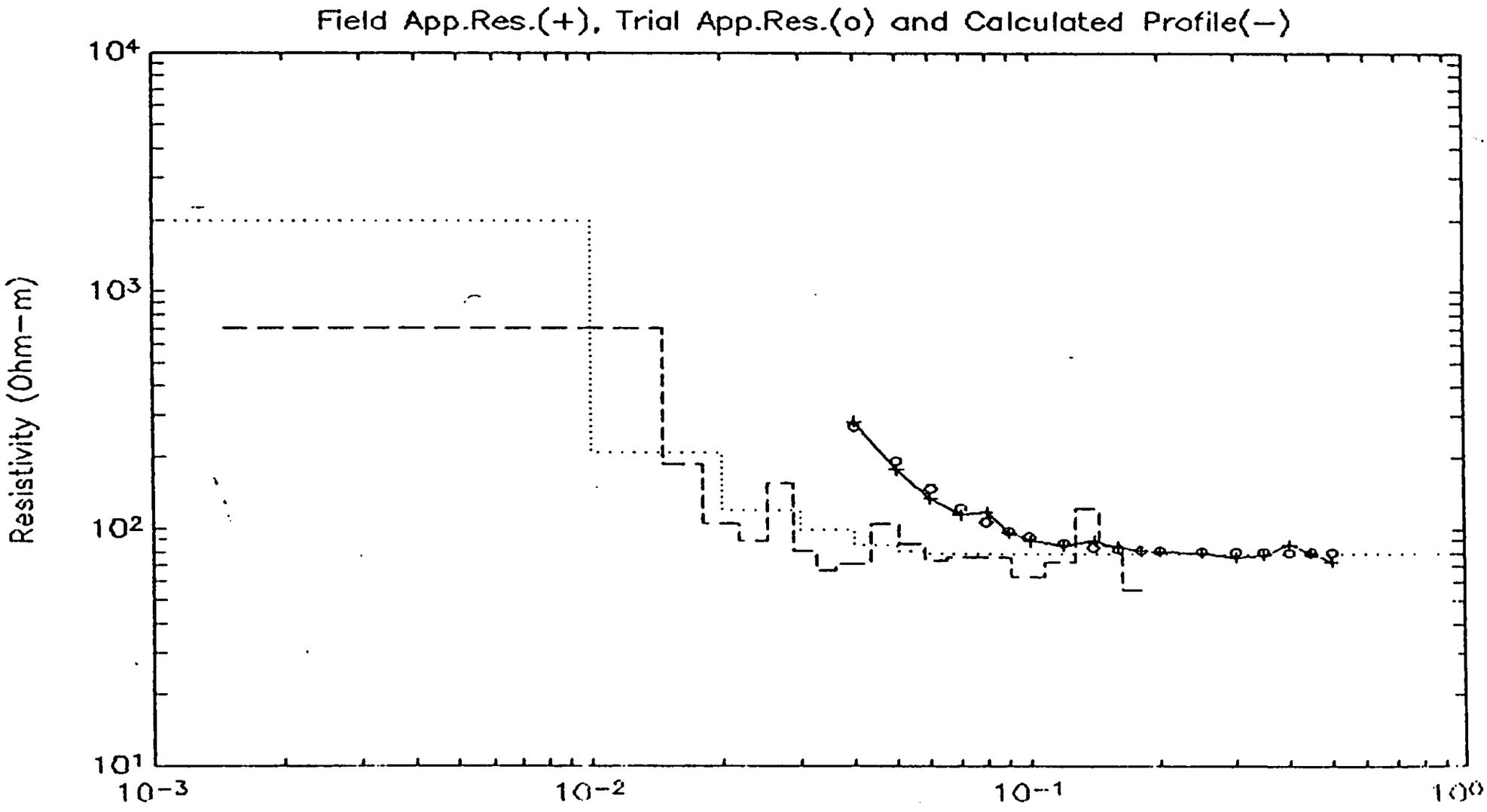

(b) Recovery with noise
..... original profile
-+-+- resultant 'field' apparent resistivity curve with noise added
------- recovered profile
-o-o- resultant best fit 'calculated' apparent resistivity curve

Figure 48: Examples of profile recovery using Zohdy's method

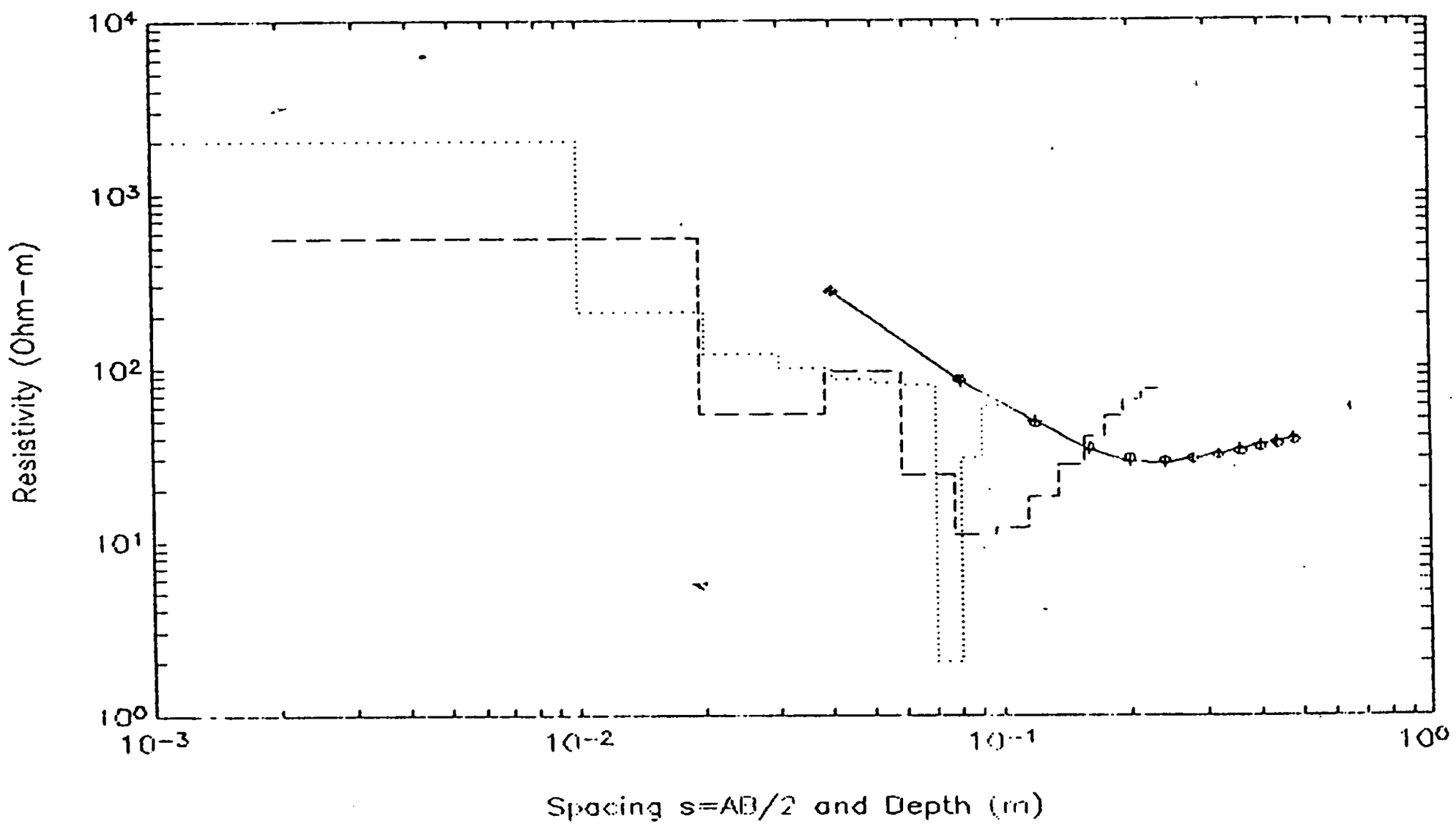

(b) Recovery of profile with simulated reinforcing bar between 7 and 8 cm depth
..... original profile
-+-+- resultant 'field' apparent resistivity curve
------- recovered profile
-o-o- resultant best fit 'calculated' apparant
resistivity curve

Figure 48 (continued): Examples of profile recovery using Zohdy's method

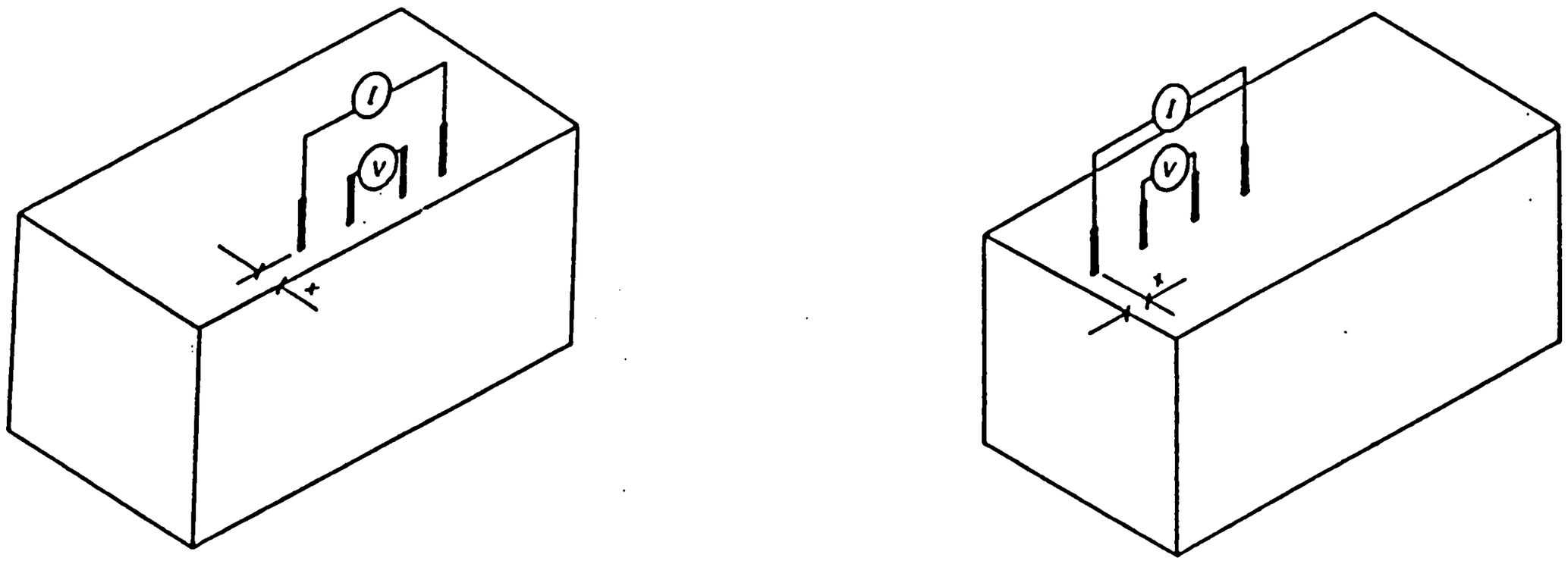

(i) Electrodes close to element edge.

(ii) Electrodes close to element end.

Figure 49: Proximities of boundary elements
(Millard 1991)

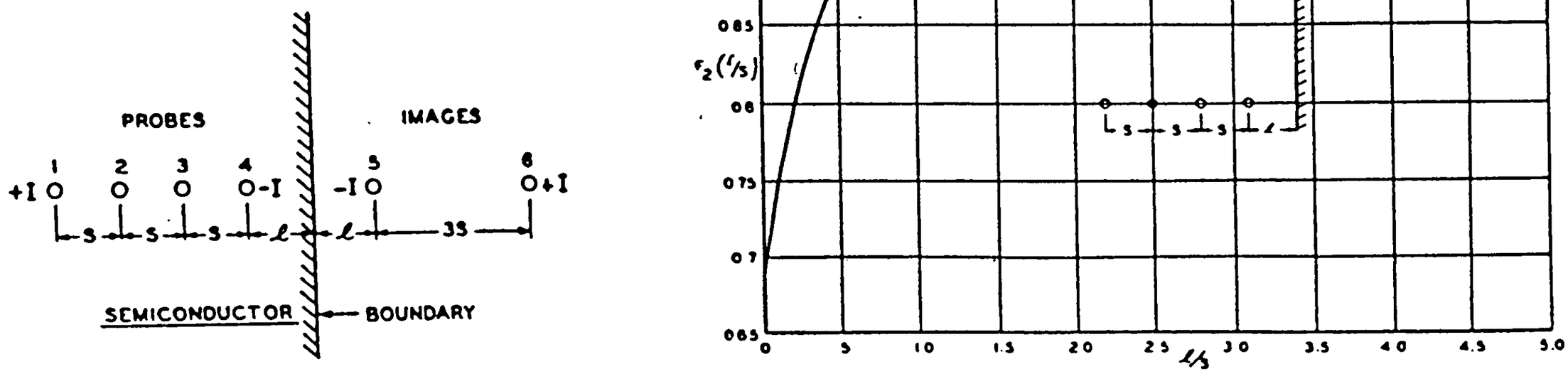

(i) Resistivity probes perpendicular to a boundary.

(ii) Correction factor for probes perpendicular to a non-conducting boundary.

Figure 50: Correction factor for boundary effects
(Valdez 1954)

A literature survey of electrical techniqu

LOVELL-SMITH, J.W.

Nov 1994

32788

Copy 1

BRANZ

THE RESOURCE CENTRE FOR BUILDING EXCELLENCE

BRANZ MISSION

To be the leading resource for the development of the building and construction industry.

HEAD OFFICE AND RESEARCH CENTRE

Moonshine Road, Judgeford
Postal Address - Private Bag 50908, Porirua
Telephone - (04) 235-7600, FAX - (04) 235-6070

REGIONAL ADVISORY OFFICES

AUCKLAND

Telephone - (09) 524-7018
FAX - (09) 524-7069
118 Carlton Gore Road, Newmarket
PO Box 99-186, Newmarket

WELLINGTON

Telephone - (04) 235-7600
FAX - (04) 235-6070
Moonshine Road, Judgeford

CHRISTCHURCH

Telephone - (03) 366-3435
FAX - (03) 366-8552
GRE Building
79-83 Hereford Street
PO Box 496